AD NUMBER

AD813590

NEW LIMITATION CHANGE

TO

Approved for public release, distribution unlimited

FROM

Distribution authorized to U.S. Gov't. agencies and their contractors; Critical Technology; Nov 1966. Other requests shall be referred to Air Force Materials Lab., Metals and Ceramics Div., Wright-Patterson AFB, OH 45433.

AUTHORITY

Air Force Materials Lab ltr, 29 mar 1972

AFML-TR-65-407
PART II

DEVELOPMENT OF DISPERSION STRENGTHENED TUNGSTEN BASE ALLOYS

HEINZ G. SELL, WILLIAM R. MJRCOM,
and GEORGE W. KING

Westinghouse Lamp Division
Bloomfield, N.J.

TECHNICAL REPORT AFML-TR-65-407, PART II
NOVEMBER, 1966

Air Force Materials Laboratory
Research and Technology Division
Air Force Systems Command
Wright-Patterson Air Force Base, Ohio

NOTICES

When Government drawings, specifications, or other data are used for any purpose other than in connection with a definitely related Government procurement operation, the United States Government thereby incurs no responsibility nor any obligation whatsoever; and the fact that the Government may have formulated, furnished, or in any way supplied the said drawings, specifications, or other data, is not to be regarded by implication or otherwise as in any manner licensing the holder or any other person or corporation, or conveying any rights or permission to manufacture, use, or sell any patented invention that may in any way be related thereto.

Copies of this report should not be returned to the Research and Technology Division unless return is required by security considerations, contractual obligations, or notice on a specific document.

FOREWORD

This report was prepared by members of the scientific staff of the Metals Research Section of the Lamp Division of Westinghouse Electric Corporation, under USAF Contract No. 33(615)-1698. The contract was initiated under Project No. 7351, "Metallic Materials", Task No. 735101, "Refractory Metals". The project was administered under the direction of the Air Force Materials Lab., Research and Technology Division, Air Force Systems Command, with Mr. J. T. Gow as project engineer. This report presents the results of research and development conducted during the period from May 1, 1965, through April 30, 1966.

The authors of this report have been engaged in the various programs of the contract as follows:

Project Manager	- H. G. Sell
Preparation, Fabrication, and Characterization of Experimental Alloys	- W. R. Morcom
Thermo-Mechanical Characterization of a Westinghouse High Strength W-3.8 v/o ThO_2 Alloy (ThDW-WHS)	- G. W. King

The authors wish to thank Drs. N. F. Cerulli and Lui Wei for analytical support and Messrs. R. K. Courtney, J. J. Corcoran, R. P. Watson, R. E. Bednarz, and W. R. Wheatley for valuable assistance.

The Dynapak extrusions were carried out at the Westinghouse Astronuclear Laboratories under the direction of R. Begley, and the large size extrusion billets were hot compacted at Aerospace Corporation, El Segundo, California, under the direction of Dr. J. White. A variety of W-Re-ThO_2 alloy samples were supplied by Chase Brass and Copper Company, Waterbury, Connecticut. The authors gratefully acknowledge these contributions.

This technical documentary report has been reviewed and is approved.

The manuscript was released by the authors November, 1966, for publication as an AFML Technical Report.

I. Perlmutter
Chief, Metals Branch
Metals and Ceramics Division
AF Materials Laboratory

ABSTRACT

The mechanical properties of a W-3.8 v/o ThO_2 alloy with superior high temperature tensile and creep strength have been determined from room temperature to 3000°C. This alloy has been produced by two separate techniques in rod form. The alloy has been found to exhibit a tensile strength as high as 15,500 PSI at 2400°C and at a strain rate of 0.05 min^{-1} and a 1 hour creep rupture strength as high as 12,500 PSI at 2200°C. The DBTT of this alloy annealed at 2400°C for 1/2 hour is 190°C.

Four experimental W-5.7 v/o ThO_2 alloys have been produced to investigate the effects of chemical processing parameters on dispersoid distribution and strength properties. The high temperature strength properties have been essentially reproduced in alloys in which the thoria dispersion was added to tungsten oxide. In those alloys in which the thoria dispersion was added to the metal powder, the strength improvements were much smaller.

Substructures and dispersoid distributions have been extensively studied by electron transmission microscopy and by various replication techniques. In the superiod strength W-ThO_2 alloys, the thoria dispersed second phase contains a high fraction of particles having diameters smaller than 1000Å. The thoria distribution is very stable and effects the retention of a polygonized substructure to 2800°C.

A high temperature strength evaluation was also made on W-Re-3.8 v/o ThO_2 alloys having 5, 10, 15 and 25 w/o Re concentration. These alloys have significantly lower strength above 2000°C than the ThDW-WHS (W-3.8 v/o ThO_2) alloy.

TABLE OF CONTENTS

TABLE OF CONTENTS (cont'd.)

ILLUSTRATIONS

ILLUSTRATIONS (cont'd.)

ILLUSTRATIONS (cont'd.)

ILLUSTRATIONS (cont'd.)

ILLUSTRATIONS (cont'd.)

ILLUSTRATIONS (cont'd.)

LIST OF TABLES

LIST OF TABLES (cont'd.)

I. INTRODUCTION

In the high temperature materials development field, it does not often occur that one can report about the successful development of a vastly improved material. This is the favorable position in which the authors of this report find themselves in regard to the alloy W-3.8 v/o ThO_2 (in preceding progress reports referred to as Westinghouse-Special alloy but from hereon designated ThDW-WHS alloy--thoria doped tungsten, Westinghouse high strength alloy). As the substantial amount of information on high temperature tensile and creep strength, low temperature ductility, and other metallurgical properties contained in this report will show, this specific W-3.8 v/o ThO_2 alloy, as well as alloys similarly produced on an experimental basis, have reproducibly superior high temperature strength characteristics to those of any other currently available tungsten base alloy or pure tungsten.

That a W-ThO_2 alloy could be made with very favorable high temperature mechanical properties was already demonstrated under the preceding contract (AFML-TR-65-407, Part I--subsequently referred to as Ref. 1) from results on 11 different alloy systems, including W-ThO_2, which were investigated on a screening basis. The fact that this should be possible was indicated during several earlier development efforts (2, 3); however, these efforts achieved only marginal success.

At the closing of the last contract period, two of the 11 alloy systems were chosen for further development work. The first choice was the W-ThO_2 alloy for the reasons given above. The second choice was the system W-Re-ThO_2 from the viewpoints of improved low temperature ductility (4) and potential high temperature strength.

The immediate effort that was required at the beginning of the contract differed for the two alloys. In the case of the W-ThO_2 alloy, previous contract results had shown that hot pressing of blends of elemental powders did not present the optimum method of consolidating a billet with a fine and mechanically effective dispersion. It was initially assumed that the lower temperature required for consolidation by hot pressing would help to retain a finer dispersion. However, electron transmission microscopy revealed various degrees of agglomeration depending on powder contamination and heat treatment after pressing. In the course of this evaluation, the observation was made that H_2 self-resistance sintered and swaged ingots produced from a certain alloy powder prepared by the Lamp Division's Engineering Department, had retained a fine dispersion which imparted significant strength improvements.

The problem reverted thus back to the powder itself and, specifically, to its chemical preparation. Therefore, four experimental alloy batches were prepared differing in the method in which the thoria was chemically introduced, and the mechanical properties were compared with those of the engineering material (ThDW-WHS). The alloys were consolidated by self-resistance sintering and by hot compaction. Fabrication was accomplished by extrusion and swaging.

In the case of the W-Re-ThO_2 alloy, the problem faced at this laboratory was poor fabricability in that swaging of die pressed and high temperature sintered ingots was only marginally successful. Additional attempts were made to swage W-5% and 10% Re alloys with a 2 w/o ThO_2 dispersion but again with very poor yield. This experience differed from that of the Chase Brass and Copper Company where fabrication of these alloys from sintered ingots was successfully accomplished. Alloy rods of the desired compositions were made available and included in the evaluation by courtesy of the Chase Brass and Copper Company.

Evaluations of the two alloy systems were primarily made with respect to high temperature tensile properties and dispersion characteristics. For the high strength alloy ThDW-WHS, the ductile brittle transition temperature (DBTT), the creep properties, and the recovery behavior were also determined in considerable detail. In all evaluations, various techniques of electron microscopy were extensively employed. The results were correlated with existing theories of dispersion strengthening and reasonable agreement was obtained with equations derived from the Orowan mechanism as modified by Kelly, et.al. (5). The work hardening characteristics of the W-ThO_2 alloys were found to be in qualitative agreement with the theory of Fisher, et.al. (6).

In the final analysis, the strongest high temperature alloy is shown to be the engineering material (ThDW-WHS) which reproducibly demonstrates in the annealed condition (1/2 hour, 2400°C) a tensile strength $\sim$ 5 times that of pure tungsten at 2400°C tested at a strain rate of 0.05 min^{-1} and a 1 hour creep rupture strength at 2200°C of $\sim$ 12500 PSI. Two of the experimental W-ThO_2 alloys exhibited equivalent tensile properties. Future efforts required for the development of sheet fabrication methods for this alloy are outlined in the summary of this report.

II. W-ThO_2 Alloys

The effect of a thoria dispersion on the mechanical properties and structural stability of tungsten was reported by Jeffries as early as 1924 (7). In recent years, a great deal of effort has been made to utilize dispersoids in other metals to improve high temperature strength. Notable success has been achieved, in some instances, with TD-nickel (Ni-2 v/o ThO_2) as one of the most outstanding examples (8).

The present research program was directed towards the development of a tungsten base dispersed second phase alloy with superior high strength properties above 0.5 T_m and with low temperature ductility at least comparable to that of pure tungsten.

One primary objective of the present work has been the detailed characterization of the most promising alloy, ThDW-WHS. Such characterization has been performed with respect to particle size and distribution, recovery, and mechanical properties.

In addition, since the chemical approach to dispersing the second phase proved more rewarding than the mechanical technique (milling), a second major objective has been to investigate several chemical dispersion techniques. To this end four W-ThO_2 alloys were prepared by new techniques chosen also to produce very fine dispersions. In all four alloys, the ThO_2 was added to the matrix tungsten or tungsten oxide as a $Th(NO_3)_4$ solution. The concentration of ThO_2 was selected to be 5.7 v/o, i.e., between the two levels previously used (1). This "compromise" concentration was chosen with the hope of further improving the strength of the 3.8 v/o alloy, but reducing the fabrication difficulties encountered with the 6.5 v/o alloy (1). For the consolidation of these alloys, hot pressing was still used as a standard method, but in one alloy (ThDW-2) a second method, self-resistance sintering, was also employed.

For the purpose of scale-up, 2.25 in. diameter billets were hot pressed at Aerospace Inc. and were conventionally extruded at the WPAFB facility. Three of the alloys processed in this fashion were also produced in the smaller billet size (1.25 in. diameter) and processed by high rate extrusion. Finally, the effect of swaging temperatures on rods of less than 0.400 in. was investigated to some extent in two of the alloys.

A. Preparation of Alloys

1. Dispersion Techniques

The techniques employed to incorporate the ThO_2 dispersoid into the base powders are described below:

ThDW-WHS (3.8 v/o ThO_2) - The starting material for this alloy is ammonium paratungstate (APT) of high purity. A typical analysis is reported in Table 1. The APT is converted to tungsten oxide at about 600°C in nitrogen or in air. The oxide formed in nitrogen is blue (approximate formula $W_{20}O_{59}$) whereas a yellow oxide (WO_3) forms in air. Mixtures of the two oxides can be employed. The oxide powders are loaded into a twin shell blender, and while the blender shell is turning, the $Th(NO_3)_4$ solution is sprayed into the oxide by the centrifugal action of a rapidly rotating "attritor" bar.

In addition to homogeneously dispersing the solution, this bar also effects some comminution of the oxide particles. After the total amount of solution is added ($\sim$10% of the oxide charge by weight) the attritor bar rotation is stopped, but tumbling of the doped oxide is continued while drying.

The dried doped oxide is subsequently reduced in hydrogen at temperatures from 750-1000°C. The resulting metal powder which has a FSSS in the range 1.2-2 μ is then sieved (250 mesh) and tumbled. Normally, this powder is processed in quantities amounting to 350 Kgs. per batch.

ThDW-1 (5.7 v/o ThO_2) - The first experimental alloy was prepared from a 50 Kg. batch of the same oxide employed for ThDW-WHS, and processing techniques were identical with the following exceptions:

(a) In addition to the $Th(NO_3)_4$ solution, solutions of KNO_3, $K_2Si_2O_3$ and $Al(NO_3)_3$ were added to give the respective weight concentrations of 0.4, 0.4 and 0.1%. These additives were included because silica and alumina were previously found to promote a finer thoria dispersion (1).

(b) The attritor bar was permitted to rotate for about 3 times the period employed in the preparation of ThDW-WHS thus promoting greater comminution.

(c) The reduction conditions were altered (temperature range 850-1000°C) to produce a finer metal powder.

The mean particle size (FSSS) of this experimental batch was 3.6μ.

ThDW-2 (5.7 v/o ThO_2) - The second experimental alloy batch was essentially a laboratory produced ThDW-WHS equivalent with a higher concentration of thoria. It provided a measure of the concentration effect and also served as a control for the alloy ThDW-1. It was prepared in the same quantity and by the same technique as ThDW-1 with the exception that the K and Al salts were omitted. The mean particle size (FSSS)* of this batch was 1.5μ.

ThDW-3 (5.7 v/o ThO_2) - The third alloy variation was prepared by the addition of a $Th(NO_3)_4$ solution directly to high purity metal powder (4 Kg. batch size). In this alloy and the fourth experimental alloy (ThDW-4), the doping was performed on the reduced powder in an attempt to achieve a more effective dispersion because of the very fine particle size of this material (0.3μ). The quantity of solution employed was just sufficient (~11 w/o) to make up a fluid slurry which was milled (1) for 3 hours to homogenize the mix. The slurry was then decanted directly into a stainless steel tray and frozen under vacuum. The frozen state was maintained until no further condensate formed in the LN trap between the container and the pump. At this point, the relatively dry powder was removed and further dried in air at 80°C. The freeze-drying technique was employed in an attempt to minimize segregation of the thorium salt during drying.

On the first run, this final drying step proved destructive to the entire batch in that relatively slow, but nearly total, oxidation occurred. This pyrophoricity was probably promoted by the exothermic decomposition of the nitrate, even at this relatively low temperature. Although the oxide formed could have been reduced for further experimentation, it was discarded, and a second batch was made with the final drying performed in N_2. The dried mix was then heated in H_2 to a temperature of 900°C to decompose the $Th(NO_3)_4$. The mean particle size (FSSS) of this batch was 1.3μ.

ThDW-4 (5.7 v/o ThO_2) - The fourth alloy in this series was prepared by the addition of an alcoholic solution of $Th(NO_3)_4$ to the same high purity tungsten (4 Kg. batch size) used for ThDW-3. Again, the amount of liquor added was just sufficient to form a fluid slurry which was milled, dried under vacuum, and finally dried at ~80°C in air. This alcohol-vacuum technique was employed to permit accelerated drying and thus possibly minimize thorium salt segregation. The thorium salt was again decomposed in H_2 at 900°C. No pyrophoricity was observed with this material. Its FSSS was 3.3μ.

---

* FSSS - Fisher Subsieve Size

W-5 w/o Cb-5.7 v/o ThO_2 - As the mechanical property data of the W-Re alloys evolved (1), doubts arose that this series of alloys would provide the high temperature strength desired. Consequently, an alternative solid solution system was sought. On the basis of other data (9), a W-Cb alloy was selected. In this case, the constituent metal powders were milled for 20 hours in the tungsten mill with a $Th(NO_3)_4$ solution. Drying in air was performed at 80°C, and the decomposition of the $Th(NO_3)_4$ was accomplished in an argon atmosphere.

B. Consolidation of Alloys

1. Hot Pressing

Previous contract work (1) demonstrated the efficacy of this technique for producing maximum density billets which could subsequently be fabricated by extrusion, although properties determined on previously hot pressed materials were somewhat inferior to those of the same material which had been self-resistance sintered. However, because of the difficulties anticipated in pressing ingots for self-resistance sintering, and in attaining satisfactory densities by that method, hot pressing was again employed as the standard consolidation technique.

Since it was desired to initiate a preliminary scale-up which required billet sizes larger than the hot press in this laboratory could consolidate (1.25 in. dia.), the hot pressing of larger billets was performed by Dr. J. White of the Aerospace Corporation.

For the small billets, the apparatus and the pressing procedure employed have been described previously (1). One variation, the use of a tantalum foil liner to reduce possible carbon contamination, was tried. However, most of the compacts prepared with the foil were found to have circumferential cracks of such a depth as to render them useless. The cracks are believed to have resulted from folds occurring in the foil during pressing. All the billets were then successfully pressed without a liner.

For the 2.25 in. dia. billets, powder of five compositions (including powder of the W-Cb-ThO_2 alloy) was forwarded to Aerospace Corporation for hot pressing in an apparatus described elsewhere (10). The W-ThO_2 powders were from the same experimental batches used for the 1.25 in. dia. billets. Contrary to the experience in this laboratory, all large billets were pressed successfully with a tantalum foil liner in a mold of different design.

Initially, attempts were made to produce the larger size billets with a length to diameter ratio approaching two. This resulted in fracture of the mold, and subsequently this ratio was reduced to slightly greater than 1, after which satisfactory billets were produced. The major differences between the pressing techniques are given below (Table 2):

Table 1

Supplier's Analysis of Ammonium Paratungstate

Element or Compound	WO_3	Mo	NVR*	NH_3	Al	Cu	Fe	Na	Si
Analysis** w/o	89.00	<.002	<.005	5.4	<.002	<.0003	<.003	<.002	<.0004

* Non-Volatile Residue
** Balance H_2O

Table 2

Comparison of Hot Pressing Techniques

Westinghouse	Aerospace Corp.
1.25 in. dia. x 1.9 in. length	2.25 in. dia. x 2.5 in. length
Single piece mold	Split mold
Single acting press	Double acting press
No liner	Ta foil liner
Handled in air prior to hot pressing	Handled in inert gas prior to hot pressing

Table 3

Carbon Analyses of a Hot Pressed ThDW-2 Billet After Conditioning

Section No.*	Carbon Content (wt. ppm) (Low Pressure Combustion)
1 (edge section)	87
2	83
3	100
4 (center sections)	74
5	68
6	81
7	101
8 (edge section)	113

* To obtain the sections a 1/8" thick disc was cut from the billet; from this a 1/4" wide diametric strip was cut and sectioned perpendicular to the diameter.

Note: Commercially pure tungsten nominally has about 40 wt. ppm. carbon.

Following pressing, all billets were conditioned by surface grinding to remove 0.03-0.05 in. from all surfaces. This removal represents roughly two to five times the depth to which contamination was metallographically observable. Carbon determinations made across the diameter of one billet after grinding are listed in Table 3. The average carbon concentration is higher than normally found in commercial purity tungsten and a small surface to center gradient is observed.

A listing of all billet compositions, dimensions, and densities is presented in Table 4.

Table 4

Dimensions and Densities of Hot Compacted Extrusion Billets

Designation	Composition	Billet*** Dimensions	Density (% Theo.)
ThDW-WHS*	W-3.8 v/o ThO_2	1.20 x 1.26	92
ThDW-1	W-5.7 v/o ThO_2**	2.10 x 2.04 1.20 x 1.45	95 87
ThDW-2	"	2.10 x 2.14 1.20 x 1.46	91 91.5
ThDW-3	"	2.10 x 2.00	95
ThDW-4	"	2.10 x 2.00 1.20 x 1.46	95 92
ThDW/Cb-1	W-5 w/o Cb-5.7 v/o ThO_2	2.10 x 1.60	96

* The Dynapak extruded ThDW-WHS is a second billet equivalent to the material referred to as Alloy No. 2 in previous work.
** ThDW-1 also contains compounds of potassium, silicon, and aluminum at levels less than 0.5 w/o.
***Dimensions given as diameter x length (inches).

2. Self-Resistance Sintering

The fact that the ThDW-WHS alloy is consolidated by self-resistance sintering made it necessary to attempt this consolidation process for the experimental alloys, in spite of the liabilities mentioned before. Consequently, two alloys (ThDW-1 and ThDW-2) were pressed at room temperature in a conventional

open mold at 40 KSI (0.375 x 0.375 x 24 in. for both alloys, and also 0.725 x 0.700 x 24 in. for ThDW-2). The alloy ThDW-2 was successfully sintered in both sizes to 93-96% of theoretical density. The schedules used (essentially the same employed for ThDW-WHS) entailed a rise time to the maximum temperature ($\sim$2850°C) of 15 min. for the small and 35 min. for the larger ingots. All ingots were held at this temperature for 20 min. Several schedules were tried on ThDW-1, but adequate density could not be obtained, and internal voids were found in the sintered ingots. These voids are presumed to be the result of premature surface sintering which precludes the escape of volatile material retained internally--probably some compound of the silica and/or alumina added to this alloy.

It is, of course, necessary throughout the foregoing processes to minimize contamination of the oxide or the metal. Iron and nickel are generally accepted as being undesirable contaminants in tungsten, and reactions of thoria with carbon have been reported in the literature which result in the formation of free thorium (11). Thorium in the form of the free metal is reported to have a very high diffusivity in tungsten (12), whereas, as will be shown later, the oxide is very stable in the completely dense tungsten matrix. Therefore, if thorium is formed as a result of carbon contamination, coarsening of the second phase can occur during subsequent high temperature processing.

C. Fabrication of Alloys

1. Direct Swaging of Self-Resistance Sintered ThDW-WHS and ThDW-2 Ingots

Sintered ingots 20 x 0.6 x 0.5 in. were warm swaged directly into rods of $\sim$0.185 in. dia. The die line was the same used for extruded alloys (Table 5). The initial preheat temperature for ThDW-WHS was 1700°C and was gradually reduced to about 1200°C as the rod diameter was decreased. For ThDW-2, a preheat temperature of 1650-1750°C was used at all sizes, because some edge cracks were present in the as sintered ingots. Intermediate anneals were employed during the reduction to the final rod size.

2. Extrusion

Previous work (1) had demonstrated the feasibility of high rate extrusion (Dynapak) for alloys of this type, and the primary breakdown of the 1.2 in. dia. billets was again performed in this fashion. The 2.1 in. dia. billets, however, were extruded in a conventional press. This variation was investigated because, from the equipment standpoint, fewer problems were anticipated in scale-up.

Table 5

General Swaging Schedule for Extruded Alloys

Machine Size	Preheat Temp. (°C)	Preheat Time (min.) 1st end	Preheat Time (min.) 2nd end	Size (in.)
#6	1700-1750	15	10	1.000 ± .010
"	"	10	10	.855 "
"	"	"	"	.740 "
"	"	"	"	.630 "
#4	"	10	6	.630* "
"	"	"	"	.560 ± .005
"	"	"	"	.470 "
"	"	"	"	.400 "
"	"	"	"	.340 "
"	"	"	"	.285 "
"	"	"	"	.240 "
"	"	"	"	.205 "
"	"	"	"	.185 "

* All of the high rate extruded material was started on the #4 swager at 0.630 in.

Prior to extrusion, all billets were encapsulated in molybdenum. Capsules of the configuration previously employed (1) were used with the 1.2 in. dia. billets, while the capsules for the larger billets were machined at WPAFB where the conventional extrusion was performed. The extrusion parameters are presented in Table 6.

The W-5 w/o Cb-5.7 v/o ThO_2 billet broke up severely on extrusion. All other billets, as extruded, had good surface characteristics (Mo capsule) and relatively uniform diameters (no indication of breaking up of the core alloy) throughout their length. Swaging was thus begun without removing the molybdenum case. Only the high rate extruded billets were sampled, as extruded, since the conventionally extruded billets were barely long enough for swaging.

3. Swaging of Extruded Billets

The swaging schedule used is shown in Table 5. Due to the short lengths involved, no continuous swaging was feasible; hence, temperatures at the point of material deformation were higher at the ends and progressively lower as the center of the rod approached the die. The maximum temperature drop due to this limitation is estimated to be $\sim$300°C. This is encountered on the smallest dies with rods exceeding $\sim$30 inches. The effect is essentially negligible with short pieces of large diameter.

Material losses during swaging were high (Table 7). Although the as extruded surface of the molybdenum capsules had indicated sound billets in two cases (ThDW-1 - large billet and ThDW-WHS - small billet), swaging breaks are believed to have resulted from pre-existing cracks. This was suggested by the almost total penetration of molybdenum into the cracks, which is not believed possible under the swaging conditions employed. The most common source of loss, however, was splitting, particularly at the ends of the rods. Such splitting is a problem in the fabrication of thoriated tungsten and in these alloys was probably aggravated by the limitations of the hand swaging process. Additional factors may have been the higher concentration of thoria and a less than optimum working schedule.

4. Rolling

Since the projected end use of the high strength alloy is sheet, a single preliminary attempt was made to roll two of the compositions being investigated (ThDW-2 and ThDW-WHS). Both were pressed at room temperature in a standard mold to 0.750 x 1.500 x 15 in. and self-resistance sintered ($\sim$2850°C, 30 min.) to densities of $\sim$17.2 gm/cm^3. The billets were subsequently cut into 4-5 in. lengths and conditioned as shown in Fig. 1. The rolling schedule is given in Table 8.

Table 6

Extrusion Parameters for W-ThO_2 Alloys

	1.20 in. dia. Billets (Dynapak Extrusion)	2.10 in. dia. Billets Standard Extrusion)
Preheat Temperature (induction)	1950°C	1980°C
Preheat Time	5 min.	25 min.
Transfer Time	10-20 sec.	N.D.*
Extrusion Ratio	6:1	6.3:1
Die Composition	Steel (ZrO_2 coated)	H-12 Steel (ZrO_2 coated)
Lubricant	None	MoS_2
Jacket Material	Molybdenum	Molybdenum
Ram Speed (Running)	N.D.*	5.5-6.0 in./sec.

* N.D. - Not Determined

Table 7

Swaging Data of Extruded W-ThO_2 Alloys

Alloy	Total R.A. by Swaging	In Process Anneals	Approximate Material Yield	
		(1) High Rate Extruded Billets		
ThDW-1	90-92%	1900°C, 3 min. at 0.400 in.	75%	Primarily end split losses. Splits were mostly circumferential slightly below rod surface.
ThDW-2	"	"	65%	End and center split losses.
ThDW-4	"	"	70%	Primarily end split losses.
ThDW-WHS	"	"	30%	Most of material loss resulted from a transverse break at 0.630 in. dia.
		(2) Conventionally Extruded Billets		
ThDW-1	96-98%	----------	0%	Transverse crack at 0.745 in. dia. Total loss in 0.625 in. die.
ThDW-2	"	1640°C, 18 hrs. at 0.565 in.	11%	Most of material loss resulted from a transverse break at 1.000 in. dia.
ThDW-3	"	"	19%	Most of material loss resulted from severe center splitting at 0.560 in. dia.
*ThDW-4 (a)	"	"	60%	Primarily end split losses.
*ThDW-4 (b)				
*ThDW-4 (c)				

*(a) Worked at standard temperature (1700°C-1750°C) from 0.400 in. dia.
(b) Worked at 1500 to 1400°C, from 0.400 in. dia.
(c) Worked at 1450 to 1300°C, from 0.400 in. dia. Annealed 1/2 hour at 1775°C at 0.286 in. and 0.243 in. dia.

Table 8

Sheet Rolling Schedule for W-ThO_2 Alloys

Mill - 10 x 12 inches

Preheat - 1600°C, 15 min., each pass

Reductions - (1) .630 - .505 in.
(2) .505 - .318 in.
(3) .318 - .170 in.

A two-high 10 in. dia. x 12 in. mill was used and all passes made in the same direction.

Neither billet was suitable for further rolling after the third pass (also shown in Fig. 1). The ThDW-WHS alloy showed slight edge cracking after the first pass, and at 0.170 in., severe edge cracks were closely spaced throughout the length of the ingot. The ThDW-2 showed no cracking in the first two passes but developed a longitudinal center crack on the third pass which separated the billet for two-thirds of its length. The surfaces of this crack showed a pronounced laminar structure (Fig. 2).

While these initial rolling attempts have not resulted in useful material, they are encouraging enough to suggest that further experimentation with rolling variables will permit production of sheet material.

D. Characterization of the ThDW-WHS Alloy

The properties of the ThDW-WHS alloy were determined in greater detail than those of the experimental alloys, hence its properties will be reported separately throughout the remainder of this report.

1. Microstructure of As Worked Rod

The optical microstructure of the as worked rod is shown in Fig. 3. The grain structure is highly elongated, and the fibers are non-uniform in width. The average grain width, which may include some subgrains as well as high angle grain boundaries, is about 16μ. The substructure was examined by electron transmission microscopy and is characterized by

Fig. 1 Rolling Billet (Center). ThDW-WHS Billet After 3 Passes (Left). ThDW-2 Billet After 3 Passes (Right).

Fig. 2 Laminar Structure of Rolled ThDW-2 Billet After 3 Passes.

Fig. 3 Microstructure of As Swaged ThDW-WHS (Etched in Murakami's Reagent) - 500X

the presence of tangled dislocations within well defined subgrains (Fig. 4). The subgrains of the as worked material are elongated and have an average width of about 3μ.

2. Particle Size Distribution

The fine particle distribution (<0.1μ) was determined from carbon extraction replicas (Fig. 5 and at higher magnification Figs. 6a and 6b). The extraction replica technique employed (with minor modifications) was reported by Koo (13). Mounted specimens are mechanically polished through 4-0 emery paper, then electropolished for about 12 minutes in a 1.5% KOH solution at temperatures below 5°C. After thoroughly rinsing in distilled water, a layer of plastic film is applied and stripped from the sample surface in order to remove surface debris. Carbon is then deposited in a vacuum evaporator ($\sim 10^{-5}$ Torr) from a source at right angles to the surface. The carbon film is scribed into small squares with a sharp tool following which the sample is chemically etched in a 1.5% H_2O_2 solution until segments of the carbon film float free. Finally, the films are thoroughly washed in distilled H_2O, collected on grids and dried in a vacuum desicator.

The extraction replicas were examined in a Hitachi HU-11A electron microscope. The structure was photographed at 20,000X and further enlarged to 40,000X. Both as worked (Fig. 6a) and annealed (Fig. 6b) specimens were replicated.

The thoria particles are present over a wide size range (<50 - >1μ). The larger particles (>10,000Å) are rod-like in shape after fabrication as shown in the optical micrograph of Fig. 3 and the extraction replica of Fig. 5, whereas smaller particles are essentially spherical (Fig. 4). However, no attempt has been made to include larger particles in the size distribution determination, because they are considered to be relatively insignificant in the strengthening process of this alloy.

The distribution was established on the basis of the method developed by Ashby, et.al. (14). The significant relationship is that which equates the number of particles per unit area in a plane of polish ($\bar{N}_S$) to the mean diameter of particles ($\bar{X}$) as follows:

$$\bar{N}_S = N_1/\bar{X} \qquad \text{Eq. 1}$$

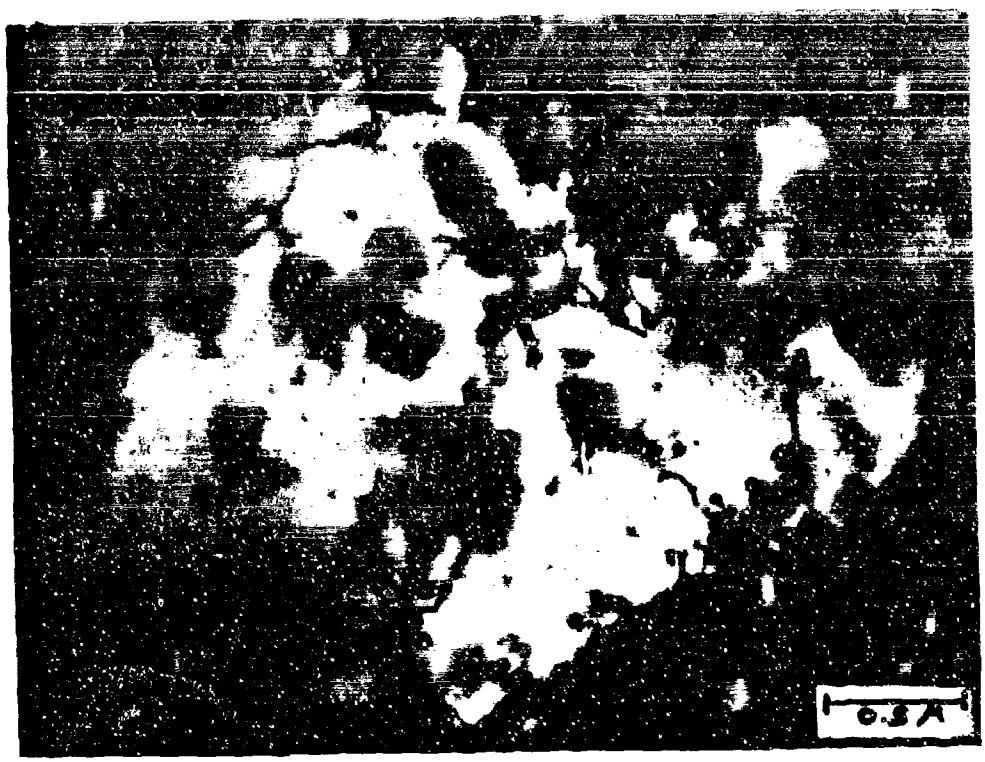

Fig. 4 Electron Transmission Micrograph of As Worked ThDW-WHS - 40,000X

Fig. 5 Extraction Replica of As Worked ThDW-WHS - 6000X

Fig. 6a Carbon Extraction Replica of Thoria Particles in As Worked ThDW-WHS - 40,000X

Fig. 6b Carbon Extraction Replica of Thoria Particles in Annealed (1/2 Hr., 2400°C) ThDW-WHS - 40,000X

where N_1 is the number of intercepts per unit length of line drawn randomly over the area of the micrographs. The parameter sought is the mean interplanar spacing $\bar{D}_s$, defined by Kochs (15) as the average distance from a particle to its next nearest two or three neighbors*. It is given by:

$$\bar{D}_s = 1.18 \left(\frac{1}{\bar{N}_s}\right)^{\frac{1}{2}} \qquad \text{Eq. 2}$$

In order to apply these equations, the mean particle diameter was first determined by counting the number of particles in intervals of 250Å (i.e., 0-250Å, 250-500Å, etc.) within randomly selected areas of six micrographs from each of the respective samples. The total number of particles in each size range was then multiplied by the median of that range, and all size ranges summed and the total averaged. In the case of the as worked material, 612 particles were counted within a total area of $12\mu^2$, and 448 particles within an area of $24\mu^2$ of the annealed specimens.

Next, an array of random lines was scribed on the micrographs and the number of intercepts counted. Five lines of 2μ length each were scribed on eleven plates of the annealed specimen to give a total length of 110μ, and lines totaling 70μ in length were scribed on 11 plates of the as worked material. The results of the evaluation are summarized in Table 9. The distribution curves are plotted in Fig. 7.

* It was originally pointed out by Kochs and further discussed by Kelly, et.al. (5) that the mean interplanar spacing and not the mean center to center spacing between particles is the appropriate measure in calculating the interaction between a gliding dislocation and a random array of obstacles.

Table 9

Particle Size Distribution Parameters of ThDW-WHS

	As Worked	Annealed
Mean particle diameter, $\bar{X}$, angstroms	402 ± 233	386 ± 236
No. of intercepts per micron, N_1	0.65	0.27
No. of particles per micron^2, N_s	16	7
Mean interplanar spacing, $\bar{D}_s$, microns	0.3	0.44

The fact that fewer fine particles are observed in the annealed samples as compared to the as worked samples, suggests that some coarsening has occurred. However, the statistical data do not permit a definite conclusion, since the large sigma values obscure any small shifts which may have occurred in the mean particle diameter.

3. Recovery

Annealing studies were made at temperatures between 1600°C and 3100°C in order to assess the effect of the dispersion on the recovery and/or recrystallization behavior. Optical and electron transmission microscopy as well as room temperature hardness measurements were employed for this evaluation.

a. Effect of Annealing on Room Temperature Hardness

All specimens were initially ground through 3-0 emery paper and then electropolished to remove at least 0.005 in. from the surface. Each specimen was annealed repeatedly in a vacuum of approximately 5×10^{-5} mm Hg. and the Vickers Hardness measured after each annealing period. At least six hardness indentations were made to obtain an average value. Periodically, when the hardness indentations became too closely spaced, the surface was reground and again electropolished. At temperatures below 2800°C, the specimens were annealed by radiation heating while at higher temperatures they were annealed in an electron beam furnace. On

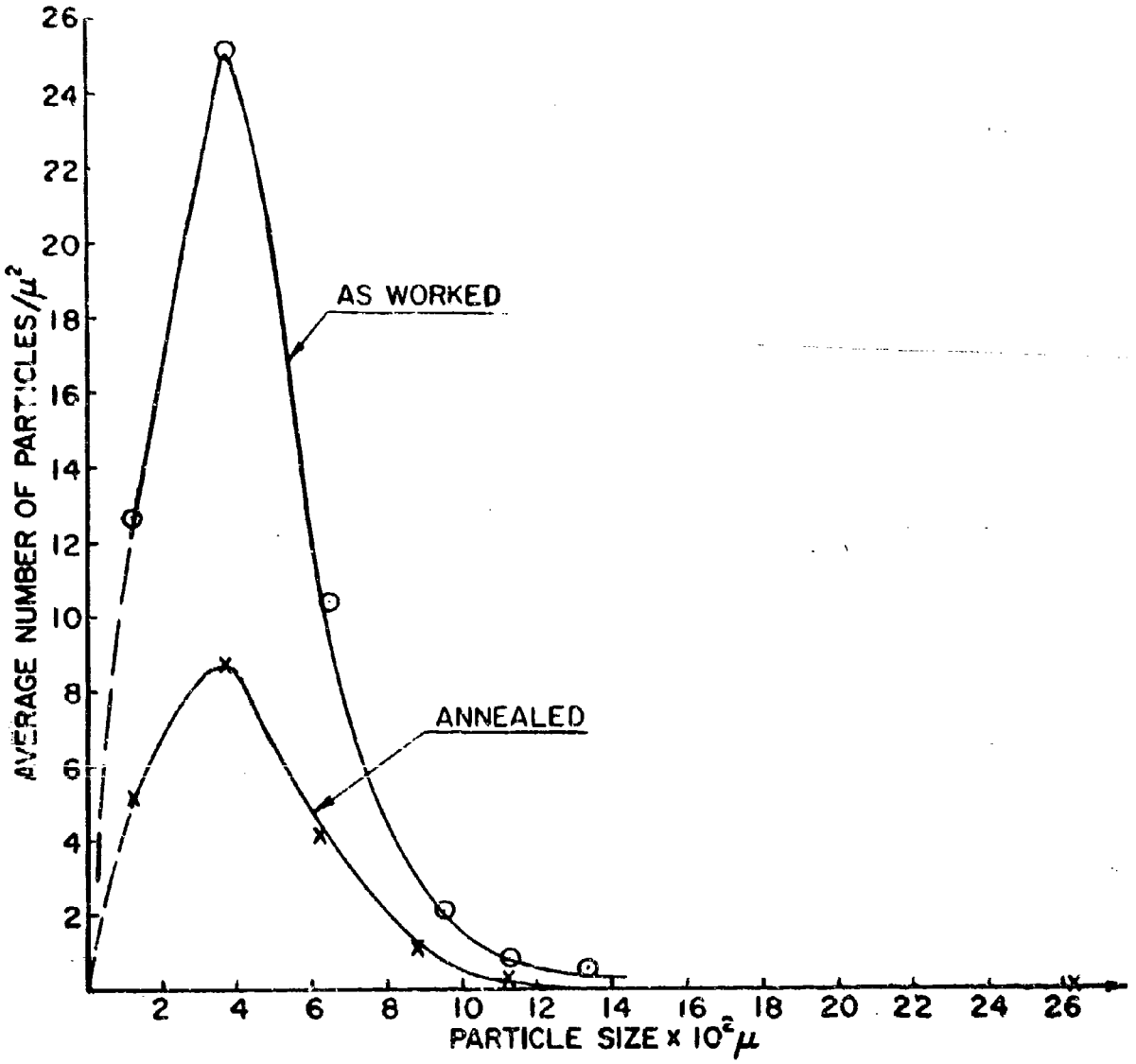

FIG. 7 PARTICLE SIZE DISTRIBUTION OF W-3.8 %TI O_2 (ThDW-WHS)

all runs, the temperature was measured by an optical pyrometer, which was calibrated against melting points of pure metals. The hardness data for a given determination varied by about ± 15 units from their average values.

The results of isothermal anneals at various temperatures on the room temperature hardness are recorded in Table 10. These data are to be compared with an average value of about 485 VHN for the as worked alloy and about 370 VHN for fully recrystallized pure polycrystalline tungsten. At temperatures up to approximately 2700°C for 10 hours, changes in hardness indicate that only recovery is occurring. The extent of recovery at temperatures below 2800°C decreases slightly with decreasing temperature. However, at or above 2800°C, the material recrystallizes after a short time anneal, and the hardness drops to that of recrystallized tungsten.

b. Effect of Annealing on Microstructure

The microstructures of the alloy after annealing for various times at temperature ranging from 1600-2800°C are depicted in Figs. 8a, b, c and d. The results of grain size measurements (width of elongated grains) are listed in Table 11 along with the grain size of the alloy as worked.

Annealing for long periods at 1600°C caused a reduction in the overall average grain size ($\bar{d}_T$) from ~16μ (as worked) to 6μ (after annealing for 65 hours). This is attributed to the formation of new subgrain boundaries by the process of polygonization. However, the average primary grain size, ($\bar{d}_p$) which does not include small recovered (or possibly recrystallized) regions within large grains, is apparently unchanged.

On the other hand, annealing at 2400°C or at higher temperatures causes the grain size to increase. In addition, after annealing at temperatures above 2400°C, small recrystallized areas, such as are typically formed by nucleation and growth processes, become clearly recognizable within the worked grains. These areas are marked "A" in Figs. 8c and 8d and were identified as being recrystallized by the fact that such areas were free of etch pits, whereas the surrounding matrix was heavily etch pitted by a boiling concentrated hydrogen peroxide solution. However, the predominant mode of recrystallization appears to be by the strain induced migration of boundaries already present, rather than by nucleation and growth, since considerable coarsening of the grain structure had occurred before such areas are seen.

Table 10

Effect of Isothermal Annealing at Various Temperatures on Room Temperature Vickers Hardness

Temp., °C	Time	Vickers Hardness Number								
1600	Hrs.	1/2 468	1 454	2 471	6 471	65 466				
2100	Hrs.	1/60 454	1/20 463	1/6 456	1/2 457	1 449	2 450	6 454		
2400	Hrs.	1/60 452	1/6 446	1/2 448	1 454	2 448	7 447			
2660	Hrs.	1/12 463	1/2 456	2 445	10 440					
2800	Hrs.	1/60 472	1/20 467	1/6 445	1/2 452	2 435	4 405	6 398	11 407	24 378
3100	Hrs.	1/60 407	1/20 417	1/6 401	1/2 384	1 371	2 372	6 366		

Table 11

Effect of Annealing on the Grain Size
(Width of Elongated Grains) of W-3.8 v/o ThO_2

Annealing Temperature, °C	Time Hrs.	(a) $\bar{d}_p$, mm	(b) $\bar{d}_t$, mm
As Worked	----	------	.016
1600	65	.012	.006
2400	.5	------	.023
2400	5	.021	.019
2800	24	.194	.168
3100	6	.135	.135

(a) $\bar{d}_p$ is the diameter of the "primary grains" after annealing

(b) $\bar{d}_t$ includes small grains and subgrains formed after annealing in addition to the primary grains.

(a)

(b)

Fig. 8 Microstructures of Annealed ThDW-WHS
(a) 65 Hrs., 1600°C - 500X
(b) 1/2 Hr., 2400°C - 250X

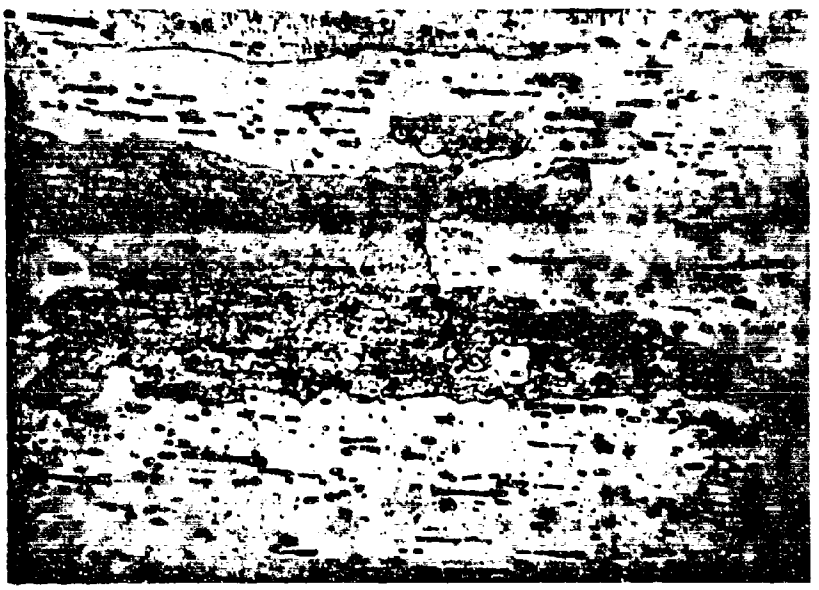

(c)

(d)

Fig. 8 (Cont'd.) Microstructures of Annealed ThDW-WHS - (c) 4 Hrs., 2800°C - 500X; (d) 24 Hrs., 2800°C - 100X.

c. Effect of Annealing on Substructure

The effect of annealing at various temperatures on the substructure was investigated by electron transmission microscopy (ETM). In some instances, the same annealed specimens which were used for hardness measurements and optical microscopy studies were subsequently thinned and examined in the electron microscope. In other instances, additional samples were annealed at various temperatures to obtain information concerning the state of the substructure at intermediate times.

The transmission specimens were prepared by first grinding ribbons ($\sim$30 mils thick) from rods. The ribbons were sectioned to an appropriate size and then electrolytically thinned further in two stages. In the first stage, a dimple was formed on opposing faces of the ribbon by an electrolytic jet of 5% KOH; in the second stage, perforation was completed by immersing the specimen in the same electrolyte and continuing to electropolish. A spotlight was located behind the foil so that the perforation could be detected at the earliest possible moment. Accelerated etching around the larger thoria particles was generally encountered and caused difficulties in obtaining large transmission areas. In all examples of the substructure shown here, the plane of the foils was parallel to the rod axis.

Examples of the substructure formed after annealing for 65 hours at 1600°C and for 30 minutes at temperatures between 2400 and 3000°C are shown in Figs. 9a, b, c and d. The anneal at 1600°C caused a reduction in the average subgrain size (width of elongated grains) of the as worked material from about 2.8μ (Fig. 4) to about 1μ (Fig. 9a). The decrease in subgrain size was caused by the formation of many simple dislocation boundaries such as marked "A" in Fig. 9c. The same area is shown in the enlarged micrograph of Fig. 10 to better resolve the nature of the boundary.

The substructure of specimens annealed for 30 minutes at 2400°C and 2720°C (Figs. 9b and 9c) is very similar to that shown in Fig. 9a except that the subgrain size is about 2μ, and, in general, there are fewer dislocations within the subgrains. Networks of dislocations such as shown by the arrow in Fig. 9c were found throughout the substructure at all annealing temperatures below 2800°C. However, many isolated dislocations pinned by the thoria particles were still retained within the subgrains. Clear evidence of sub-boundary pinning by particles is seen in Fig. 9b (see arrows). In this case, the boundary is moving away from its center of curvature.

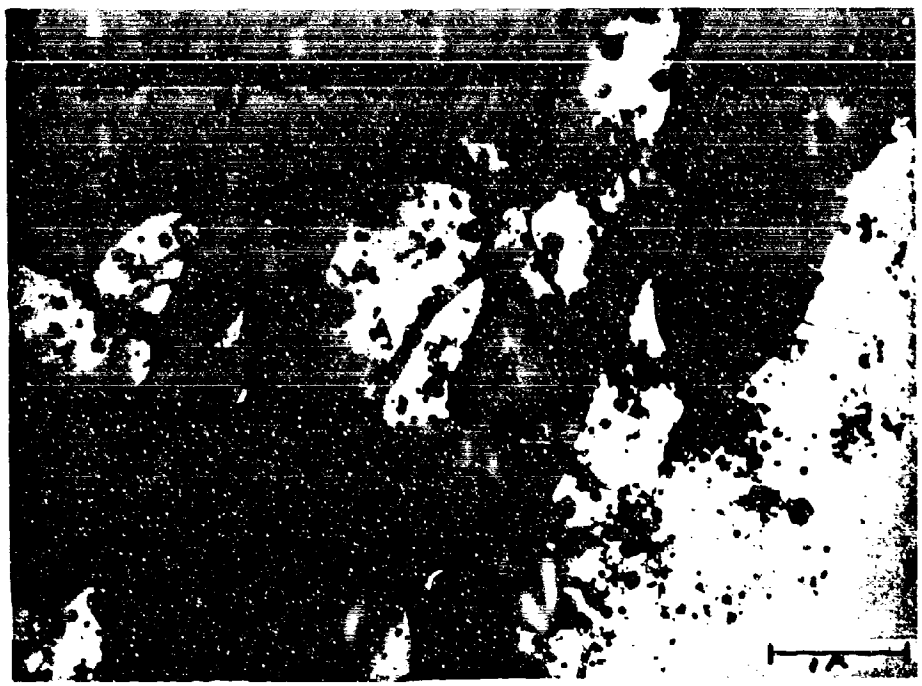

(a)

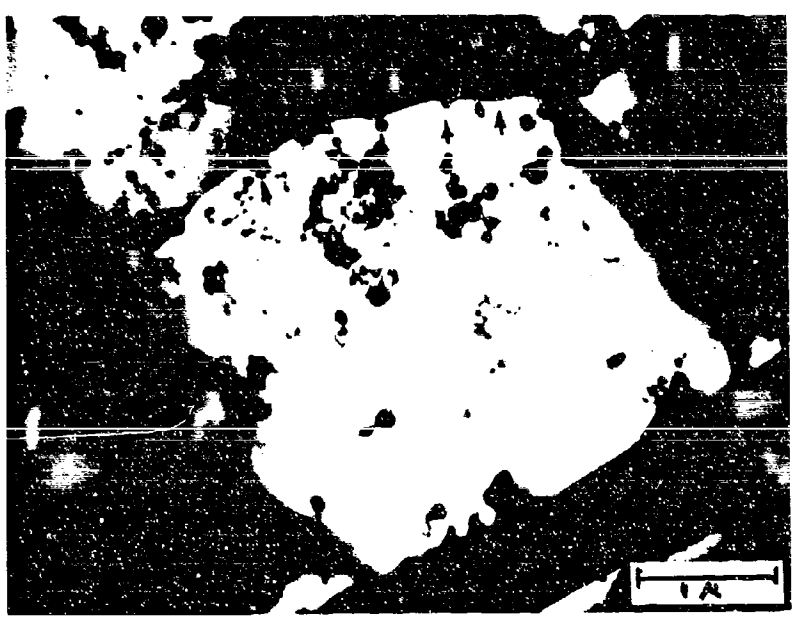

(b)

Fig. 9 Electron Transmission Micrographs of Annealed ThDW-WHS - (a) 65 Hrs., 1600°C; (b) 1/2 Hr., 2400°C - 20,000X

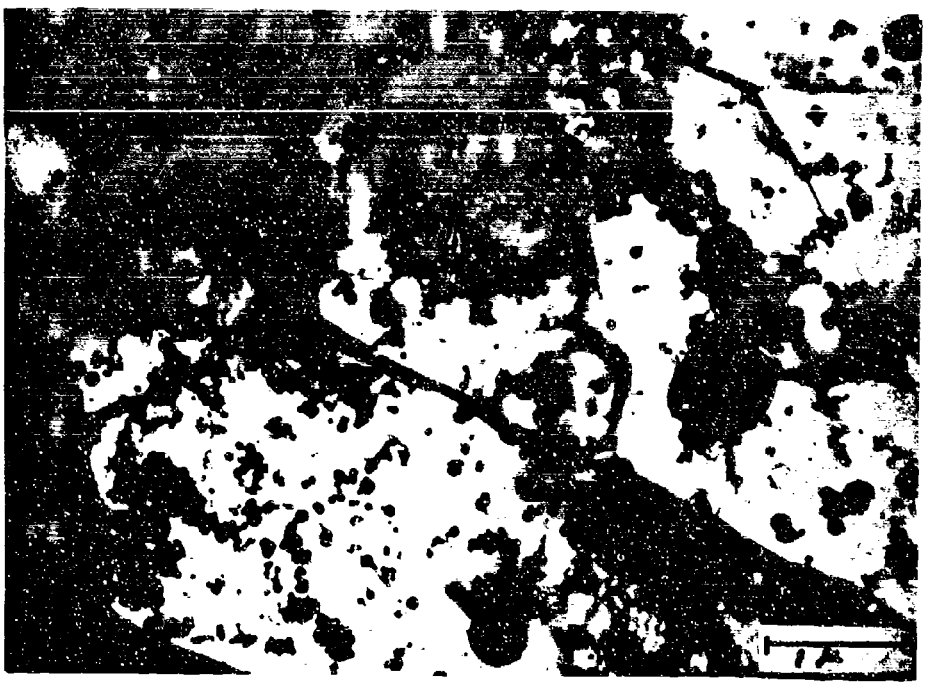

(c)

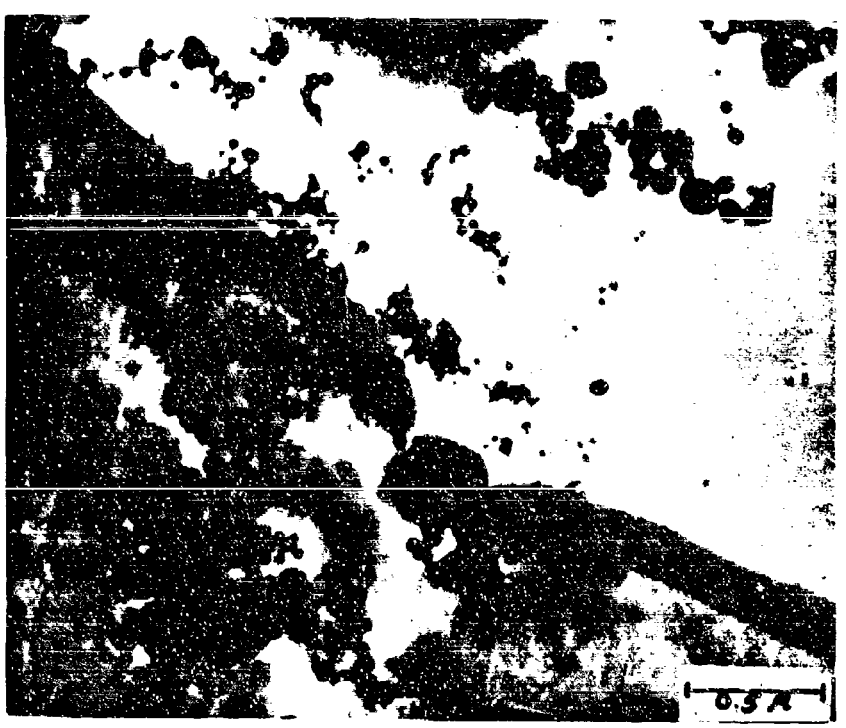

(d)

Fig. 9 (Cont'd.) Electron Transmission Micrographs of Annealed ThDW-WHS - (c) 1/2 Hr., 2720°C; (d) 1/2 Hr., 3000°C - 40,000X

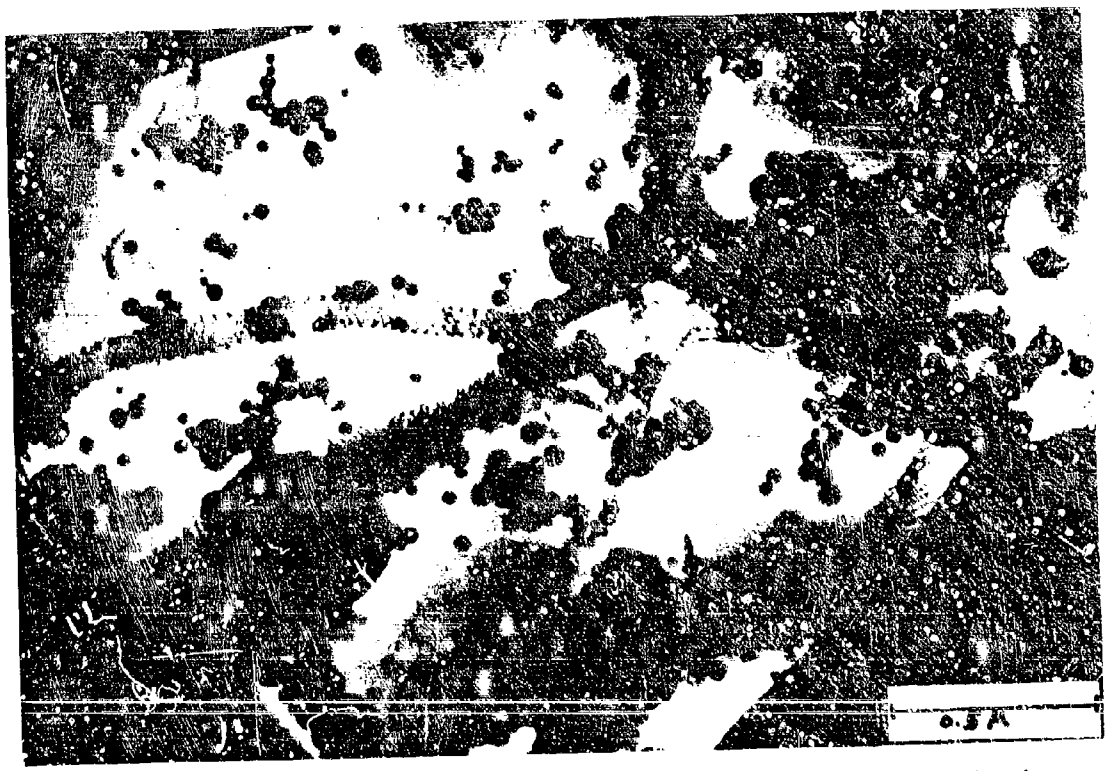

Fig. 10 Enlarged Area of Fig. 9c Showing Low Angle Boundaries Formed by Arrays of Dislocations - 50,000X

After annealing for 1 hour at 2800°C or for 1/2 hour at temperatures above 2800°C, the subgrain size, in general, has increased to a size too large to be measured at the lowest magnification possible in the electron microscope. One subgrain was located within a foil annealed for 1 hour at 2800°C. The analysis of selected area diffraction patterns taken across its boundaries established the fact that the misorientation was small.

Only in one case, in fact, was it possible to identify a high angle grain boundary. This boundary which was located in a specimen annealed for 1/2 hour at 3000°C (Fig. 9d) had a misorientation equal to or greater than 13°. This boundary was also pinned by a thoria particle.

d. Summary and Discussion of Recovery Data

The combined information from hardness tests, optical and electron microscopy presents a coherent picture of the effect of the dispersion on the recovery and recrystallization of the warm worked ThDW-WHS alloy. There is a first stage which only involves recovery, and has been found to prevail at 2720°C for at least 10 hours and at all less rigorous annealing conditions. At temperatures of 2800°C or higher, a second stage, namely, recrystallization occurs.

The hardness data as well as optical and electron microscopy show that, at 2800°C, it takes about 30 minutes before recrystallization commences. During this period, there is a drop in hardness which is accompanied by the development of a well defined substructure of elongated subgrains (average width about 2μ), largely made up or simple dislocation type boundaries. Annealing for slightly longer times results in a rapid disappearance of the subgrains and an increase in the grain size of primary grains, and a further decrease in the hardness to that of recrystallized pure tungsten.

At 3100°C, the entire sequence occurs very rapidly. The recrystallized structure remains highly elongated, and grains which extended the entire length of a 1/2 inch sample were sometimes observed. Thus, the growth in the direction parallel to the rod axis is much greater. The substructure during the recovery stage was also elongated in the working direction. The recrystallization "nuclei", when first detected, are almost spherical but at latter stages of annealing become elongated (Fig. 8d - see arrows). The preferential directional growth can be attributed to the stringers of large particles parallel to the working direction (Fig. 5).

The mechanism of recovery is primarily the formation of low angle sub-boundaries by polygonization. For recrystallization, two competitive processes occur. One is the formation and

growth of "nuclei", and the second is the growth of pre-existing boundaries by strain induced grain boundary migration. Strain induced grain boundary migration is, however, the chief mode of recrystallization, but there is an incubation period required before it takes place.

The conclusions drawn from this annealing study of the ThDW-WHS alloy find support in the literature. Cahn (16) has recently discussed, among others, two models which could apply. One is the "bulge" model, attributed to Bailey and Hirsch (17), which is analogous to the model for strain induced grain boundary migration with the exception that an incubation period is required in some cases. The second model describes recrystallization by the growth of preformed nuclei (18). This model is quite similar to the original model of Cahn (19) except that the incubation period represents the gradual "healing" of the preformed nucleus (which in part can consist of high angle boundaries) by polygonization rather than by the formation and growth of a new subgrain. The recovery and recrystallization phenomena observed can be correlated, to some degree, with either of these two models. However, the authors consider recrystallization by growth of preformed nuclei (second model) to be the rate controlling process because of the extensive polygonization that precedes migration of boundaries.

Whatever the mechanism, however, it is clear that the dispersoid has greatly increased the recrystallization temperature above that of pure tungsten. Recrystallization in similarly worked pure tungsten will occur in less than 30 minutes at temperatures as low as 1400°C. However, in the ThDW-WHS alloy, the matrix does not recrystallize even after 30 minutes at 2600°C. The effects which recovery and recrystallization have on strength properties will become apparent later.

E. Mechanical Properties of ThDW-WHS Alloy

1. Ductile-Brittle Transition Temperature (DBTT)

The DBTT was determined in tension on specimens annealed for 1/2 hour at 2400°C. In addition, one specimen was tested in the as worked condition and a second after an anneal at 1850°C for 1/2 hour. The specimens were electropolished to remove approximately 0.005 in. from the gage diameter before testing at a strain rate of 0.005 min^{-1}. The test temperatures were measured with two iron-constantan thermocouples. Because of the gripping arrangement, only one thermocouple could be attached to the gage section. The other was attached to the tensile head. The average temperature difference between the two locations ($\sim$0.5 in. apart) was $\pm$ 5°C and considered to be inconsequential.

The stress-strain behavior is depicted schematically in Fig. 11. In Region I (<140°C), the material fractured in a completely brittle manner. In Region II (140-200°C), yield points were observed and the mode of fracture changed from brittle to ductile. Examination of the surfaces of the gage sections of the fractured tensiles did not reveal Lüders band markings, although most specimens fractured within the Lüders strain region. The specimens tested at 176°C and 193°C had a yield point followed by a Lüders strain, work hardening, and necking prior to fracture (Fig. 11). In Region III (>200°C), the alloy exhibited the typical flow curve of a ductile material.

The ductility (% R.A.) is plotted in Fig. 12. Included in this figure are data on pure tungsten. The DBTT of the alloy is about 190°C with a ductility tail extending to below 150°C. This compares with a DBTT of about 300°C for the pure tungsten control.

The strength properties are recorded in Table 12 and selected parameters from this table are plotted in Fig. 13. In cases of ductile fracture, the true fracture stress (corrected for necking) is reported (20). In those cases where fracture occurred prior to necking, the maximum engineering stress is reported. The temperature dependence of the yield stress and the fracture stress is typical of bcc metals in the DBT region. In the fully ductile condition, the true fracture stress of the alloy and of pure tungsten is approximately the same.

A DBTT of about 200°C was previously reported at this laboratory for high purity tungsten and for a W-3.8 v/o ThO_2 alloy tested in the stress-relieved (1560°C, 1/2 hour) condition (2, 21). When compared with the DBTT (~400°C) of commercially pure tungsten annealed at high temperatures, the DBTT of the ThDW-WHS alloy is significantly lower. The latter alloy also has higher strength at low temperatures than pure tungsten or the previously tested W-3.8 v/o ThO_2 alloy.

The effect of prior deformation in the ductile temperature region on the DBTT is confirmed in this alloy, in that an as swaged specimen exhibits 6% R.A. at room temperature. Annealing as low as 1800°C destroys this ductility. Nevertheless, after annealing at 2400°C for 1/2 hour, the alloy is more ductile than pure tungsten. The difference in the DBTT's (exceeding 100°C) may be attributable to the retention of a substructure in the alloy. More investigation is required, however, to elucidate this supposition.

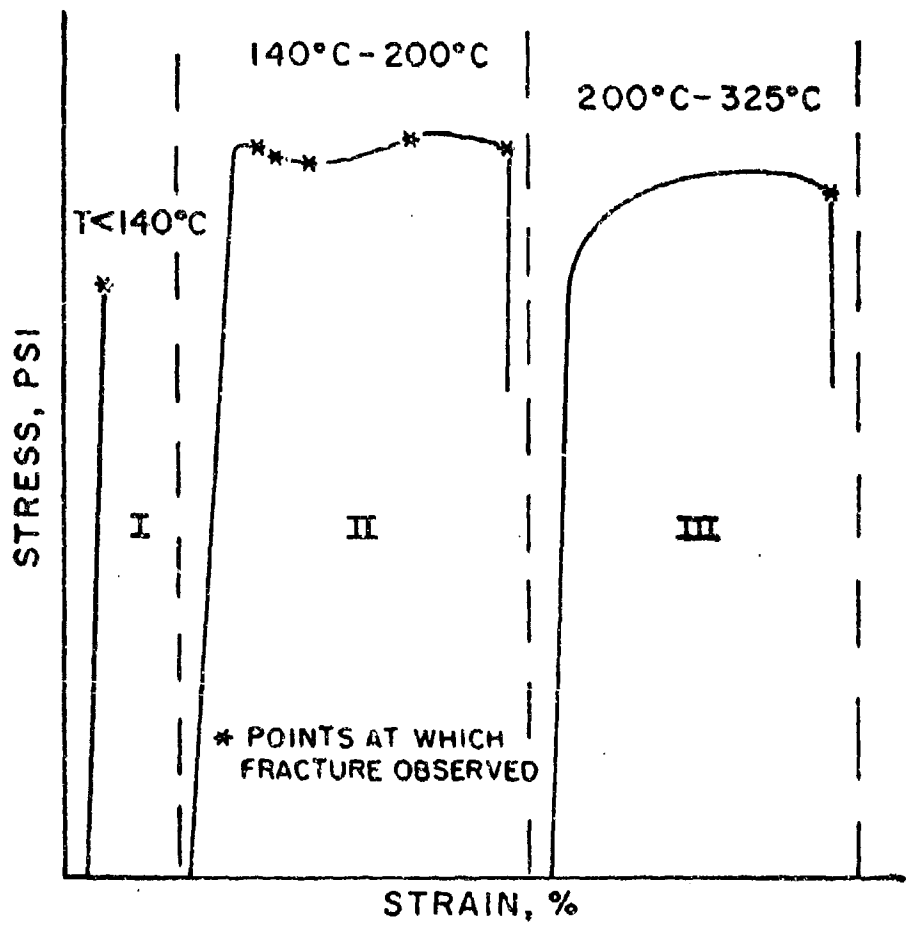

FIG. II SCHEMATIC REPRESENTATION OF ENGINEERING STRESS STRAIN CURVES OF ThDW—WHS AT VARIOUS TEMPERATURE REGIONS.

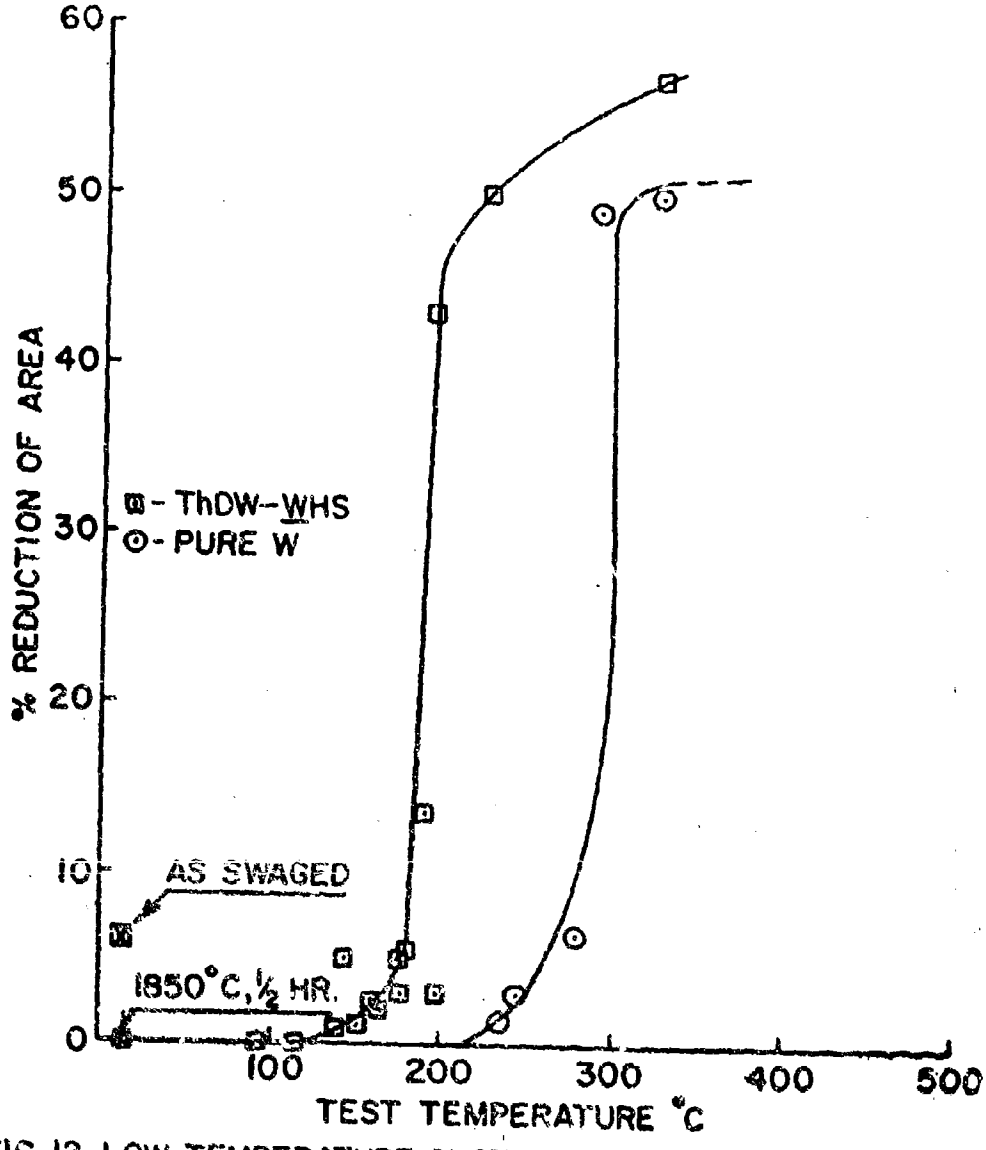

FIG. 12 LOW TEMPERATURE DUCTIL.. / OF ThDW-WHS AND PURE TUNGSTEN

Table 12

Low Temperature Tensile Properties of Pure Tungsten and ThDW-WHS, Annealed at 2400°C, 1/2 Hr. Except as Shown, Tested at 0.005 min^{-1}

Temp. °C	Prop. Limit, KSI	Yield Stress, KSI	Ult. Stress, KSI	Fract. Stress, KSI	% Elong.	% R.A.
		ThDW-WHS				
15*	169	(c) 191	191	203	0.4	6
15**	---	-------	---	145	0	0
93	---	-------	---	99	0	0
115	---	-------	---	96	0	0
141	123	(a) 134	---	134	1.1	1
143	132	(a) 141	---	141	0.4	5
152	119	(b) 127	---	130	2.0	1.2
161	122	(a) 133	---	134	1.0	2.5
163	139	(a) 144	---	147	0.6	2.2
175	122	(b) 131	---	139	2.8	5.0
176	109	(b) 123	127	131	5.2	3.0
181	119	(b) 128	---	136	1.9	5.5
190	106	(b) 118	---	132	8.0	13.5
193	95	(b) 109	111	126	11.5	43.0
198	122	(a) 133	---	135	1.1	3.0
225	86	(c) 91	95	116	15.3	56.0
326	49	(c) 67	85	104	15.2	57.0
		Pure Tungsten				
235	34	(c) 42	---	52	1.1	1.5
244	32	(c) 38	---	61	2.3	3.0
278	20	(c) 33	---	65	5.3	6.5
289	14	(a) 15	57	110	32.0	49.0
325	10	(c) 14	55	107	32.0	50.0

* Annealed 1/2 Hour at 1850°C.
** As Swaged
(a) Upper Yield Stress
(b) Lower Yield Stress
(c) 0.2% Yield Stress

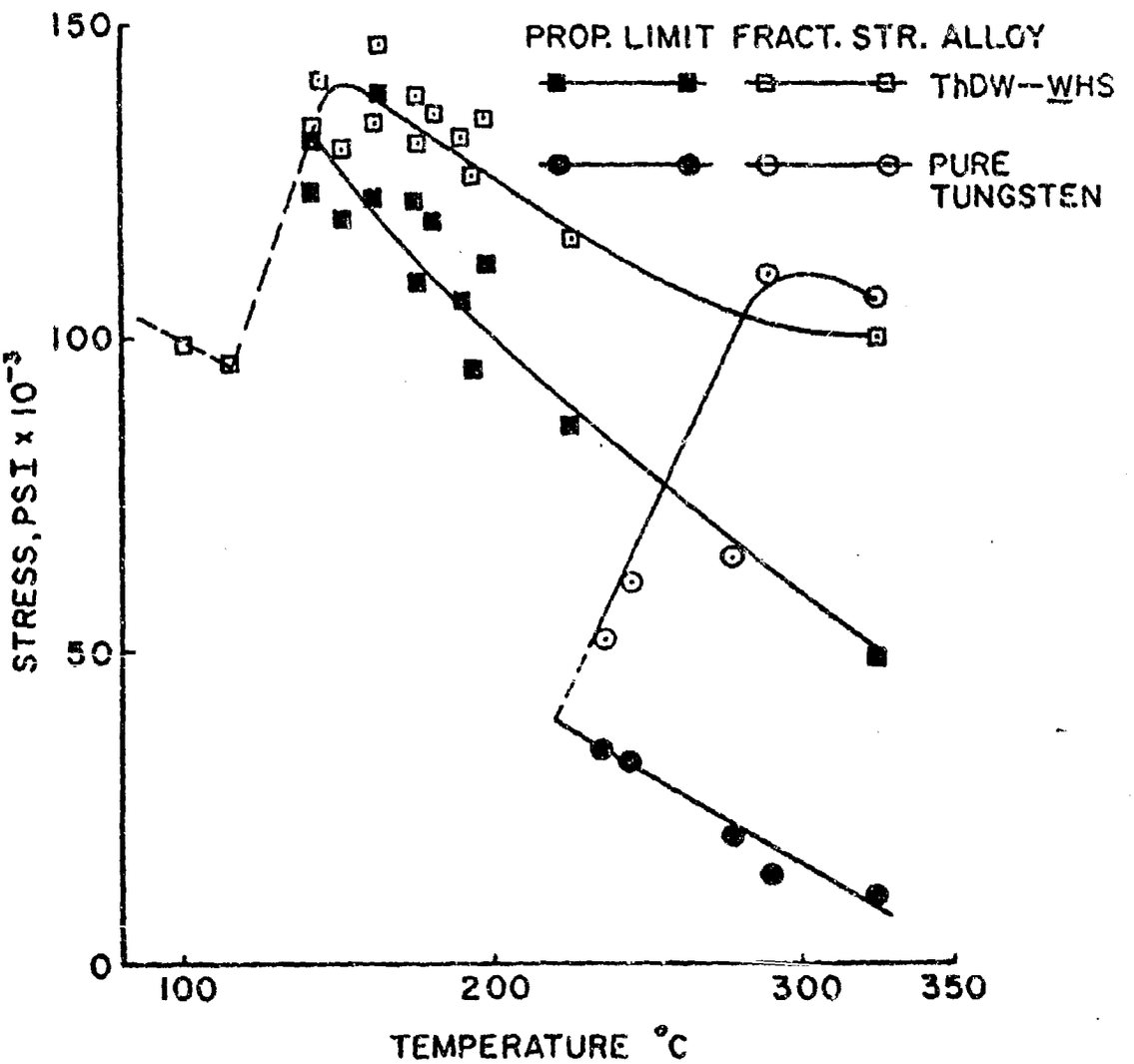

FIG. 13 LOW TEMPERATURE STRENGTH PROPERTIES OF PURE TUNGSTEN AND ThDW-WHS

2. Elevated Temperature Tensile Properties

The tensile properties of the ThDW-WHS alloy, processed both by self-resistance sintering and swaging, and by hot pressing, extruding and swaging (the latter is designated Alloy No. 2 in accordance with previous work (1)) were determined over the temperature ranges of 300-3000°C and 1500-2400°C, respectively. As a control, pure tungsten was tested over the range 300-2400°C.

The materials were ground into buttonhead tensile specimens (0.092 in. gage dia. x 1.00 in. gage length) for tests up to and including 2400°C and into longer tensile specimens designed for gripping outside the hot zone (Fig. 14) for tests above 2400°C.

Tests were performed on an Instron tensile machine, and most tests were run at a cross head speed of 0.05 min^{-1} on specimens annealed for 1/2 hour at 2400°C. The tests above 2400°C were made on as worked material at a strain rate of 0.1 min^{-1}, except as noted. The effect of strain rate was determined to some extent by comparing the slower strain rate data with test results obtained at a strain rate of 2 min^{-1}. All tests were carried out in vacuum of $\sim 5 \times 10^{-5}$mm Hg. Specimens were heated by radiation. A cursory evaluation of the effect of annealing was made by comparing data from an as worked material, with data from material annealed at 2400°C for 1/2 hour and, in one instance, annealed at 2825°C for 1/2 hour.

a. Test Results

All tensile test results are summarized in Table 13. Pertinent parameters are plotted in Figs. 15 and 16, and true stress-true strain curves for ThDW-WHS and pure tungsten at various temperatures are presented in Fig. 17.

Fig. 15 clearly shows the outstanding strength properties of the alloy ThDW-WHS. At the lowest test temperatures, the alloy is stronger than pure tungsten by a factor of 1-1/2 to 2. The ultimate strength ratio increases with increasing temperature, and it reaches the value of about 5 at 2400°C. The yield strength ratios are even more striking, varying from about 4 at the lowest test temperatures to about 6 at 2400°C. These ratios are plotted in Fig. 18 for the complete temperature range. Included in Fig. 18 are the same ratios for Alloy No. 2. The property improvements in Alloy No. 2 are not as favorable as in the alloy ThDW-WHS.

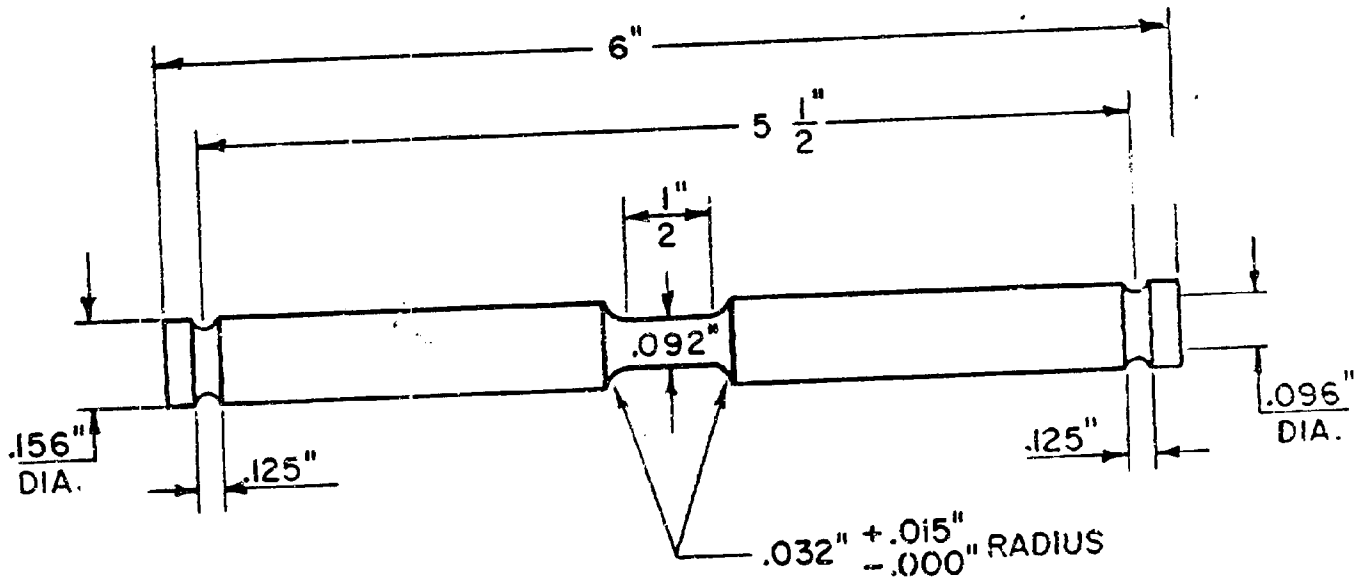

FIG. 14 SPECIMEN DESIGNED FOR CREEP TESTING AND FOR TENSILE TESTING ABOVE 2400 °.

Table 13

Elevated Temperature Tensile Properties of
ThDW-WHS, Alloy No. 2 and Pure Tungsten

Test Temp.,°C	Prop. Limit,KSI	0.2% Y.S.,KSI	Ult. Str.,KSI	Uniform Strain,%	Tot. Elong.%	% R.A.	Work Hardening Coefficient, n
			ThDW-WHS				
		Strain Rate: 0.05 min^{-1}; Annealed 2400°C, 1/2 Hr.					
432	58	65	79	13	20	64	.103
615	52	60	67	8	18	67	.071
700	51	60	65	6	15	71	.067
1000	34	46	53	5	12	79	.113
1200	42	46	48	3	13	77	.031
1500	33	36	37	1	12	76	.042
1850	24	26	29	2	11	46	.078
2200	12	15	18	3	15	24	.111
2400	11	14	15	3	17	43	.111
2400	13	15	16	2	20	30	.091
2800	6	7	8	5	29	51	.067
2400(a)	10	11	13	4	21	27	.088
		Strain Rate: 0.1 min^{-1}; As Swaged					
2620	10	11	12	3	28	26	.046
2720	8	9	10	6	21	28	.088
2800	8	8	9	1	17	50	.060
3000	7	7	8	2	10	27	.077
		Strain Rate: 2 min^{-1}; Annealed 2400°C, 1/2 Hr.					
1400	42	43	44	3	19	79	----
1650	32	34	34	3	18	75	----
1850	33	34	34	--	15	64	----
2200	27	27	27	--	9	65	----
2400	24	24	24	--	21	56	----

(a) Annealed 2825°C, 1/2 Hr.

Table 13 (cont'd.)

Elevated Temperature Tensile Properties of ThDW-WHS, Alloy No. 2 and Pure Tungsten

Test Temp.,°C	Prop. Limit,KSI	0.2% Y.S.,KSI	Ult. Str.,KSI	Unf. Strain,%	Tot. Elong.%	% R.A.	Work Hardening Coefficient, n
			Strain Rate: 2 min^{-1}; As Swaged				
1400	45	46	46	0	13	74	----
1650	39	42	42	1	16	79	----
1850	33	34	34	0	15	64	----
2200	28	28	28	0	13	54	----
2400	23	24	24	0	17	55	----
			Alloy No. 2				
			Strain Rate: 0.05 min^{-1}; Annealed 2400°C, 1/2 Hr.				
1500	20	23	31	11	41	74	.104
1650	18	20	23	5	34	70	.07
1850	12	13	15	9	42	79	.056
2200	7	8	10	9	36	72	.075
2400	4	6	8	5	25	59	.096
			Strain Rate: 2 min^{-1}; Annealed 2400°C, 1/2 Hr.				
1500	21	25	34	15	22	63	----
1650	19	22	33	11	42	68	----
2200	16	16	16	4	32	62	----
2400	11	12	12	4	40	78	----
			Strain Rate: 2 min^{-1}; As Swaged				
1850	39	40	40	--	11	48	----
2200	13	13	13	6	46	60	----
2200	12	13	14	9	43	70	----

Table 13 (cont'd.)

Elevated Temperature Tensile Properties of
ThDX-WH3, Alloy No. 2 and Pure Tungsten

PURE TUNGSTEN

Strain Rate: 0.05 min^{-1}; Annealed 2400°C, 1/2 Hr.

Test Temp.,°C	Prop. Limit,KSI	0.2% Y.S.,KSI	Ult. Str.,KSI	Unf. Strain,%	Tot. Elong.%	% R.A.	Work Hardening Coefficient, n
380	13	15	56	29	33	62	.364
430	8	11	54	41	59	72	.438
544	13	17	46	44	53	72	.329
708	13	17	38	40	52	91	.289
840	11	14	34	45	53	92	.299
1500	3	5	19	25	51	82	.296
1650	5	5	13	20	47	62	.235
1850	5	6	10	18	41	48	.210
2200	1.7	2.4	4	7.5	17	59	.156
2400	1.9	2.3	3.5	4	13	15	.150

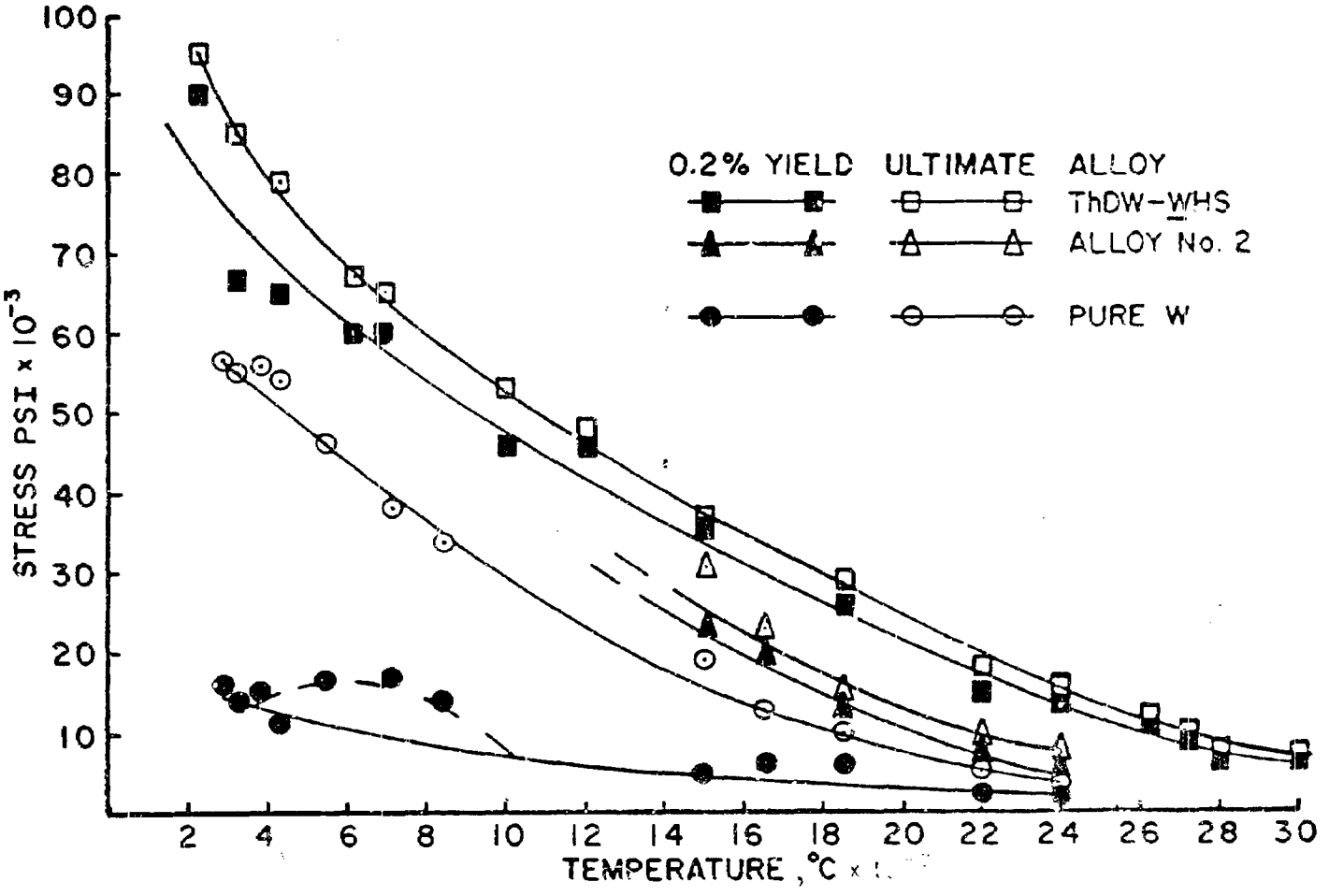

FIG. 15 ENGINEERING STRENGTH PROPERTIES OF PURE TUNGSTEN AND W-3.8V/0ThO_2 ALLOYS

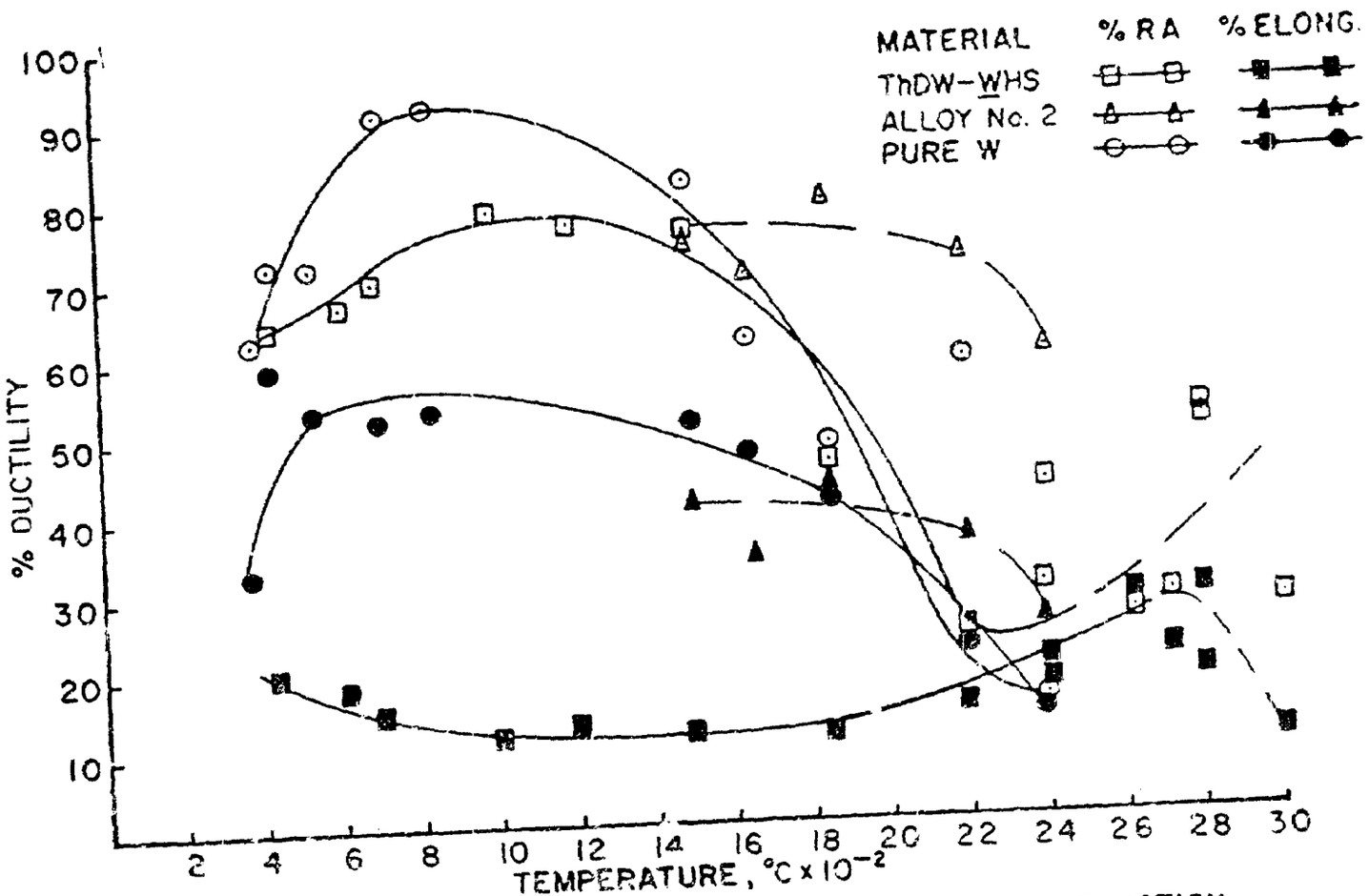

FIG. 16 DUCTILITY OF PURE TUNGSTEN AND W-ThO_2 ALLOYS AS A FUNCTION OF TEMPERATURE

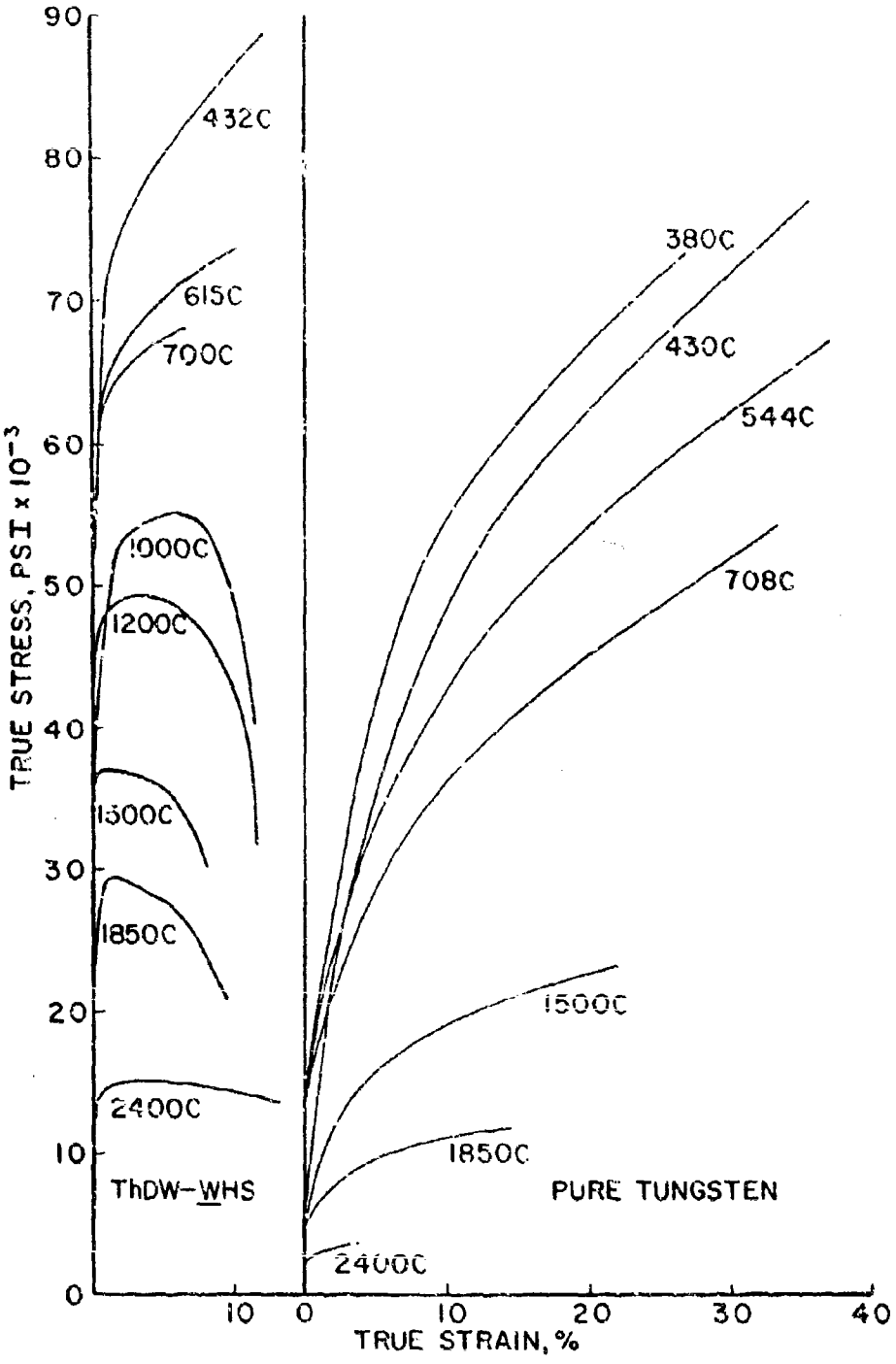

FIG. 17 TRUE STRESS-TRUE STRAIN TENSILE CURVES OF ThDW-WHS AND PURE TUNGSTEN AS A FUNCTION OF TEMPERATURE (CURVES PLOTTED BY COMPUTER)

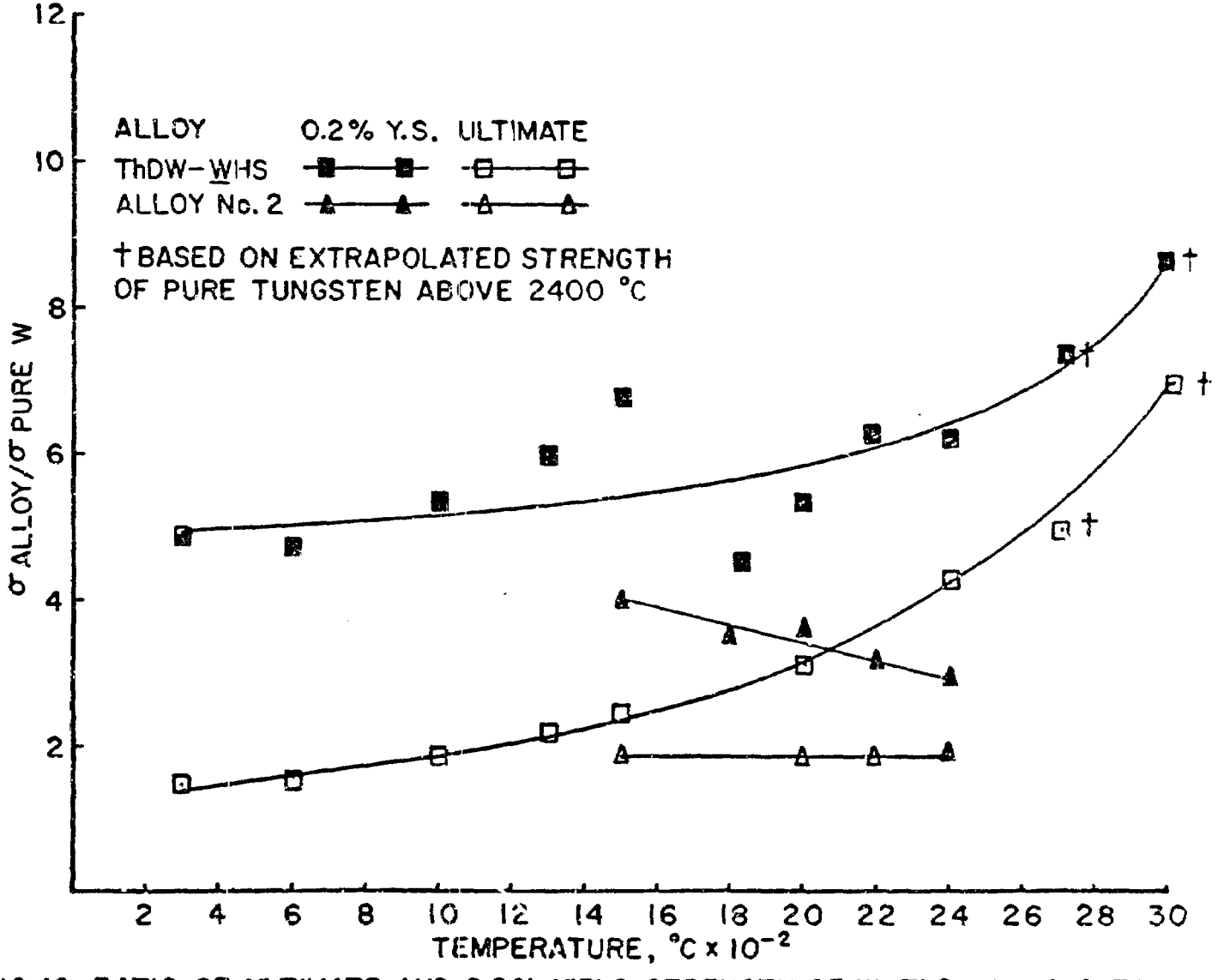

FIG. 18 RATIO OF ULTIMATE AND 0.2% YIELD STRENGTH OF W–ThO_2 ALLOYS TO THOSE OF PURE TUNGSTEN AS A FUNCTION OF TEMPERATURE

The ductility (% Elong. and % R.A.) is plotted in Fig. 16. ThDW-WHS has lower ductility than pure tungsten up to about 2000°C. Above that temperature, the ductility of ThDW-WHS is equal to or better than that of pure tungsten. Alloy No. 2 is more ductile than ThDW-WHS in the temperature range investigated.

The deformation behavior of ThDW-WHS is significantly different from that of pure tungsten. While the stress-strain behavior of pure tungsten was normal at all temperatures, both ThDW-WHS and Alloy No. 2 exhibited, at or above 1000°C, a behavior which could be attributed to work softening (22) or early plastic instability. To distinguish between these two possible causes, tests at 2200°C were repeatedly interrupted and the diameter of the gage section measured. It was thus determined that no necking was occurring through an extensive plastic region, although the slope of the stress-strain curves is negative after a few per cent of plastic strain. The observed behavior must therefore be attributed to work softening.

The effect of strain rate is as expected in that the strength increases with increased strain rate. The increase of the strain rate from 0.05 min^{-1} to 2 min^{-1} results in a strength increment of about 20%.

For the test conditions employed, annealing at 2400°C for 1/2 hour has an effect on strength of ~20% at or below 1650°C. The effect becomes negligible above that temperature. Annealing for 1/2 hour at 2825°C (one test) further slightly reduces the strength at 2400°C.

The work hardening coefficients were calculated from the relationship $\sigma = K\varepsilon^n$ for ThDW-WHS and pure tungsten over the entire temperature range for the specimens annealed at 2400°C for 1/2 hour and strained at 0.05 min^{-1}. The results for the alloy show (Table 13 and Fig. 19) that the work hardening coefficient varies little over the whole temperature range with a small minimum indicated at 1200°C and a plateau in the temperature range 2000°C to 3000°C. The average value for n of 0.08 confirms the high work hardening rate of the alloy. On the other hand, the work hardening coefficients for pure tungsten are higher throughout the entire temperature range and show a clear trend to lower values at higher temperature. A plateau is apparent in the temperature range 800-1400°C.

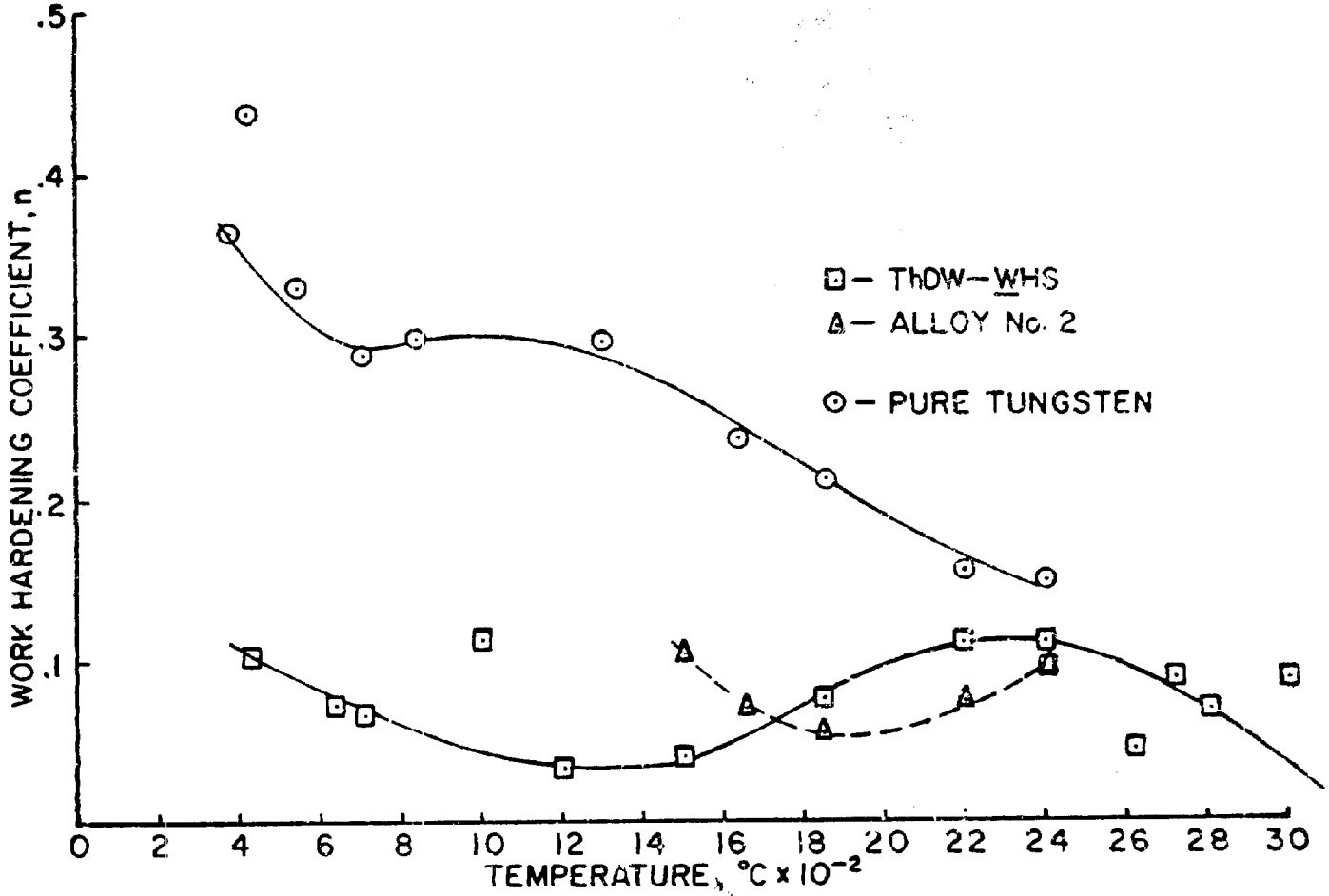

FIG.19 EFFECT OF TEMPERATURE ON WORK HARDENING COEFFICIENTS OF PURE TUNGSTEN AND TUNGSTEN THORIA ALLOYS

b. Discussion of Tensile Results

There can be no question that significant dispersion strengthening has been achieved. It was, therefore, of interest to compare the yield strength ($1/2\,\sigma_0 = \tau_0$, where τ_0 is the initial flow stress) of the alloy and its temperature dependence with theoretical predictions. For this purpose, calculations were made on the basis of the simple Orowan model as extended by Kelly and Nicholson (5) (Eq. 3 below):

$$\tau = \tau_m^\circ + \frac{Gb}{4\pi} \phi \ln \left[\frac{d-2r}{2b}\right] \frac{1}{(d-2r)/2} \qquad \text{Eq. 3}$$

where $\phi = 1/2\ (1 + \frac{1}{1-\nu})$

The following values have been used:

G (shear modulus) = 3/8 E(Young's modulus)

b (Burgers vector) = 2.74×10^{-8}cm

d (interpl. spacing) = 4.4×10^{-5}cm

ν (Poissons ratio) = 0.33

2r (mean particle dia.) = 4.0×10^{-6}cm

τ_m° (matrix shear strength of pure tungsten)

The temperature dependence in this equation is essentially that of the shear modulus, as calculated from dynamic modulus data (23). Fig. 20 compares the experimental results with theoretical predictions.

The comparison shows reasonable agreement in the values of the critical resolved shear stress up to about 1200°K but appreciable deviation at higher temperatures. Obviously, the temperature dependence of the experimentally determined flow stress is greater than that of the shear modulus which is the only temperature dependent parameter in the theoretical model. Since prismatic dislocation loops and jogs were seen in fractured tensile specimens (Fig. 21), the deviation may be explained on the basis

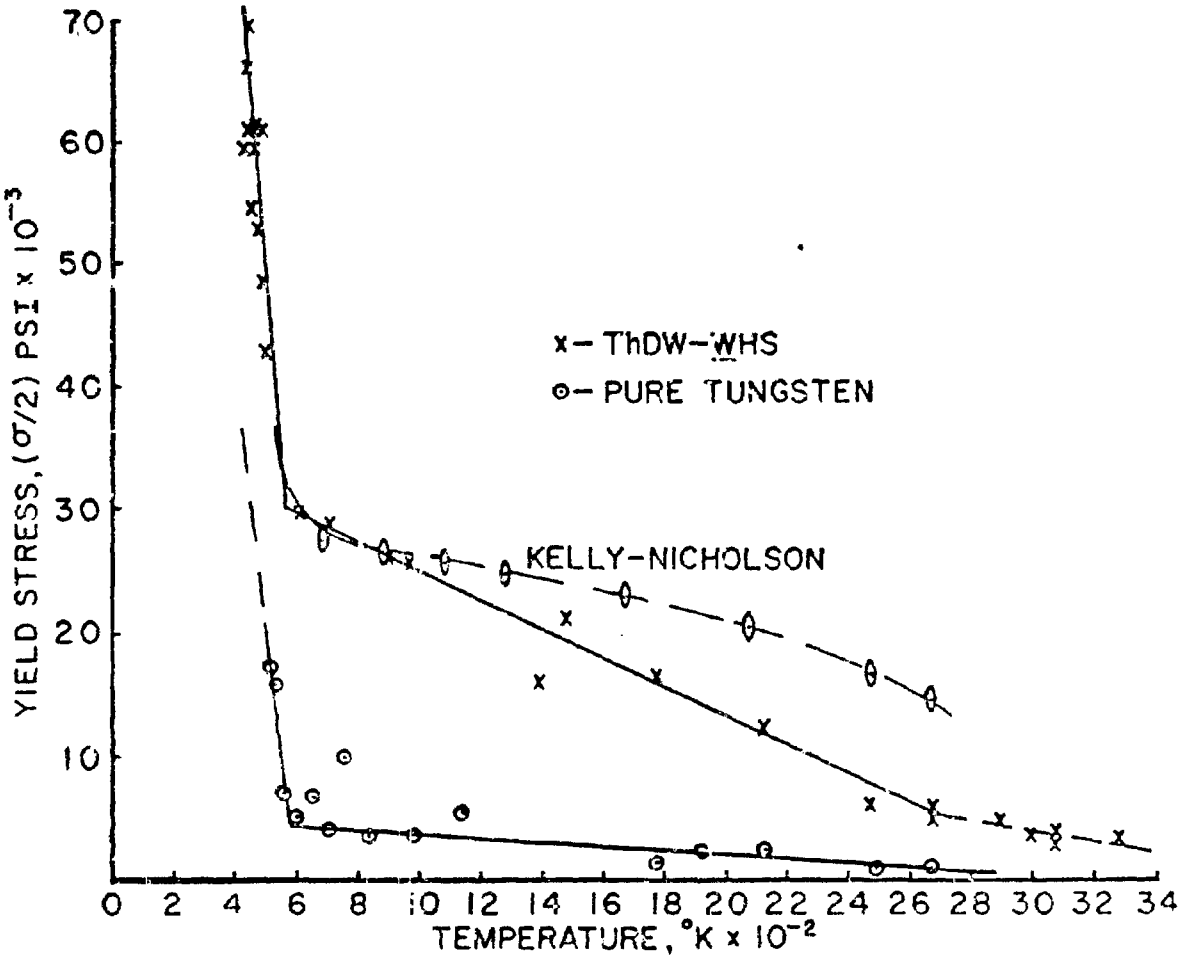

FIG. 20 TEMPERATURE DEPENDENCE OF THE YIELD STRESS OF PURE TUNGSTEN AND ThDW–WHS

Fig. 21 Electron Transmission Micrograph of ThDW-WHS, Tensile Tested at 2800°C, at 0.05 min^{-1} - 7500X

of thermally activated cross slip, as postulated by Hirsch (24). The latter would result in an increase in the effective interplanar spacing, as suggested by Ashby (25).

A calculation of the activation energy which can be derived from the effect of strain rate on the temperature dependence of the flow stress should further elucidate the rate controlling mechanism. In accordance to Seeger (26), the flow stress is related to the energy U_o needed to overcome an internal stress or to cut through an obstacle by the following equation:

$$\dot{\varepsilon} = NAb\gamma_o \exp - \frac{(U_o - V_f\tau^*)}{KT} \qquad \text{Eq. 4}$$

where τ^*, the effective stress acting on the dislocation is equal to τ (the applied stress) minus τ_G (the internal stress due to other obstacles). The other parameters have their usual meaning. Eq. 4 can be rearranged to read as follows:

$$\tau = \tau_G + U_o/V_f - KT \ln (NAb\gamma_o/\dot{\varepsilon})/V_f \qquad \text{Eq. 5}$$

A plot, therefore, of τ versus temperature should give a straight line with an intercept at 0°K equal to $\tau_G + U_o/V_f$, or as expressed in the following equation:

$$\tau = \tau_G + \tau^* \quad \text{with} \quad \tau^* = U_o/V_f \qquad \text{Eq. 6}$$

In order to calculate U_o, the activation volume V_f must be determined and an estimate of τ^* must be made. The slope, M, of the straight line is:

$$M = -K \ln (C/\dot{\varepsilon})/V_f \qquad \text{Eq. 7}$$

where $C = NAb\gamma_o$ and is assumed to be constant. Hence, V_f can be calculated by applying Eq. 7 to two different strain rates which yields:

$$V_f = -K \ln (\dot{\varepsilon}_2/\dot{\varepsilon}_1)/\Delta M \qquad \text{Eq. 8}$$

A plot of τ versus temperature for ThDW-WHS at the two strain rates, 0.05 min^{-1} and 2 min^{-1}, is shown in Fig. 22. The two strain rate curves have a common intercept at about 37,000 PSI (25.5 x 10^8dynes/cm^2) at 0°K. By substituting the experimental values, the activation volume is calculated to be about 3 x $10^{-21}cm^3$.

The agreement, at low temperatures, between experimental data and the extended Orowan model (Fig. 20) implies that τ_G in the alloy is no greater than τ_G of pure tungsten, i.e., neither the incoherent particles nor the retained defect structure increases the effective internal stress acting in the slip plane. By extrapolating τ of pure tungsten to 0°K (Fig. 22), the maximum value of τ_G is found to be about 6.2 x 10^8dynes/cm^{-2}, and hence τ^* of the alloy is about 19 x 10^8dynes/cm^{-2}. Substituting for V_f and τ^* in Eq. 6. the activation energy U_o is calculated to be equal to about 3.8 eV.

On the basis of Schoeck, et.al. (27) an activation energy of 3.8 eV is higher than required for the thermal activation of cross slip in bcc metals. However, jogs in screw dislocations, formed here by cross slip, will move non-conservatively, and hence, the activation energy of 3.8 eV could represent the energy required for the non-conservative motion of jogs. Indeed, energies of that magnitude for the formation of a vacancy have been predicted by Schoeck (28) for the non-conservative motion of jogs. The value of 3.8 eV is in good agreement with that expected for the formation of vacancies in tungsten (approximately 1/2 the activation energy for self-diffusion (29)).

A theory of work hardening by Fisher, et.al. (6) predicts that work hardening in dispersed second phase alloys will result in a greater strength increment than in the pure matrix due to an Orowan type particle-dislocation interaction. The maximum strength increment predicted is 0.1 of the shear modulus, and this maximum would be reached after a finite strain corresponding to a critical stress acting on the particles and depending on the particle size. For particles smaller than 1000Å, this critical stress is directly proportional to the shear modulus and inversely proportional to the particle radius.

As shown in Fig. 23, the strength increment in both alloys (ThDW-WHS and Alloy No. 2) reaches a maximum after less than 3% strain. However, while the theory predicts this strength to remain constant, i.e., no further work hardening to occur, the strength decreases by work softening as discussed earlier.

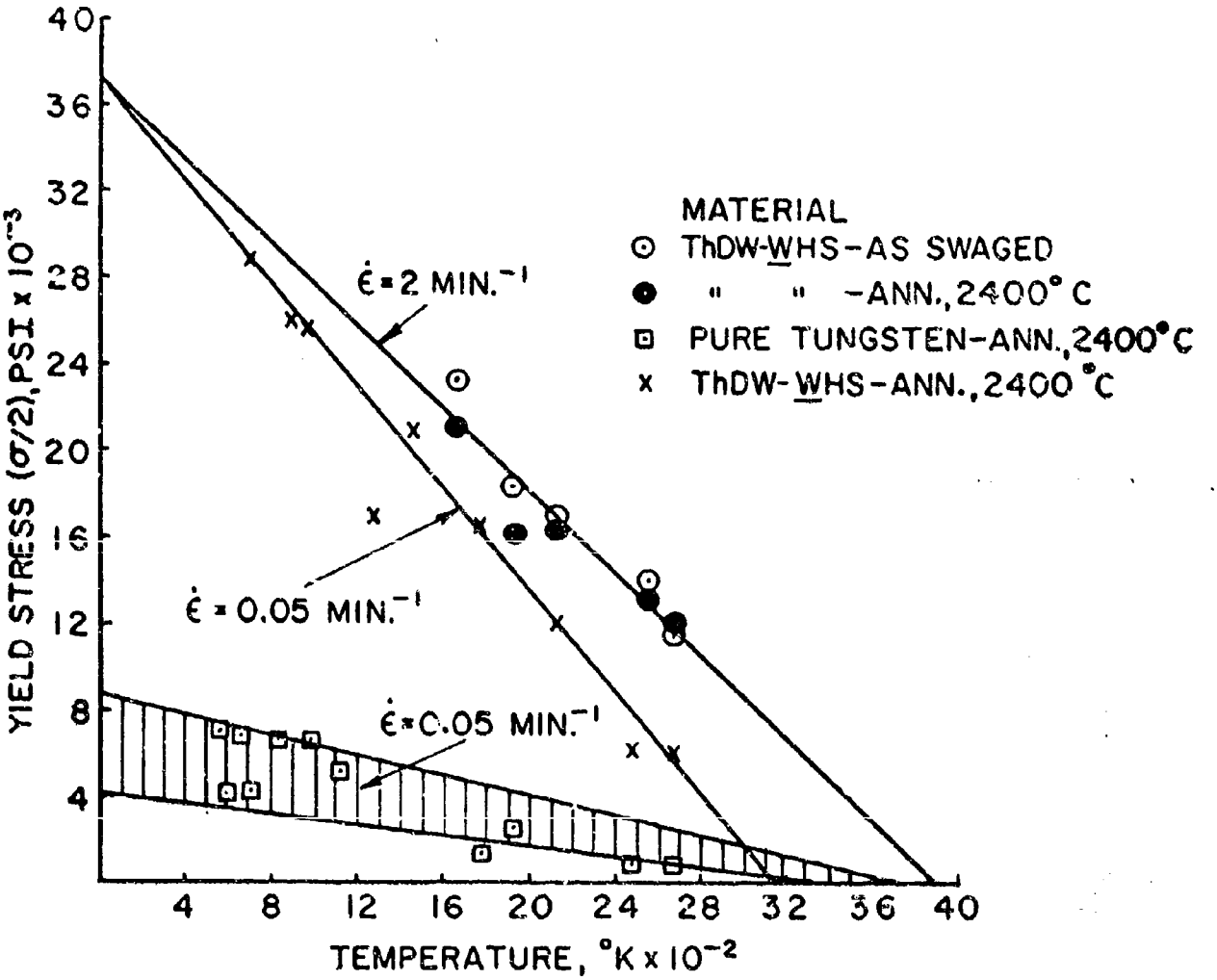

FIG. 22 EFFECT OF STRAIN RATE ON THE INITIAL FLOW STRESS OF ThDW-WHS AND PURE TUNGSTEN

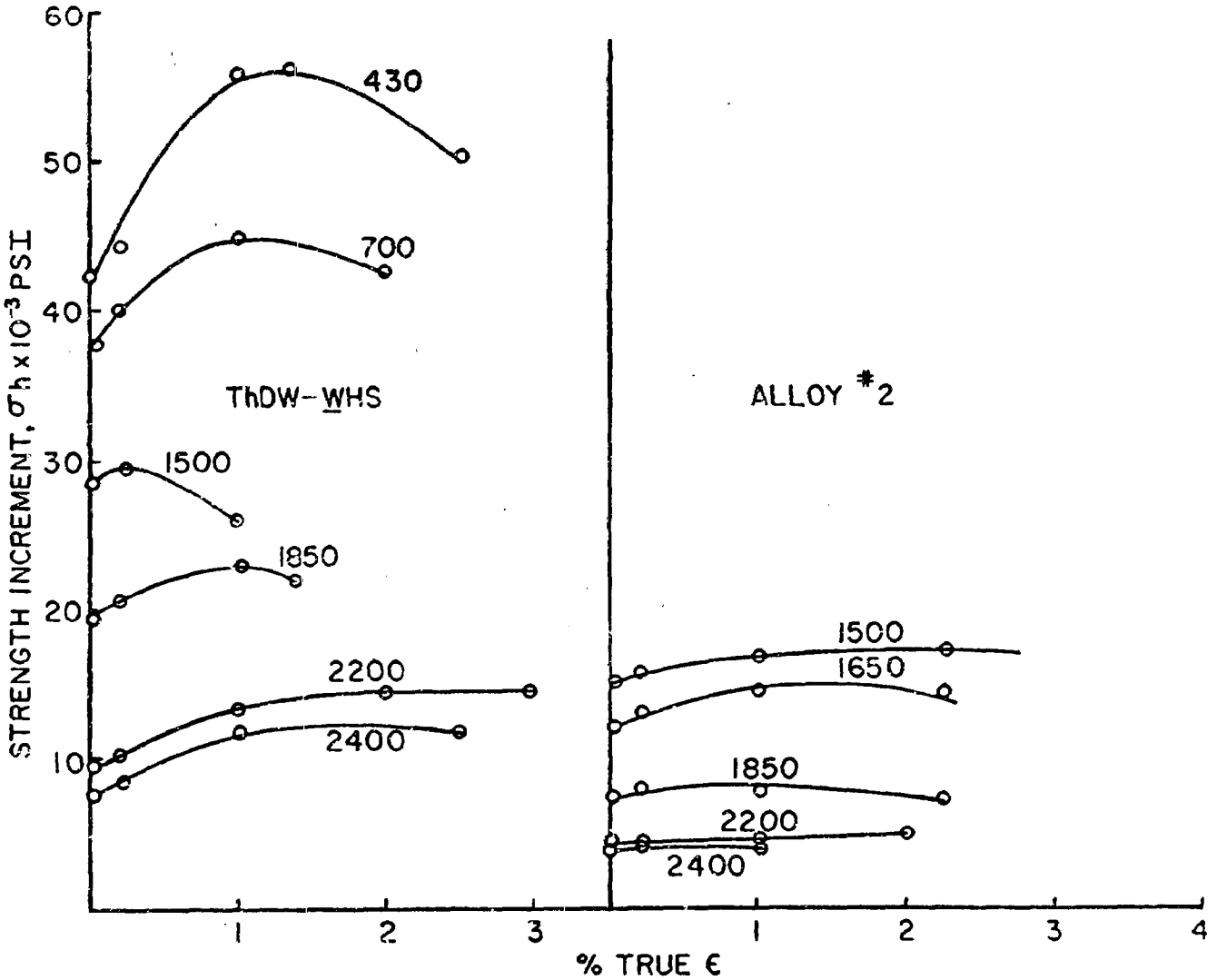

FIG. 23 STRENGTH INCREMENT ($\sigma_{ALLOY} - \sigma_{PURE\ TUNGSTEN}$) IN ThDW-WHS AND ALLOY No. 2 AS A FUNCTION OF STRAIN.

Another factor in agreement is that the ThDW-WHS alloy reaches a much higher strength increment than does Alloy No. 2, which has a coarser dispersion (1). In addition, the maximum increment in the tensile flow stress is about 0.01E (Hart (30) predicts 0.1E).

The temperature dependence of the strength increment is greater than that of the shear modulus, in disagreement with the model. However, as pointed out earlier, an additional temperature dependent mechanism is operating in these alloys.

3. Cree Properties

Creep tests were performed in the same Instron machine used for tensile testing by suspending dead weight loads from the lower pull rod. The vacuum at test temperature was about 5 x 10^{-5} torr, and the specimens were heated by radiation from a tungsten heating element. The loads included a tare weight of 8.2 lbs. representing the effect of vacuum on the pull rod and the slight friction caused by the vacuum compression seal, a Neoprene gasket in contact with the pull rod surface. The compression seal was later replaced by a bellows seal to determine whether or not the friction seal had affected the creep measurements; the data obtained were, however, essentially identical to those obtained with the friction seal.

Extension of the specimen during creep was measured by a dial gage which reads directly to one micron. The uncertainty in the dial position was less than 0.5μ. Hence, the lowest creep strain which could be detected was approximately 4 x 10^{-5}.

The tests performed were creep rupture tests, temperature cycling tests, and tests involving changes of stress at constant temperature. All test materials were annealed at 2400°C for 1/2 hour except where otherwise indicated in Table 14. Pure tungsten was used as the control.

In order to avoid spurious effects which might arise through maintaining the specimen under load while the furnace was not at thermal equilibrium, a specimen was loaded to a stress level insufficient to cause measurable creep in periods of hours, and the temperature cycled. Reproducibly, the temperature could be changed 100°C in either direction, and the system returned to complete equilibrium within 5 minutes. Therefore, in subsequent runs when changing temperature, the test specimens were unloaded and reloaded after 6-7 minutes.

Table 14

Creep Rupture Data for ThDW-WHS and Pure Tungsten at 2200°C

Stress, KSI	Annealing Temp., °C	$\dot{\epsilon}$ (Steady State) $min^{-1} \times 10^4$	Time to Rupture (min.)
		ThDW-WHS	
10	2400	4.6	Cooled under load after 75 min.
11	"	9.5	144
13	"	26.0	39
14	"	56.0	22
10	3100	7.5	45
11	2900	4.3	Cooled under load after 30 min.
		Pure Tungsten	
3.5	2400	13.0	39
3.4	"	9.0	55
7.6	"	----	1

a. Experimental Results

The creep rupture data of ThDW-WHS and pure tungsten at 2200°C are summarized in Table 14. The one and 10 hour creep rupture strengths of the two materials at 2200°C, as calculated from a Larson-Miller plot (Fig. 24), is, respectively, 12,500 PSI and 9,500 PSI for ThDW-WHS and 3,700 PSI and 2700 PSI for pure tungsten. The alloy has a creep rupture strength which is higher than that of pure tungsten by a factor of ~4. It can be further seen (Table 14 and Fig. 24) that annealing at 3100°C does not substantially lower the creep rupture strength of the alloy.

Data derived from temperature cycling tests have been compiled in Table 15. Typical creep curves for ThDW-WHS and for the pure tungsten control obtained by cycling between 2200°C and 2100°C are reproduced in Fig. 25. The ThDW-WHS creep behavior was characterized by the following distinct features:

1. When the test temperature was decreased, delay times from 3 to 14 minutes duration were observed with one exception. In some cases, these were preceded by a transient creep stage.

2. When the temperature was increased, delay times were absent; however, a transient creep stage was normally observed.

3. Creep tended to become more erratic after annealing at temperatures above 2400°C and/or after strains in excess of 1-2%.

Creep of pure tungsten occurred in an erratic fashion and was accompanied by transient creep following a temperature change. Data obtained as the result of changes in stress at constant temperature are summarized in Table 16. This table includes activation volumes calculated in the usual fashion in accordance to Eq. 9.

$$V_f = \frac{KT}{\Delta\sigma} \ln \left(\frac{\dot{\epsilon}_2}{\dot{\epsilon}_1}\right) \qquad \text{Eq. 9}$$

Delay times were not observed on decreasing the load, and transient creep was negligible.

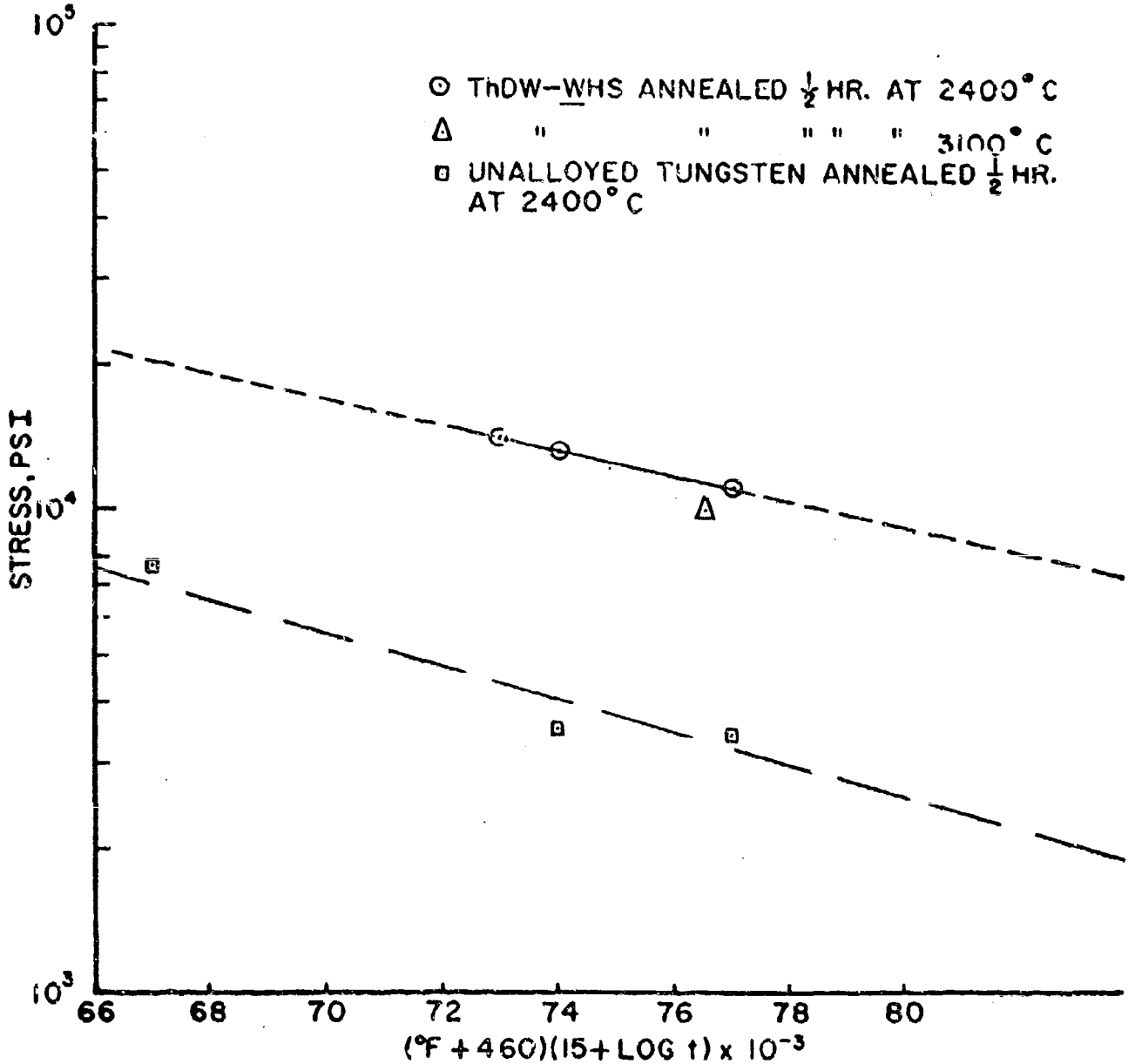

FIG.24 LARSEN—MILLER PLOT OF CREEP RUPTURE DATA

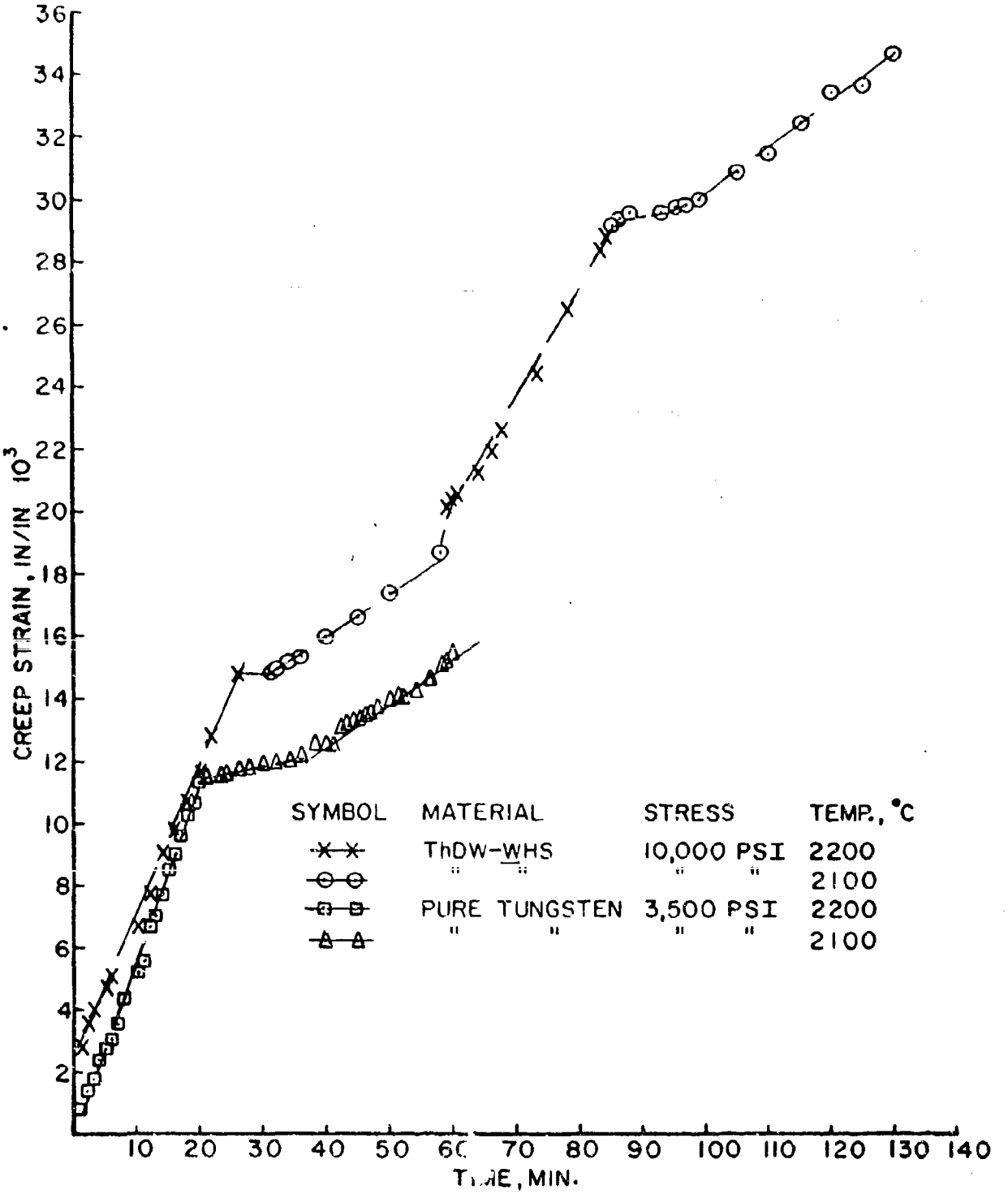

FIG. 25 TYPICAL CREEP CURVES OF ThDW-WHS AND PURE TUNGSTEN RESULTING FROM TEMPERATURE CYCLING TESTS AT CONSTANT STRESS

Table 15

Steady State Creep Rates ($\dot{\epsilon}, 10^4 \times min^{-1}$) and Apparent Activation Energies (Q' in KCal/mole) ThDW-WHS and Pure Tungsten

(Temperatures are Listed Below in °Kelvin)

Specimen No.	Stress, KSI	Temp. T_1	$\dot{\epsilon}_1$	Temp. T_2	$\dot{\epsilon}_2$	Q_1'	Temp. T_3	$\dot{\epsilon}_3$	Q_2'	Temp. T_4	$\dot{\epsilon}_4$	Q_3'
					ThDW-WHS							
1	10	2473	4.9	2373	1.4	147	2473	3.6	115	2373	1.6	95
2	10	"	5.1	"	1.3	160	----	---	---	----	---	--
3	10	"	16.0	"	4.6	146	----	---	---	----	---	--
4	11	"	6.8	"	1.8	156	----	---	---	----	---	--
4(a)	10	"	3.4	"	0.9	154	2473	3.8	169	----	---	--
5	10	2373	2.4	2473	5.1	88	----	---	---	----	---	--
5(b)	10	2473	6.9	2373	1.7	164	2473	6.4	155	2373	2.5	110
6	10	"	4.3	"	1.6	116	"	3.8	101	----	---	--
6(c)	10	"	4.5	"	1.4	137	"	4.4	135	2373	1.9	99
7	8	"	3.1	"	1.1	127	----	---	---	----	---	--
					Pure Tungsten							
1	3.6	2473	2.3	2373	0.3	236	2473	0.8	155	----	---	--
2	3.5	"	5.6	"	0.4	200	----	---	---	----	---	--
3	7	2123	32.6	2033	25.7	228	----	---	---	----	---	--

(a) Reannealed at 2400°C after above test (~3% Strain).
(b) Reannealed at 2800°C after above test (~2% Strain).
(c) Reannealed at 2620°C after above test (~3% Strain).

Table 16

Effect of Change in Stress (KSI) at Constant Temperature (2473°K) on the Creep Rate ($min^{-1} \times 10^4$), and the Calculated Activation Volumes ($cm^3 \times 10^{-21}$), Vf

Specimen No.	Material	σ_1	$\dot{\epsilon}_1$	σ_2	$\dot{\epsilon}_2$	Vf (b)	σ_3	$\dot{\epsilon}_3$	Vf (c)
1	ThDW-WHS	8	4.0	10	10.0	2.3	9	7.2	1.6
2(a)	Pure Tungsten	3.0	4.5	3.34	6.9	6.3	-	---	---
3	" "	2.96	0.19	3.26	2.1	40	-	---	---
4	" "	3.0	0.28	3.4	5.8	38	-	---	---

(a) Pre-strained (~2%) prior to test.

(b) $Vf = \frac{KT}{(\sigma_2 - \sigma_1)} \ln (\dot{\epsilon}_2/\dot{\epsilon}_1)$

(c) $Vf = \frac{KT}{(\sigma_3 - \sigma_2)} \ln (\dot{\epsilon}_3/\dot{\epsilon}_2)$

b. Discussion of Creep Results

The exceptional high strength of ThDW-WHS is also confirmed in the creep rupture properties of this alloy. Of particular significance is the fact that after annealing at 3100°C, good creep rupture strength is retained. In this case, this must be attributed directly to the dispersion, since the substructure, as discussed earlier in this report, is completely removed by this anneal ($>0.9\ T_m$).

The mechanism responsible for the creep strength of ThDW-WHS is not clearly evident. The attempt to determine the apparent activation energy controlling the creep rate from Eq. 4 is complicated by the transient creep effects and the erratic creep behavior of both the alloy and pure tungsten. However, by ignoring the inaccuracies introduced by these factors, one can tentatively interpret the data.

As Table 15 shows, the activation energy of pure tungsten at low strain ($<3\%$) is $\sim$220 Kcal/mole and the activation energy of the alloy at similar strains is $\sim$140 Kcal/mole. This compares with an activation energy for self-diffusion of tungsten of about 150 Kcal/mole (29).

Following Schoeck (28), it is assumed that the climbing of edge dislocations is the rate controlling process in high temperature creep and that jogs must be present for this process to occur. If the jogs are formed by thermal fluctuations, then the activation energy will be equal to that for self-diffusion plus the energy of formation of a jog. However, if jogs are formed by intersection with the "forest" dislocations, then the activation energy will be equal to that for self-diffusion.

Using Seeger's Equation (26):

$$\Delta H_J = Gb^2\ \Delta l/10 \qquad \text{Eq. 10}$$

where Δl is the increase in length of the dislocation when a jog forms and is estimated to be about $b/2$. Substituting for Δl and using the empirical relationship $Gb \simeq 50KT_m$, one calculates the energy of formation of a jog in tungsten to be about 0.8 eV.

The comparison of these theoretical predictions with the experimental results indicates that for initial creep to occur in pure tungsten, thermal activation of jogs is required. Other investigators have determined creep activation energies in pure tungsten of 170 Kcal/mole (31). In the alloy, on the other hand, jogs are formed by intersection with the retained substruc-

ture. This interpretation is supported by the observed decrease in the activation energies of both materials with increasing strain.

To explain the observed higher creep strength of the alloy, in view of its lower activation energy in relation to pure tungsten, and in terms of Eq. 4, one must consider the relative magnitudes of the activation volumes of the two materials (Table 16). The activation volume of the alloy is about an order of magnitude lower than that of pure tungsten, whereas U_o of the alloy is only about 0.65 U_o of pure tungsten. Hence, the activation volume is the dominating term in the exponent of Eq. 4.

F. Characterization of Experimental Alloys

1. Optical Microstructures

The alloys which exhibited significantly improved strength were examined by conventional metallography in the as worked condition. These were compared with head and gage sections of specimens which were tensile tested at 2400°C after 1/2 hour anneal at 2400°C. Figs. 26 and 27 demonstrate changes effected by the anneal alone and the anneal plus strain. For comparative purposes, micrographs of ThDW-WHS are included (Fig. 28).

As distinct from the ThDW-WHS alloy, all the as worked experimental alloys show a finer but also elongated grain structure with grain width varying from one to several microns. Following the anneal, the grain widths increase by a factor of 2 to 3. Some particle coarsening is also observed (Figs. 26 and 27). In addition, although it is not demonstrated in the micrographs, exaggerated grain growth was observed in both the head and gage sections of ThDW-2 (conventional extrusion) and ThDW-WHS (Alloy No. 2-2) with some grains reaching a size $\geq$1mm. The strained gage sections in most cases show still greater grain broadening, and a higher area of abnormally large grains. This may possibly be the result of strain induced growth.

No attempt was made to analyze ThO_2 particle size or distribution by optical microscopy. As has been pointed out earlier, magnifications $\geq$5000X are essential to even qualitatively assess these parameters.

2. Replica Electron Microscopy

Electron microscopy of carbon replicas was used in the program to observe particularly the nature and behavior of the second phase particles and structural changes at sequential

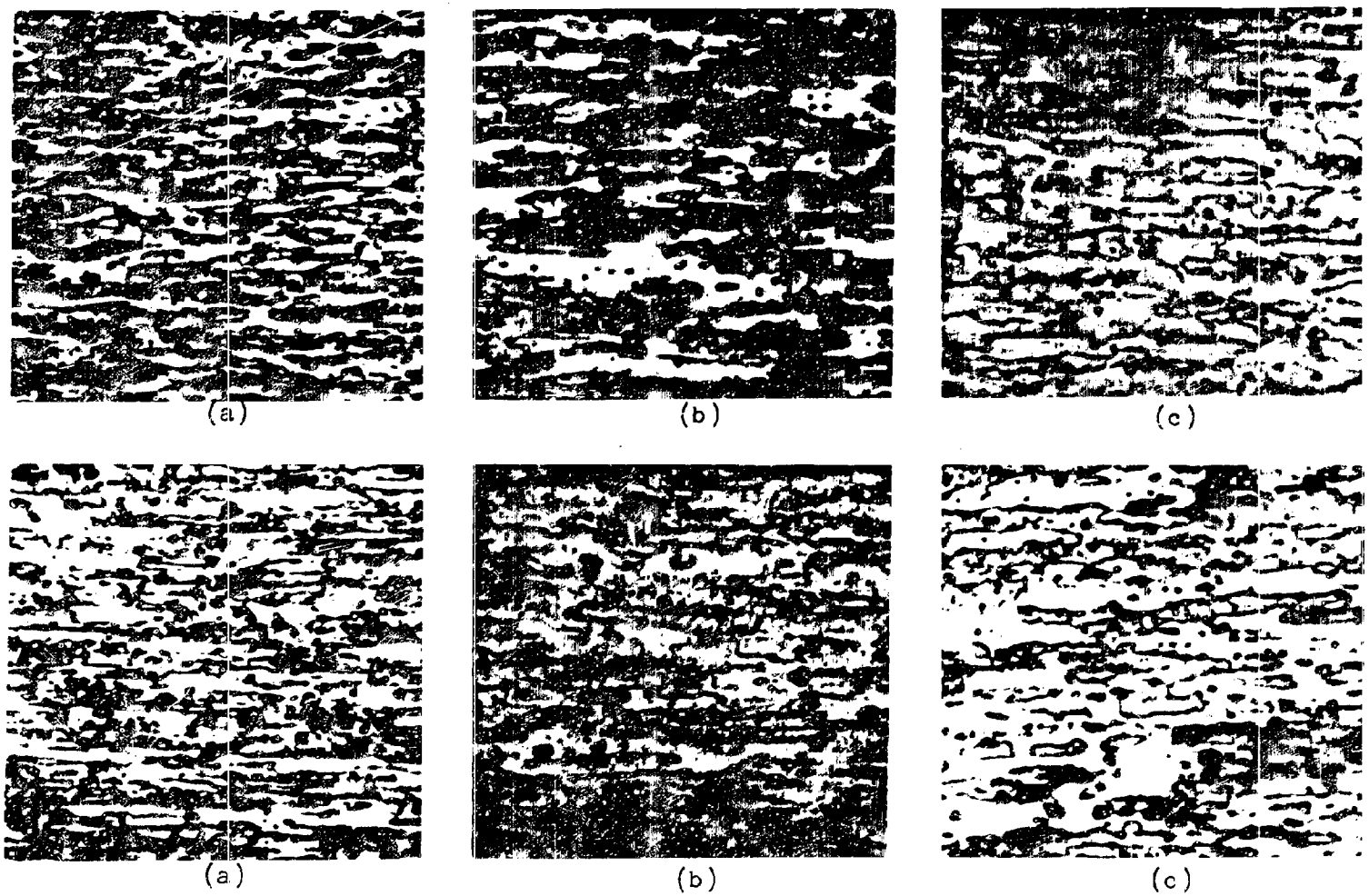

Fig. 26 Optical Micrograph of W-ThO_2 Alloys - 1500X
Top: ThDW-1 (High Rate Extrusion) Bottom: ThDW-2 (High Rate Extrusion)
(a) As Worked $\geq$90% R.A. by Swaging; (b) Head Section of Fractured Specimen Annealed at 2400°C for 1/2 Hr. Before Testing at 2400°C; (c) Gage Section of Fractured Specimen Annealed at 2400°C for 1/2 Hr. Before Testing at 2400°C.

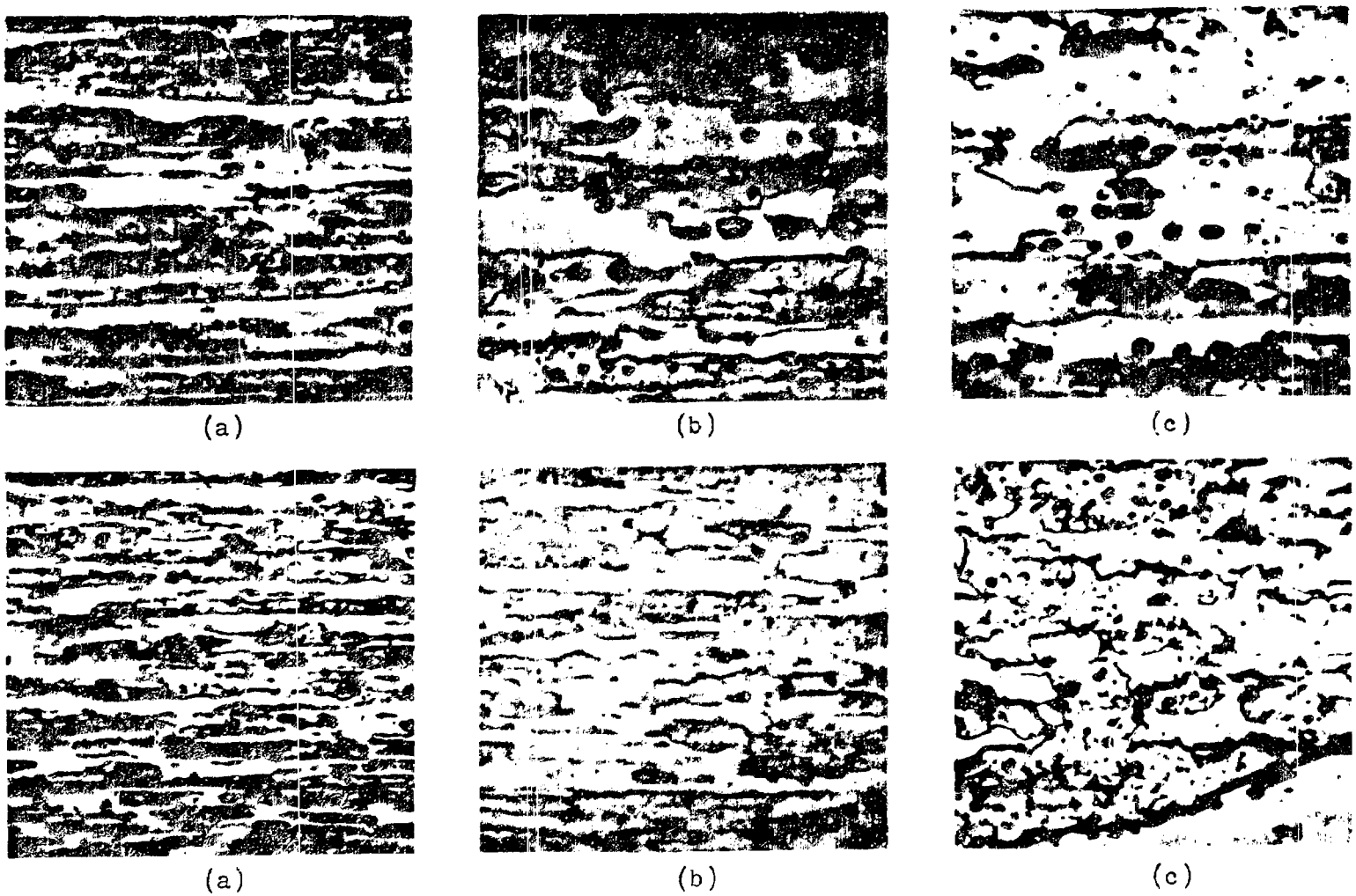

Fig. 27 Optical Micrographs of W-ThO_2 Alloys - 1500X
Top: ThDW-2 (Conventional Ext.) Bottom: ThDW-WHS (Alloy #2-2 High Rate Ext.)
(a) As Worked >90% R.A. by Swaging; (b) Head Section of Fractured Specimen Annealed at 2400°C, 1/2 Hr. Before Testing at 2400°C; (c) Gage Section of Fractured Specimen Annealed at 2400°C, 1/2 Hr. Before Testing at 2400°C.

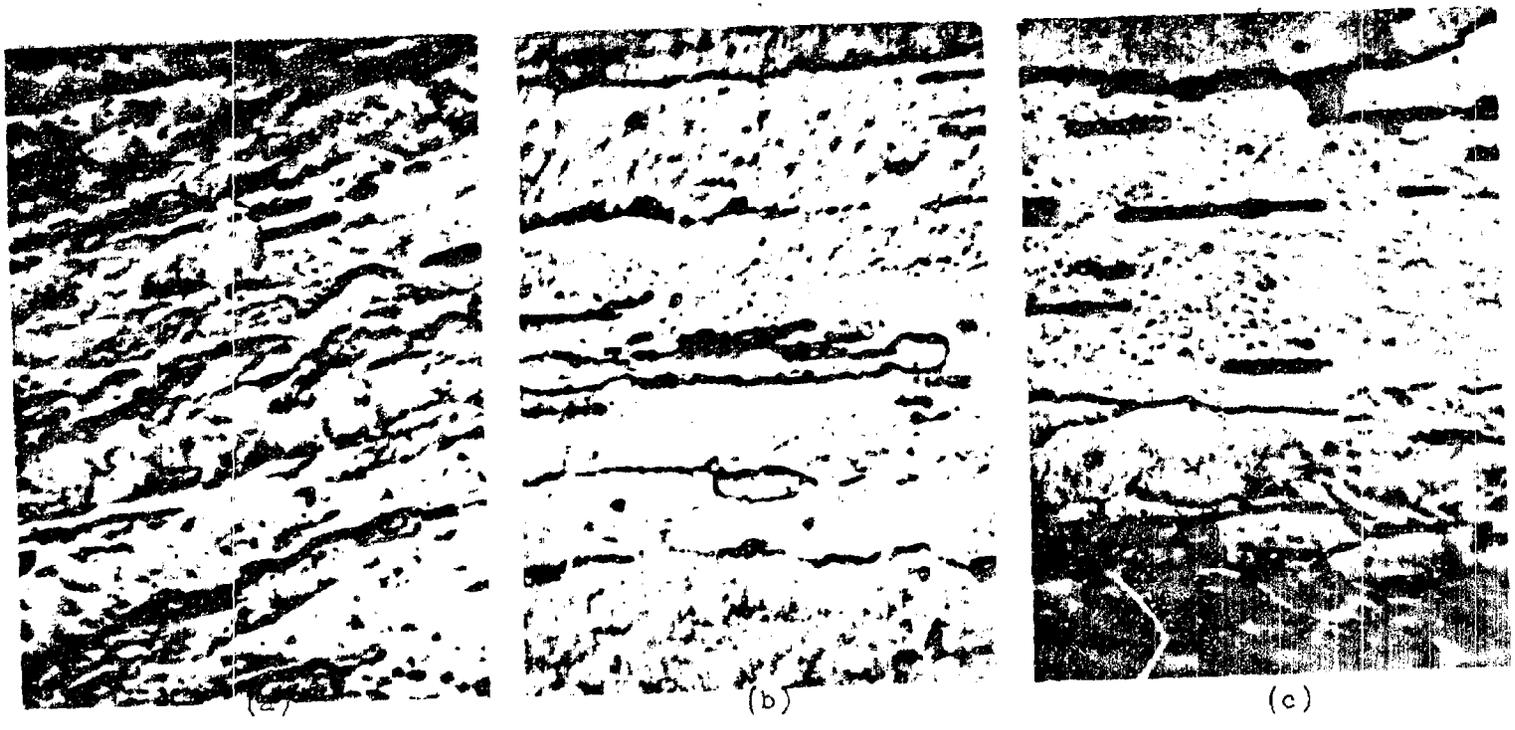

Fig. 28 Optical Micrograph of ThDW-WHS (Self-Res. Sintered) - 1500X
(a) As Worked $\geq$90% R.A. by Swaging; (b) Head Section of Fractured Specimen Annealed at 2400°C for 1/2 Hr. Before Testing at 2400°C; (c) Gage Section of Fractured Specimen Annealed at 2400°C for 1/2 Hr. Before Testing at 2400°C.

stages throughout processing. Numerous modifications in the sample preparation technique were made during the investigation to improve efficiency and quality of the resulting specimens. The technique ultimately arrived at is shown in Table 17. The C-Pt pellets which were used were established to be superior to WO_3, Au, or Pt from the standpoint of resolution. All micrographs were taken on the Hitachi HU-11, at 100 KV (75 KV was used in a few instances).

Fig. 29 pictures the alloys (1.25 in. dia. billets) after hot pressing. At this stage, the density of the alloys ranges from 87% to 92% of theoretical density (Table 4). In relation to the fine powder used for preparation, it is evident that some grain growth has occurred. It will be noted that the second phase particles are not clearly brought out, at this stage of processing, by the technique employed so that any particle size differences which may exist cannot be deduced from these replicas. The alloy W-5 w/o Cr-3.8 v/o ThO_2 appears to have undergone the greatest grain growth during hot pressing.

Figs. 30 and 31 show the W-ThO_2 alloys after extrusion. Marked structural differences are already evident. Replicas of all alloys show further grain growth in varying degrees, with ThDW-1 showing a distinctly elongated structure. ThDW-3, the only conventionally extruded alloy shown, reveals the most marked growth (Fig. 30). Thoria particles are distinctly visible in all alloys and range in size from $\sim$0.1μ to 2μ. ThDW-1 is seen to have the finest distribution ($\sim$0.3μ mean size estimated), while ThDW-3 contains almost exclusively particles on the order of 2μ dia.

Figs. 32, 33, 34, 35, and 36 depict the condition of the alloys after deformation by swaging (>90% R.A.). At this stage of processing, the differences among the alloys are very marked, and particles are distinctly resolved in all systems. Alloys ThDW-1 and 2, and ThDW-WHS (Alloy No. 2-2) show extremely fine dispersions (estimated mean particle size $\sim$0.1μ), while ThDW-3 and 4 show essentially no fine dispersion. It should be noted, however, that fine particles are considerably less distinct (in some cases not seen at all) in transverse sections.

Figs. 37, 38, 39, 40, and 41 represent the condition of the alloys after tensile testing. The replicas were made from fractured tensile specimens which were annealed for 1/2 hour at 2400°C and tested at 2400°C. An obvious change from the as worked structures is the rounding of all larger particles. With regard to the fine particles the micrographs reveal some areas where their density is significantly higher than observed in the as worked specimens. This is believed to result from an etching phenomenon. With regard to particle coarsening, examination of many micrographs leads to the tentative conclusion that it occurs to only a slight extent, if at all.

Table 17

Flow Sheet for the Preparation of Replicas

1. Polish specimens through papers in standard fashion. Perform final polishing on automatic polisher-lapper with Linde B alumina until structure begins to appear without etching.
2. Etch with Murakami's reagent for 2 seconds.
3. Immerse in ultrasonic cleaner (detergent in water) for ~5 minutes. Rinse several times.
4. Using BioDn and Methylacetate "blot" specimen surface 2 or 3 times.
5. Make plastic replica with BioDn and Methylacetate and, after drying, strip from specimen.
6. Shadow plastic replica with C-Pt mixture at $\sim 5 \times 10^{-6}$ torr (15-20° inclination).
7. Deposit carbon perpendicularly on plastic replica in 1μ Argon.
8. Place plastic-carbon replica, carbon side down, on drop of melted BioDn wax on glass slide.
9. Gently score replica into sections of appropriate size.
10. Immerse slide and replica in Methylacetate and slowly heat to ~60°C. Hold at that temperature for ~1 hour.
11. Pick up detached pieces of carbon on grid, and straighten them by dipping them first in an 80 acetone/20 water solution and then immediately in distilled water.
12. Dry for ~1 hour at 30-40°C.

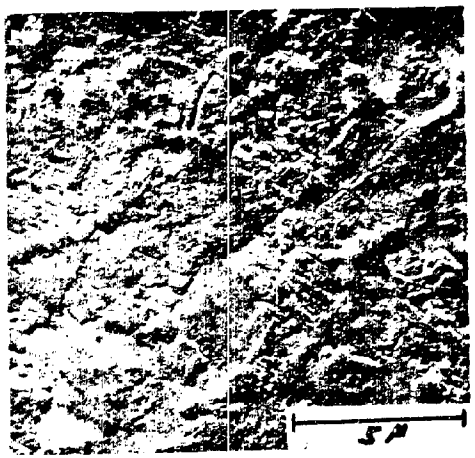

(a) ThDW-1

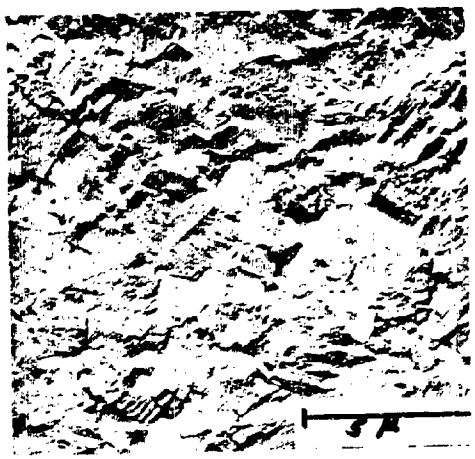

(b) ThDW-2

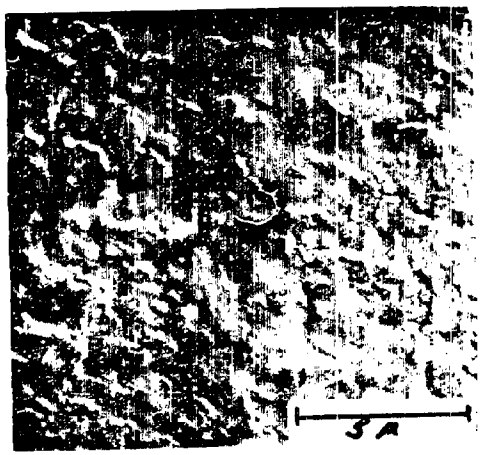

(c) ThDW-3

(d) ThDW-4

(e) ThDW-WHS (Alloy #2-2)

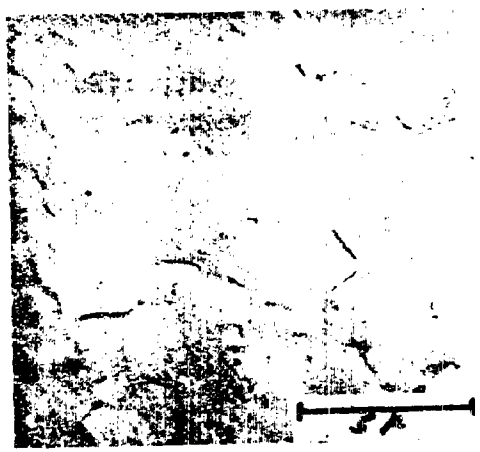

(f) W-5 w/o Cb-3.8 w/o ThO_2

Fig. 29 Carbon Replicas of As Pressed Alloys; Billet Diameter 1.25 in. - 5000X

(a) Longitudinal

(a) Longitudinal

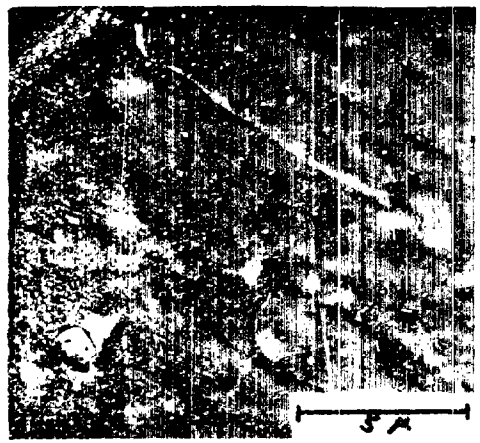

(a) Longitudinal

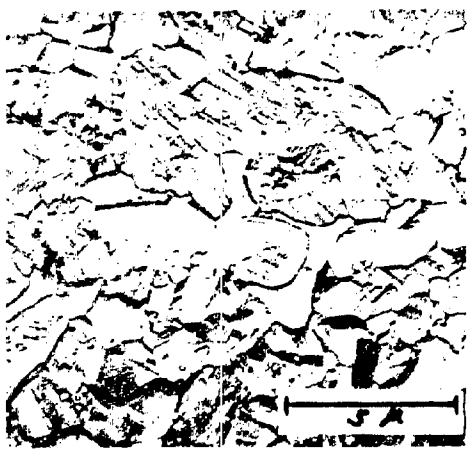

(b) Transverse

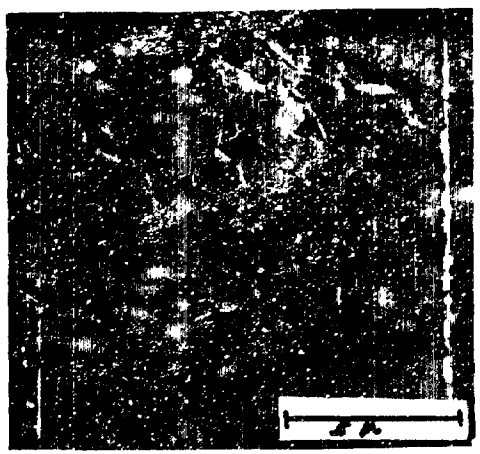

(b) Transverse

(b) Transverse

Fig. 30 Carbon Replicas of the As Extruded W-ThO_2 Alloys - 5000X
Left: ThDW-1 (High Rate Extrusion) Center: ThDW-2 (High Rate Extrusion)
Right: ThDW-3 (Conventional Extrusion)

(a) Longitudinal

(b) Transverse

(a) Longitudinal

(b) Transverse

Fig. 31 Carbon Replicas of W-ThO_2 Alloys As (High Rate) Extruded
Left: ThDW-4 Right: ThDW-WHS (Alloy #2-2) - 5000X

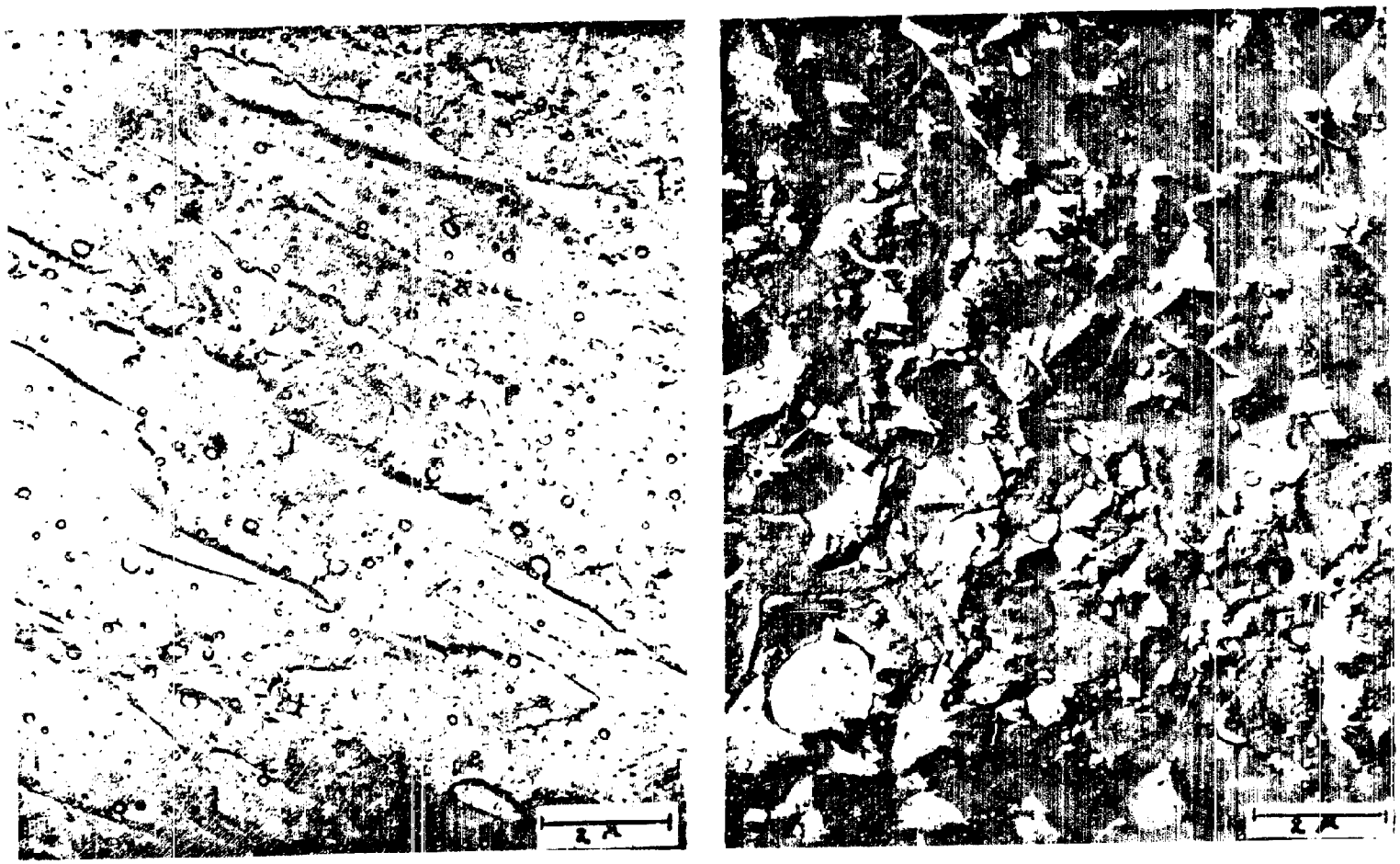

Fig. 32 Carbon Replica of ThDW-1 (High Rate Extrusion) As Worked ≥90% R.A. by Swaging - 10,000X
Left: Longitudinal Right: Transverse

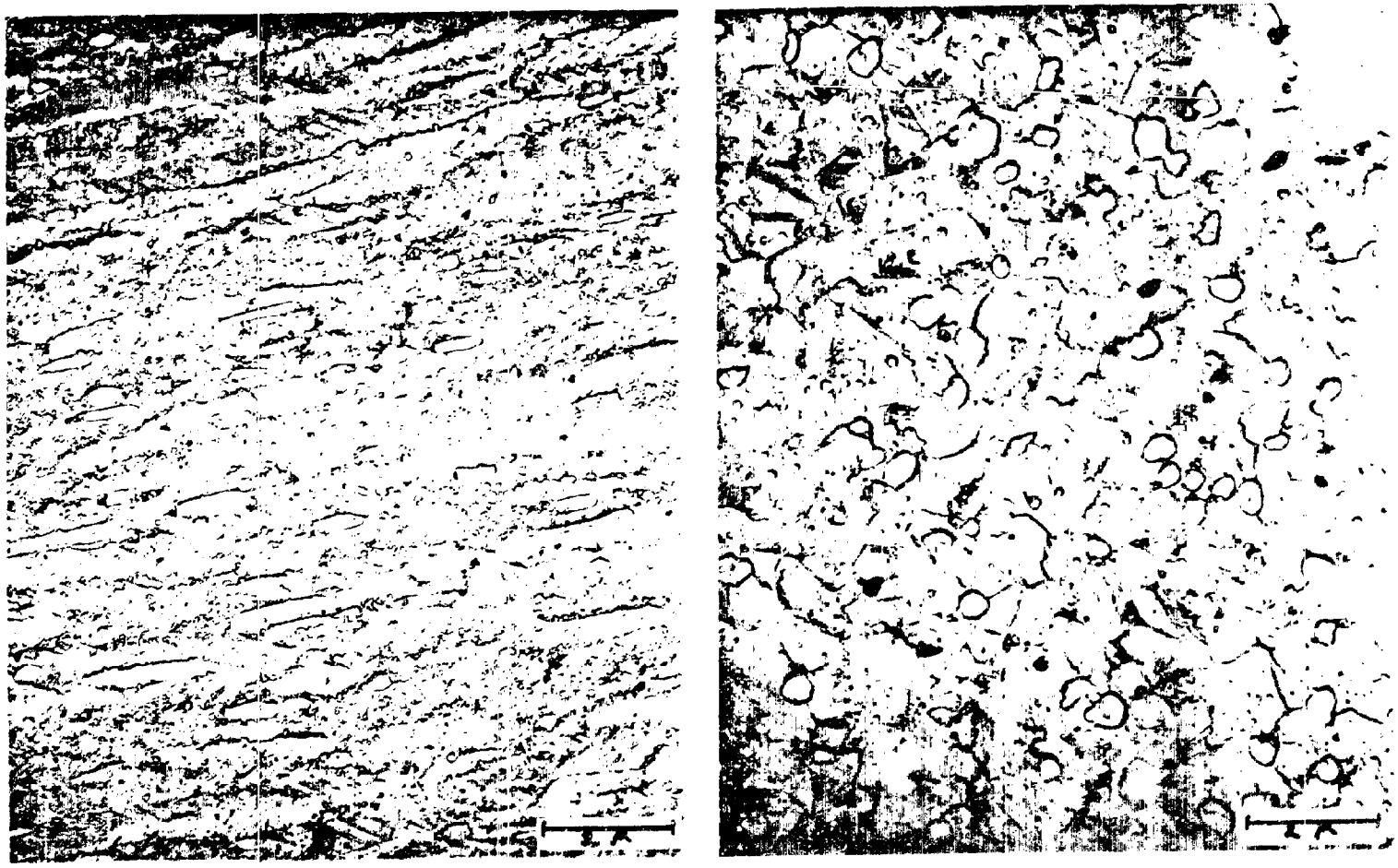

Fig. 33 Carbon Replica of ThDW-2 (High Rate Extrusion) As Worked >90% R.A. by Swaging - 10,000X
Left: Longitudinal Right: Transverse

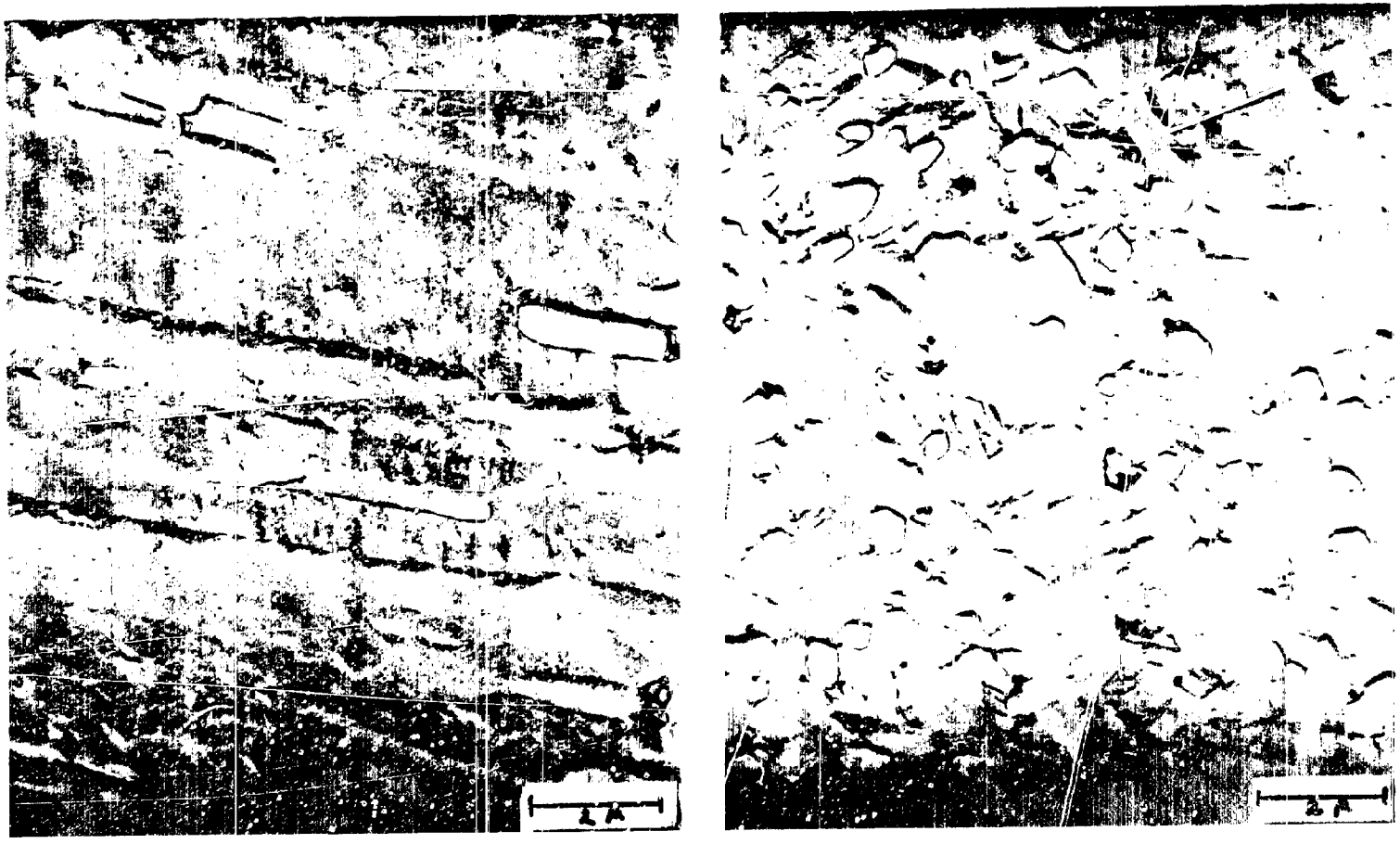

Fig. 34 Carbon Replica of ThDW-2 (Conventional Extrusion) As Worked >90% R.A. by Swaging - 10,000X
Left: Longitudinal Right: Transverse

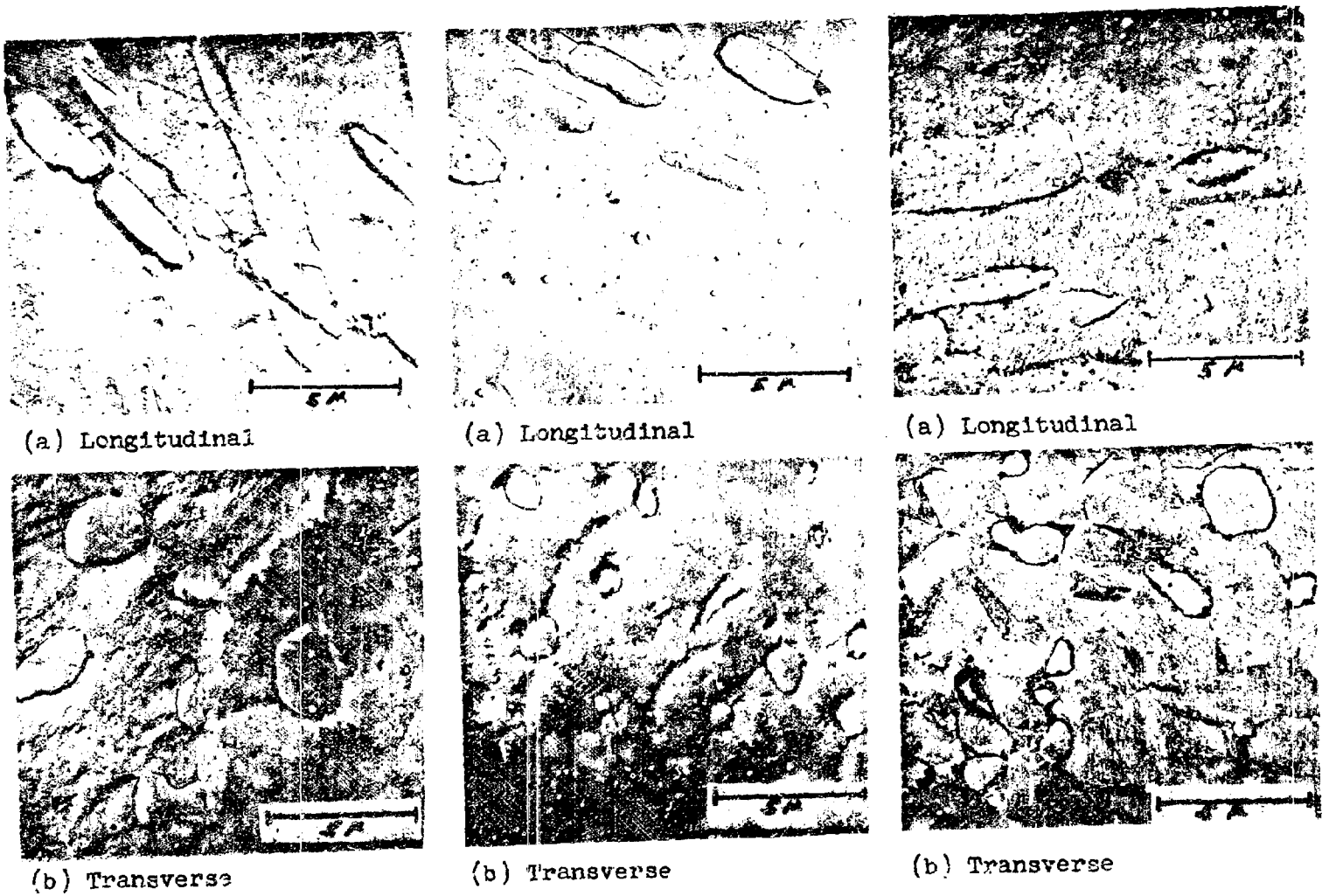

Fig. 35 Carbon Replicas of W-ThO_2 Alloys As Worked >90% R.A. by Swaging - 5000X
Left: ThDW-3 (Conventional Extrusion) Center: ThDW-4 (High Rate Extrusion)
Right: ThDW-4 (Conventional Extrusion)

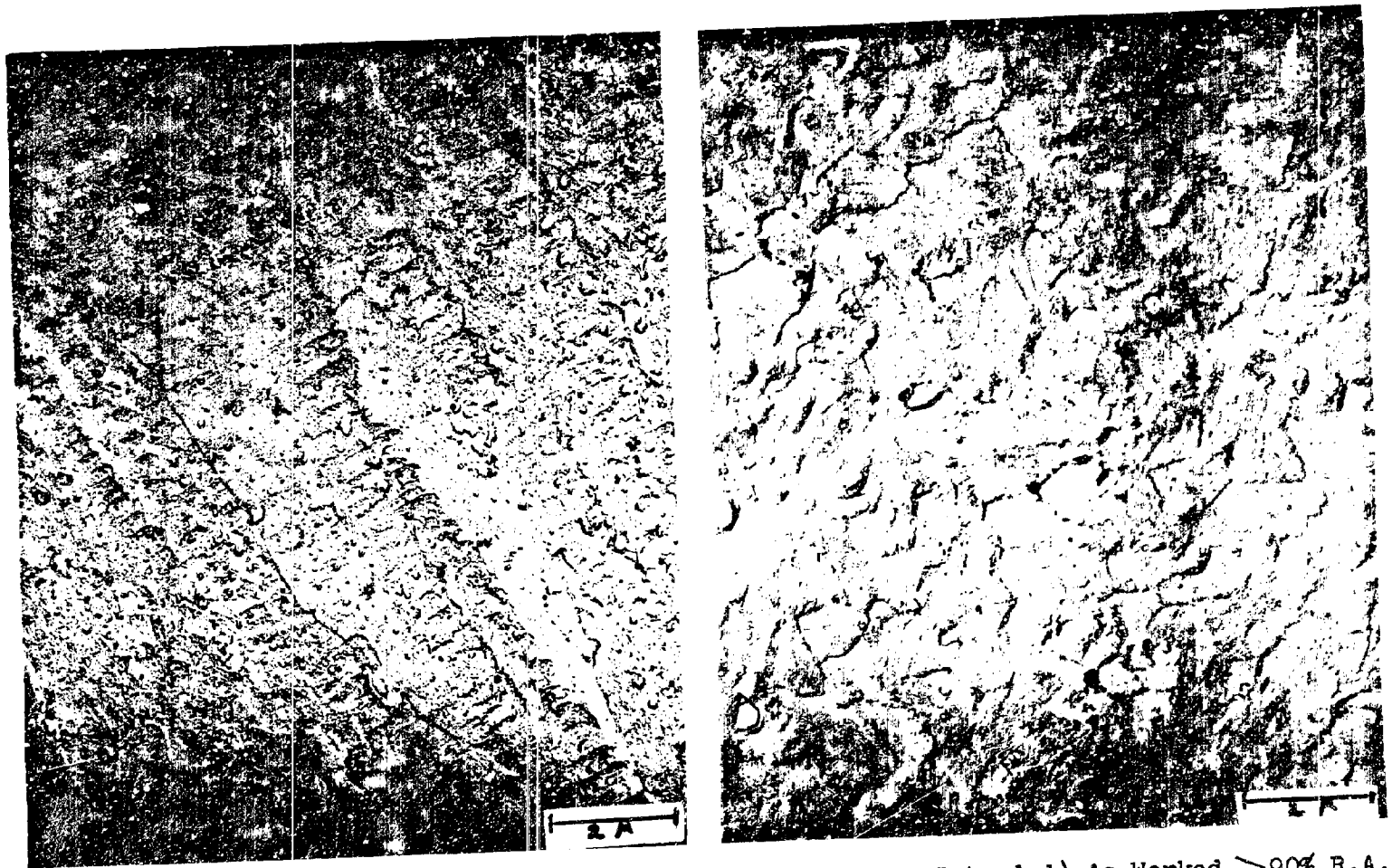

Fig. 36 Carbon Replica of ThDW-WHS (Alloy #2-2, High Rate Extruded) As Worked >90% R.A. by Swaging - 10,000X
Left: Longitudinal Right: Transverse

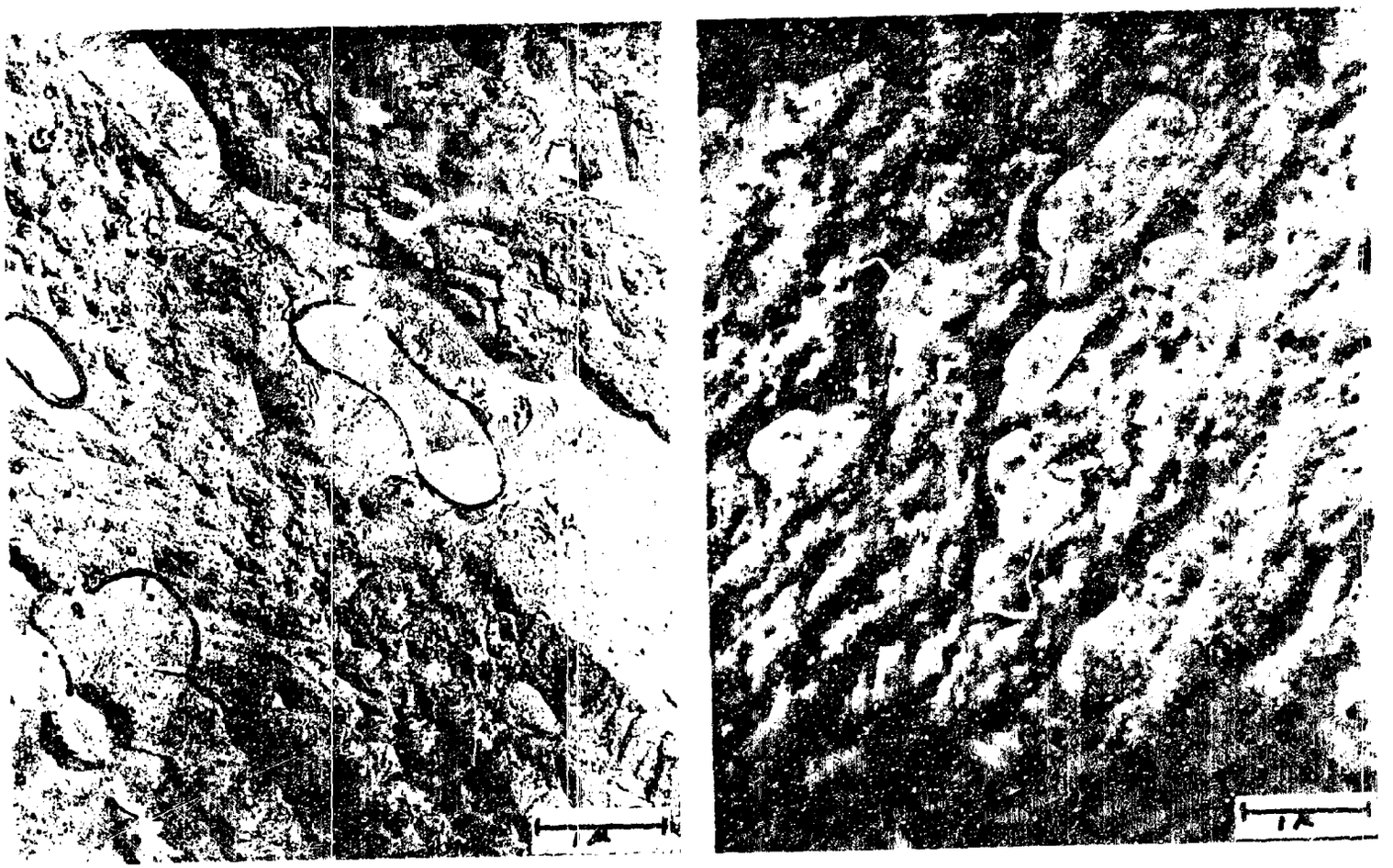

Fig. 37 Carbon Replica of Fractured ThDW-1 (High Rate Extrusion) Tensile Specimen Annealed at 2400°C for 1/2 Hr. Before Testing at 2400°C - 20,000X
Left: Head Section Right: Gage Section

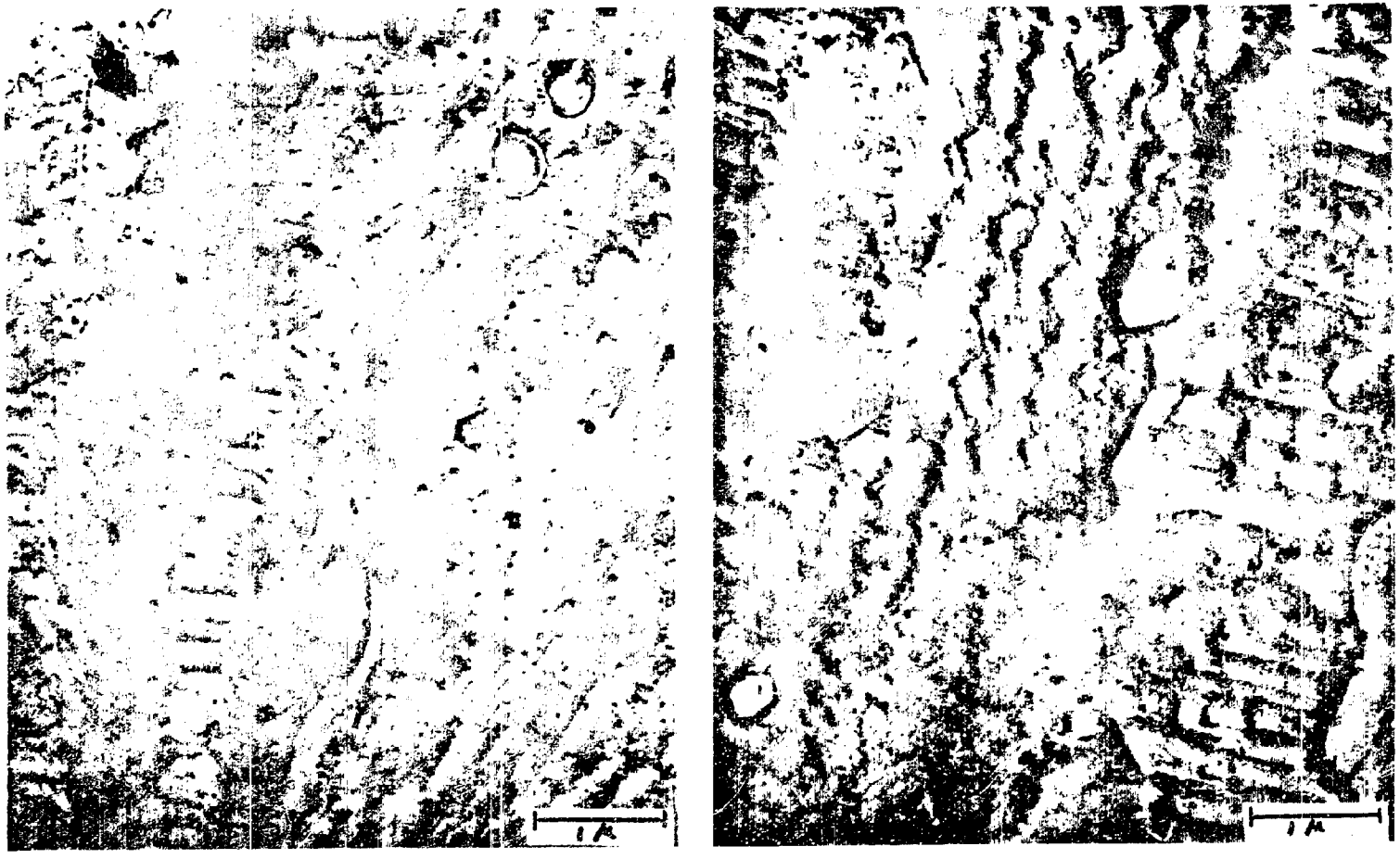

Fig. 38 Carbon Replicas of Fractured ThDW-2 (High Rate Extrusion) Tensile Specimen, Annealed at 2400°C for 1/2 Hr. Before Testing to Fracture at 2400°C - 20,000X
Left: Head Section Right: Gage Section

Fig. 39 Carbon Replica of Fractured ThDW-2 (Conventional Extrusion) Tensile Specimen Annealed at 2400°C for 1/2 Hr. Before Testing at 2400°C. - 20,000X
Left: Head Section Right: Gage Section

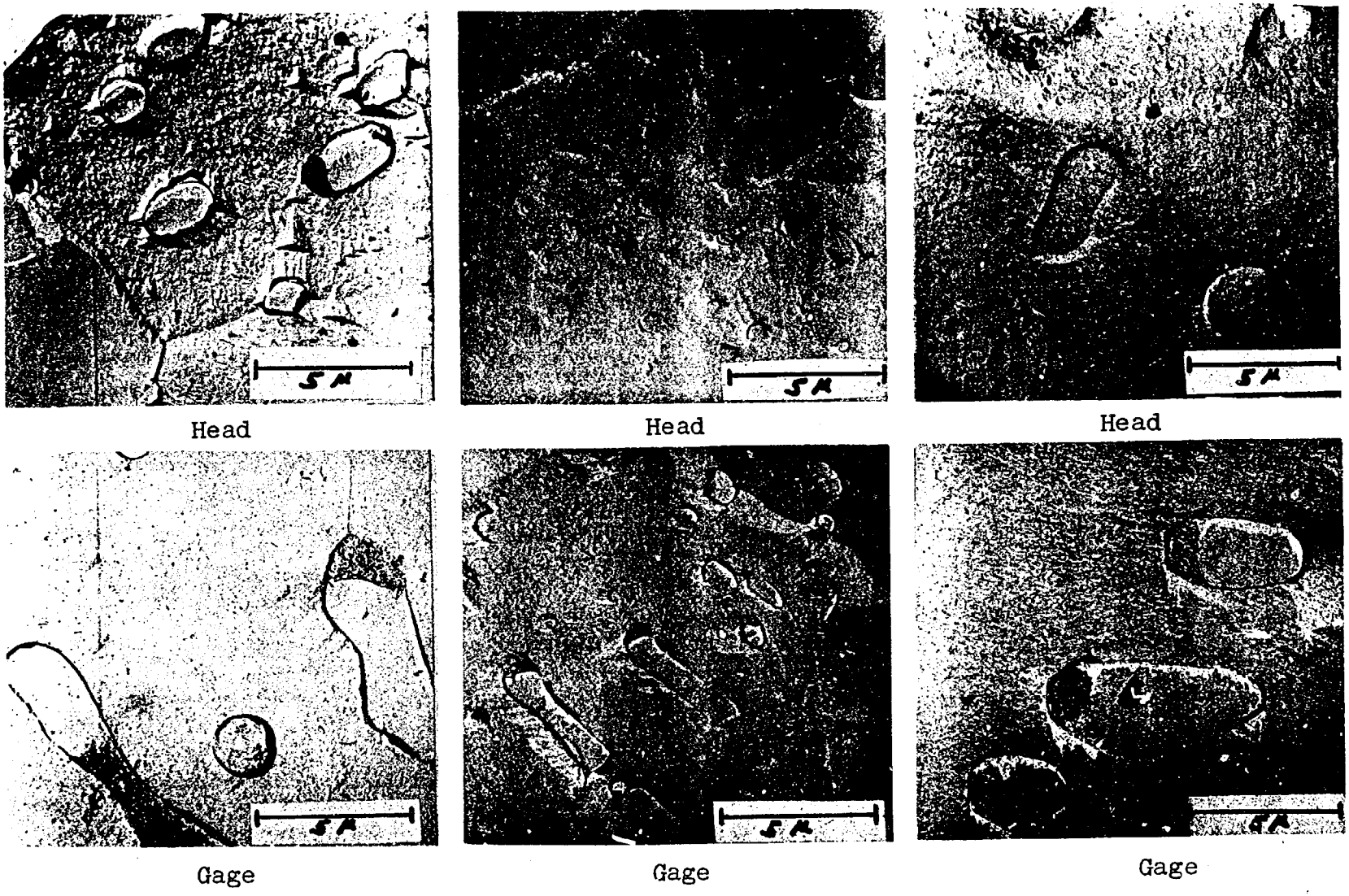

Head Head Head

Gage Gage Gage

Fig. 40 Carbon Replicas of Fractured Tensile Specimens of W-ThO_2 Alloys. Specimens Were Annealed at 2400°C for 1/2 Hr. Before Testing at 2400°C - 5000X
Left: ThDW-3 (Conventional Extrusion) Center: ThDW-4 (High Rate Extrusion)
Right: ThDW-4 (Conventional Extrusion)

Fig. 41 Carbon Replica of Fractured ThDW-WHS Tensile Specimen Annealed at 2400°C for 1/2 Hr. Before Testing at 2400°C — 20,000X
Left: Head Section Right: Gage Section

G. Mechanical Properties of Experimental Alloys

Tensile testing was conducted on specimens of the dimensions used throughout this work (Buttonhead with 0.093 in. gage dia. x 1 in. gage length). All specimens were annealed at 2400°C for 1/2 hour in vacuum (10^{-5} torr) before testing. Strain rate was 0.05 min^{-1}, and standard temperatures of testing were 1500°C, 1850°C, and 2400°C. The tensile properties derived from tests are presented in Table 18 and the ultimate tensile strengths plotted in Fig. 42. The properties of the ThDW-WHS and Alloy No. 2-2 are also listed for comparison.

It is readily evident at the higher test temperatures that the tensile strengths of the alloys prepared by doping in the reduced metal powder stage (ThDW-3 and 4) are inferior to those doped on the oxide (ThDW-1 and 2). The properties of ThDW-1 show the greatest strengthening observed in any of the alloys tested at the lowest test temperature (1500°C), but its strength decreases rapidly with increasing temperature until it is about equal to that of ThDW-2 at 2400°C. The strength of ThDW-2 is about the same or slightly less than that of the ThDW-WHS alloy.

Since the quantity of the material for test was limited, a thorough evaluation of all the parameters was not possible. However, three rather definite comparisons are warranted:

1. Hot Pressing vs. Self-Resistance Sintering: Two alloys--ThDW-WHS and ThDW-2--were prepared by both techniques. In both cases, the self-resistance sintered materials display a slightly greater ultimate tensile strength and, generally, a slightly higher ductility.

2. Low vs. High Swaging Temperature: Variations in swaging temperature (ThDW-4) showed improved properties for the 1500°C preheat temperature as compared to the 1700°C temperature.

3. Dynapak vs. Conventional Extrusion: The comparison of high rate vs. standard extrusion (ThDW-2 and ThDW-4) is not consistent, i.e., high rate extrusion is marginally more effective for strengthening in ThDW-4 while standard rate is distinctly more effective in ThDW-2. However, it must be kept in mind that ThDW-4 was doped on the metal powder.

Table 18

Tensile Data of Experimental W-ThO_2 Alloys Annealed 1/2 Hr. at 2400°C

Material	Test Temp., °C	Prop. Limit, KSI	0.2% Y.S., KSI	Ult. Str., KSI	Unf. Strain, %	Tot. Elong. %	% R.A.
ThDW-WHS (Self-Res. Sintered)	1500	33.00	36.00	36.80	1.2	11.9	76
	1850	20.60	25.50	29.20	1.5	11.0	46
	2200	11.80	15.20	18.20	3.0	14.5	24
	2400	11.10	13.50	15.10	2.5	16.7	43
ThDW-WHS (Alloy No.2-2) (Dyna.)	1500	22.60	27.60	31.90	2.5	8.8	54
	1850	17.50	19.20	22.30	2.9	8.5	28
	2200	12.60	14.00	15.70	3.7	9.8	18
	2400	11.10	11.80	13.30	2.4	5.3	15
ThDW-1 (Dyna.)*	1500	46.60	53.20	60.30	4.0	11.5	30
	1850	17.30	19.75	21.30	1.8	4.8	3
	2400	9.10	10.60	13.00	5.0	12.2	10
ThDW-2 (Ext.)	1500	40.50	43.20	45.50	1.8	6.0	51
	1850	17.00	23.20	27.30	2.0	7.8	20
	2400	6.00	8.40	11.50	3.8	8.0	6
ThDW-2 (Dyna.)	1500	12.00	13.80	22.00	12.5	20.7	24
	2400	5.55	7.20	11.80	5.5	11.0	13
ThDW-2 (Self-Res. Sintered)	1500	35.00	37.20	37.65	1.0	13.7	58
	1850	27.20	29.90	30.30	1.0	10.2	55
	2400	9.45	11.70	15.40	5.2	15.2	16
	2400	7.10	8.90	12.70	4.6	9.3	11
ThDW-3 (Ext.)	1500	10.20	12.35	17.35	19.0	53.2	64
	1850	6.40	7.40	10.10	12.0	43.7	72
	2400	2.40	3.25	4.25	11.0	44.0	42

Table 18 (Cont'd.)

Tensile Data of Experimental W-ThO_2 Alloys Annealed 1/2 Hr. at 2400°C

Material	Test Temp., °C	Prop. Limit, KSI	0.2% Y.S., KSI	Ult. Str., KSI	Unf. Strain, %	Tot. Elong. %	% R.A.
ThDW-4 (Dyna.)	1500	23.60	25.30	28.65	5.8	24.0	53
	1850	11.50	13.70	15.90	5.5	25.4	38
	2400	3.15	4.60	7.80	5.2	16.7	19
ThDW-4 (Ext. and Swaged at 1700°C)	1500	11.75	15.10	23.90	12.5	28.8	60
	1850	9.25	10.70	14.40	10.5	25.7	45
	2400	4.35	5.00	6.15	5.0	22.5	
ThDW-4 (Ext. and Swaged at 1500°C)	1500	17.30	20.50	26.40	8.7	18.5	57
	1850	14.80	16.50	17.80	2.2	10.8	51
	2400	5.20	5.85	6.45	3.5	15.5	34
ThDW-4 (Ext. and Swaged at 1300°C, with interm. Anneals)	1500	11.90	14.00	24.30	14.0	32.1	64
	1850	8.15	10.05	14.15	12.2	27.3	64
	2400	4.75	5.20	6.45	6.2	14.7	10

* All alloys not otherwise designated were swaged at 1700°C.

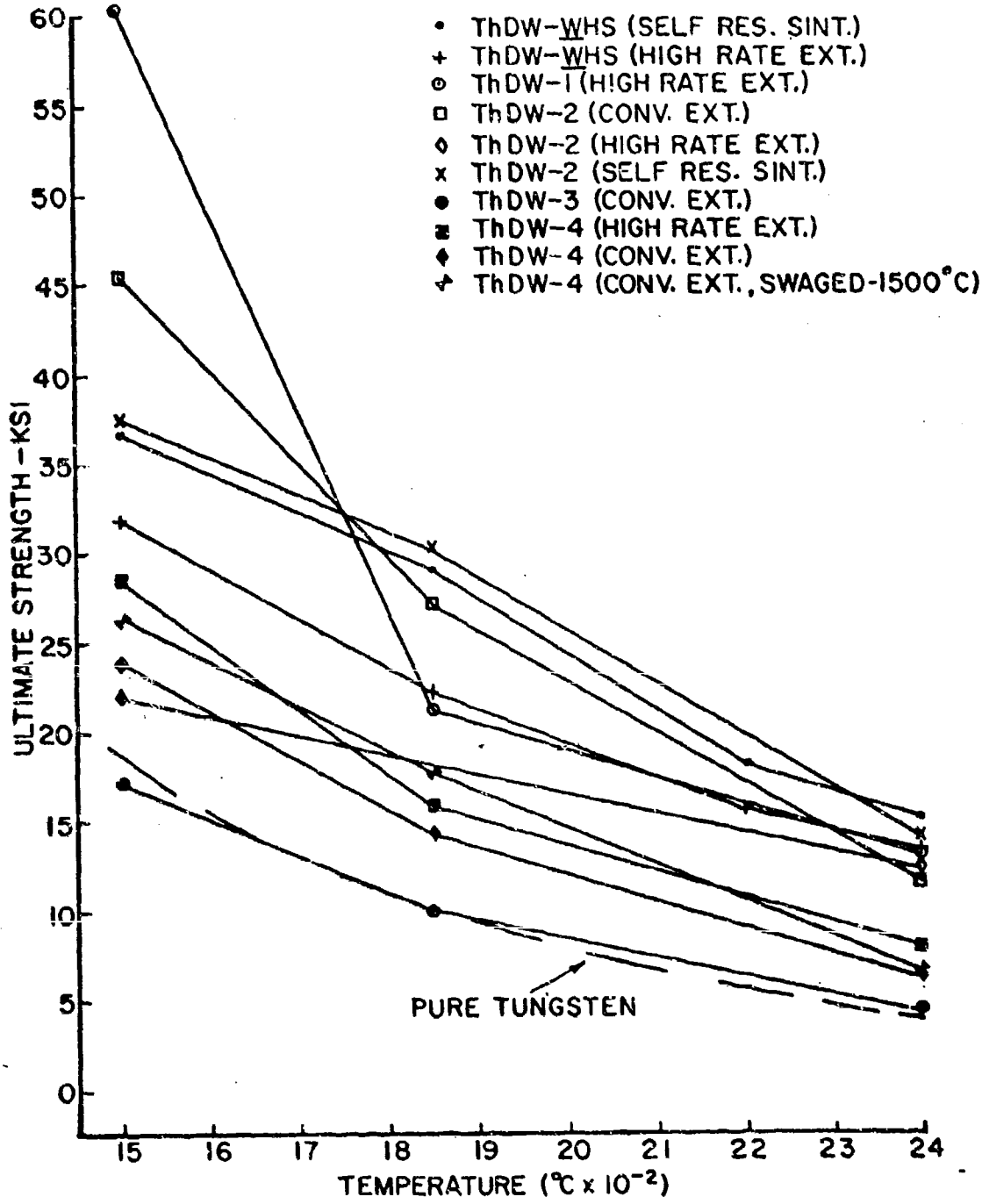

FIG. 42 ULTIMATE TENSILE STRENGTHS OF W-ThO_2 ALLOYS AS A FUNCTION OF TEMPERATURE.

H. Discussion of Experimental Alloy Results

The preparation and processing of the four experimental alloys were planned to explore the effects of a number of parameters on tensile properties. The data which resulted will be discussed as it relates to the areas of chemical processing, agglomeration inhibitors, thoria concentration, consolidation method, break-down method and thermo-mechanical effects, in that sequence. A final section will be concerned with replication results.

The properties determined demonstrate unequivocally that major property differences arise in the W-ThO_2 system as a function of mode of incorporation of the second phase. In the two superior alloys (ThDW-1 and 2), the most notable difference is the addition of the $Th(NO_3)_4$ solution to the oxide powder prior to reduction, rather than to the metal powder after reduction. The use of tumble drying in the preparation of these alloys may have contributed to strength improvement, but, in view of the poor properties of the freeze dried batch (ThDW-3), in which it is difficult to conceive appreciable $Th(NO_3)_4$ segregation during drying, it is believed that tumble drying is not the influential factor. This leads to the conclusion that porosity in the oxide powder (or some other morphological characteristics) is the cause in promoting the desired dispersion. This result is in general agreement with earlier experiences at this laboratory in that the introduction of ultrafine thoria powder to WO_3 did not yield a significant increase in high temperature tensile strength (32). Maykuth, et.al. (4) have also reported severe agglomeration of thoria during consolidation in a system in which the $Th(NO_3)_4$ solution was added to a reduced metal powder.

In previous work (1), it was indicated that Al and Si compound additions were effective in inhibiting agglomeration of ThO_2 particles. In the present work, the same effect is also indicated. The exceptional tensile strength of the ThDW-1 alloy at 1500°C may reflect a finer dispersion or may simply reflect the additional concentration of second phase which results (as in the case of commercial lamp tungsten) from the addition of these salts. The sharp drop in strength at higher temperatures can be explained on the basis that the Al and Si compounds would be expected to begin liquefying around the lowest test temperature and to become completely liquid above 2050°C (this does not consider possible two and three component phases with ThO_2). Fabrication results show that the workability of this alloy has been impaired by the addition of the Al and Si compounds.

In regard to dispersoid concentration, the direct comparison of the properties of ThDW-2 (self-resistance sintered) and ThDW-WHS, with 5.7 v/o and 3.8 v/o ThO_2, respectively, shows that the increased amount of ThO_2 did not appreciably enhance the high temperature strength. A similar effect was observed by Fraser, et.al. (33) in a Ni-ThO_2 system. This result may be attributed

to a higher degree of agglomeration in the 5.7 v/o alloy which might be expected to arise either from the closer proximity of the particles during processing or conceivably from the inability of the tungsten oxide particles, as a result of their morphology to effectively retain additional ThO_2.

The strength advantage of alloys consolidated by self-resistance sintering over those consolidated by hot pressing, though small, is believed to be significant. It is suggested that the difference observed may be due to a more thorough removal of trace impurities by self-resistance sintering in H_2 and/or to a minor pick-up of carbon from the mold in hot pressing.

The mechanical property data derived from materials in which the breakdown technique was varied (high rate extrusion vs. conventional extrusion, vs. direct swaging) can be interpreted to show that the material properties are relatively insensitive to the range of techniques employed. This broad latitude of feasible breakdown techniques is quite encouraging for future work.

The slightly improved strength of the ThDW-4 alloy swaged at the lower temperature does not necessarily predict similar improvements in the higher strength alloys. However, in view of the marked dependence of the strength of TD-nickel on thermo-mechanical treatment (34), such a prediction is believed reasonable, and further work is warranted in this area. At this point, it is significant to note that grain size (which is a result of thermo-mechanical treatment) is not reflected in the relative strengths of the alloys. In fact, the strongest alloy at 2400°C (ThDW-WH3) having a lower ThO_2 concentration and a particle size and distribution quite similar to ThDW-1 and 2, has a grain size orders of magnitude larger (Figs. 26, 27, and 28). In this light, the strength of that alloy must arise solely as a result of retained substructure and/or of the second phase particles.

The large number of replica micrographs taken (80-90 specimens, $\sim$ 500 plates) to implement the present study reveal numerous interesting but--in many cases--incompletely understood effects. As noted earlier, transverse sections consistently showed fewer fine particles than longitudinal ones; also, as may be seen from the replica micrographs as a whole, different surface features were developed in various alloys as the result of etching (e.g. many micrographs show a clear effect of anisotropic etching). All of these effects compounded the uncertainty in attempting to quantitatively evaluate particle size and distribution from surface replicas.

The frequency with which fine particles are observed at the apices of etch pits is construed to indicate either a strain field associated with the particles (contrast effects of such a field have not been observed in transmission) or the association of particles with dislocations (this has been observed in transmission on the ThDW-WHS alloy). Quite frequently, small "pits" are observed around the periphery of larger particles (e.g. Fig. 36, right, a and b). No concrete explanation can be advanced for this phenomenon, though it may be conjectured to result from impurity segregation and subsequent selective etching. In a number of specimens (e.g. Fig. 40, gage section), an apparent porosity is frequently evident at necks and ends of the larger particles in the gage sections of tensile specimens tested at 2400°C. This can tentatively be attributed to fracturing of these particles as a result of stresses applied to them due to the matrix deformation. Such fracturing would presumably be inhibited under the essentially hydrostatic compressive stresses applied during fabrication.

It should be noted, as a final point, that there is reasonable correspondence between the replica observations on ThDW-WHS and the extraction and transmission observations presented earlier. Of course, with particles as fine as those present in transmission specimens, a greater density of particles will be observed because of the thickness of the foil. Nevertheless, estimates of both particle size and interparticle spacing from the ThDW-WHS replicas are in fair agreement with the same parameters presented in Table 9 for extraction specimens.

III. W-Re-ThO_2 Alloys

The development of a dispersed second phase alloy with a tungsten-rhenium solid solution matrix has retained considerable interest because of the beneficial effects of rhenium on the low temperature ductility of tungsten (35) and the insignificant strength improvement by rhenium alone at temperatures exceeding 2000°C (36, 37). Recently, Maykuth, et.al (4) have found low temperature ductility in a W-5 w/o Re-2.2 w/o ThO_2 alloy produced by a special powder metallurgy technique, but the high temperature strength properties of this alloy (determined only to ~1930°C in the recrystallized condition) were not much better than those of pure tungsten. Earlier high temperature results in this laboratory on W-25 w/o Re-1.9 v/o ThO_2 (37) also have not been encouraging.

The work discussed in the following was concerned only with the effects of a thoria dispersion on the high temperature strength properties of W-Re alloys of varying Re concentration. This emphasis on high temperature strength rather than on low temperature ductility was in line with the basic objective of this contract program.

The experimental program had the benefit of material contributions by the Chase Brass and Copper Company.

A. Preparation of Alloys

The alloy compositions listed in Table 19 were selected for this program. Unfortunately, attempts to produce alloys No. 4 and No. 5 were not successful. The alloys prepared in this laboratory were prepared by the following technique:

Elemental powders were first sieved through a 325 mesh sieve and then blended together in a twin shell blender for 20 hours. The two elemental powders used for alloys ThDW/Re-1 and ThDW/Re-2 were powder from the experimental batch ThDW-2 (Section II-A-1) and pure rhenium powder purchased from the Chase Brass and Copper Company.

The blended compositions were pressed at 30 KSI into 24 in. long x 0.375 in. sq. bars. With the exception of composition No. 4, no problems were encountered in pressing. Composition No. 4 (W-5 w/o Re-5 v/o ThO_2) did not press readily, in that the pressed ingot was very fragile. The fourth pressing attempt finally yielded two pieces of swagable length. All pressed bars (including two sections from Alloy No. 4) were presintered in H_2 at 1100°C for 1 hour. Bars of alloys Nos. 1, 2, 3, and 5 were then self-resistance sintered in H_2 to the densities listed in Table 19 by raising the temperature within 10 minutes from room temperature to about 2800°C and holding at 2800°C for 20 minutes. Composition No. 4 which did not yield a pressed bar of sufficient length for self-resistance sintering was vacuum sintered (two 7 inch lengths) at 2750°C for 45 minutes. As normally observed in tungsten sintering, the vacuum treatment did not result in as high densities as the self-resistance sintering, in an H_2 atmosphere. The final densities were 16.0 and 16.5 gm/cc, respectively.

Attempts were made to swage the sintered ingots from preheat temperatures of about 1850°C. When severe cracking was encountered in alloys Nos. 2, 4, and 5, the remaining sound pieces were encapsulated in Mo. In spite of this precaution, material suitable for the machining of tensile specimens was not obtained from the Alloy No. 4 (W-5 w/o Re-5 v/o ThO_2), and only a piece long enough for two tensiles was obtained from

Alloy No. 5 (W-10 w/o Re-5 v/o ThO_2). Some difficulty was also encountered in swaging the W-10 w/o Re, W/Re-Control No. 2 (Table 19).

In contrast to the poor material yield at this laboratory, the alloys (CBC Nos. 6-9) from Chase Brass and Copper Company, which were consolidated by a similar technique, could be fabricated. The supplier provided the following processing information:

> "Dry blended powders were pressed into 9 inch long x 9/16 in. sq. bars at 60 KSI. The pressed bars were consolidated by presintering at 1650°C followed by sintering at 2550°C brightness for 3 hours, both steps carried out in hydrogen. The sintered ingots were hot worked by swaging. When at 1/2 in. dia., the rods were annealed in hydrogen for 5 minutes at 2550°C brightness in a resistance bell. The material was then further hot swaged down to size with about 15% reduction per pass. After the finishing pass (0.188 in. dia.), the samples furnished were given a stress relieving treatment of 15 minutes in H_2 at 1650°C."

B. High Temperature Tensile Properties

A relatively complete set of high temperature strength data was obtained up to 2400°C. Tests were conducted in vacuum of $\sim 10^{-5}$ torr on specimens annealed for 1/2 hour at 2400°C. The strain rate was 0.05 min^{-1}, and for the CBC-alloys (Nos. 6-9), 2.0 min^{-1} was also employed. The test data have been compiled in Table 20. Included in this table are test results for pure tungsten.

The effect of various rhenium concentrations on the tensile strength of pure tungsten and the effect of thoria on W-Re solid solutions at the strain rate 0.05 min^{-1} are seen in Fig. 43. To better delineate the effect of thoria and facilitate the comparison with the temperature dependence of the tensile strength of pure tungsten and the superior W-3.8 v/o ThO_2 alloy (ThDW-WH3), the data are replotted in Fig. 44. In addition, the effect of strain rate is displayed in Fig. 45.

It will be noted that rhenium strengthens tungsten up to 2400°C. The strength increment (Fig. 46) is directly proportional to rhenium concentration and is temperature dependent but drops to an insignificant value above 2000°C ($<$5000 PSI), being essentially concentration independent above that temperature. The decrease in strength with increasing temperature

Table 19

W-Re and W-Re-ThO_2 Alloys Prepared by Powder Blending, Sintering of Cold Pressed Bars and Swaging

No.	Designation	Composition	Sintered Density g/cm^3
1	W/Re-Control 1	W-5 w/o Re	18.35
2	W/Re-Control 2	W-10 w/o Re	18.45
3	W/Re-Control 3	W-25 w/o Re	18.00
4	ThDW/Re-1	W-5 w/o Re-5.0 v/o ThO_2	16.0 and 16.5
5	ThDW/Re-2	W-10 w/o Re-5.0 v/o ThO_2	18.2
6*	CBC-1	W-5 w/o Re-3.8 v/o ThO_2	----
7*	CBC-2	W-10 w/o Re-3.8 v/o ThO_2	----
8*	CBC-3	W-15 w/o Re-3.8 v/o ThO_2	----
9*	CBC-4	W-24 w/o Re-3.8 v/o ThO_2	----

* Supplied by the Rhenium Division of the Chase Brass and Copper Company, Waterbury, Connecticut.

Table 20

High Temperature Tensile Properties of Annealed (1/2 Hr. 2400°C)
W-Re and W-Re Dispersed Phase Alloys Tested at 0.05 min^{-1}

Alloy	Test Temp.,°C	0.2% Y.Str., KSI	Ult.Str. KSI	% Unf.Strain*	% Elong.	% R.A.
Pure W	1500	4.7	18.6	25	51	82
	1850	5.6	10.2	18	41	48
	2200	2.4	5.0	8	17	59
	2400	2.3	3.5	4	13	15
W-5 w/o Re	1500	17.7	28.9	19	61	89
	1850	9.6	14.7	15	42	56
	2200	3.8	6.4	10	28	24
	2400	2.8	4.6	6	26	25
W-10 w/o Re	1500	22.7	34.0	18	47	60
	1850	13.8	17.1	11	28	27
	2400	4.7	5.0	2.5	31	25
W-25 w/o Re	1500	33.6	40.5	11	35	36
	1850	16.1	16.7	1.7	24	35
	2200	6.9	7.0	1.2	36	37
	2400	4.0	4.0	1.5	22	27

* Derived from Engineering Stress-Strain Curve.

Table 20 (cont'd.)

High Temperature Tensile Properties of Annealed (1/2 Hr. 2400°C)
W-Re-ThO2 Alloys Tested at Two Strain Rates, 0.05 min^{-1} and 2.0 min^{-1}

Alloy	Test Temp., °C	0.2% Y.Str., KSI		Ult.Str., KSI		% Unf.Strain*		% Elong.		% Red. in Area	
		a	b	a	b	a	b	a	c	a	b
CBC-1	1500	23.3	26.3	34.7	45.9	15	22	31	37	33	41
	1850	16.8	16.9	19.6	25.5	5	16	17	36	21	36
	2400	4.2	10.2	5.2	10.8	6	4.3	25	54	26	44
	"	----	11.3	----	11.9	--	8	--	55	--	47
CBC-2	1500	27.8	30.7	39.1	53.8	11	19	24	38	26	35
	1850	16.9	28.4	19.3	28.4	7	4	17	22	21	26
	2400	5.8	13.3	6.5	13.3	4	0	22	41	20	39
CBC-3	1500	34.7	40.5	42.3	54.0	12	14	28	29	31	30
	1850	20.2	28.9	21.3	33.1	1.8	9	25	20	27	26
	2400	5.6	14.6	6.5	14.6	2.7	0	34	52	32	48
CBC-4	1500	43.5	44.2	47.0	57.2	7	14	16	28	20	30
	1850	23.5	31.0	23.5	32.2	0	4.4	14	22	16	21
	2400	6.1	12.7	6.2	12.7	0.8	0	22	38	21	34
ThDW/Re-2	1500	50.5	----	53.1	----	1.6	----	9	--	14	--
	2200	4.2	----	5.6	----	3.5	----	16	--	13	--

* Derived from Engineering Stress-Strain Curve.

a - 0.05 min^{-1} strain rate

b - 2.0 min^{-1} strain rate

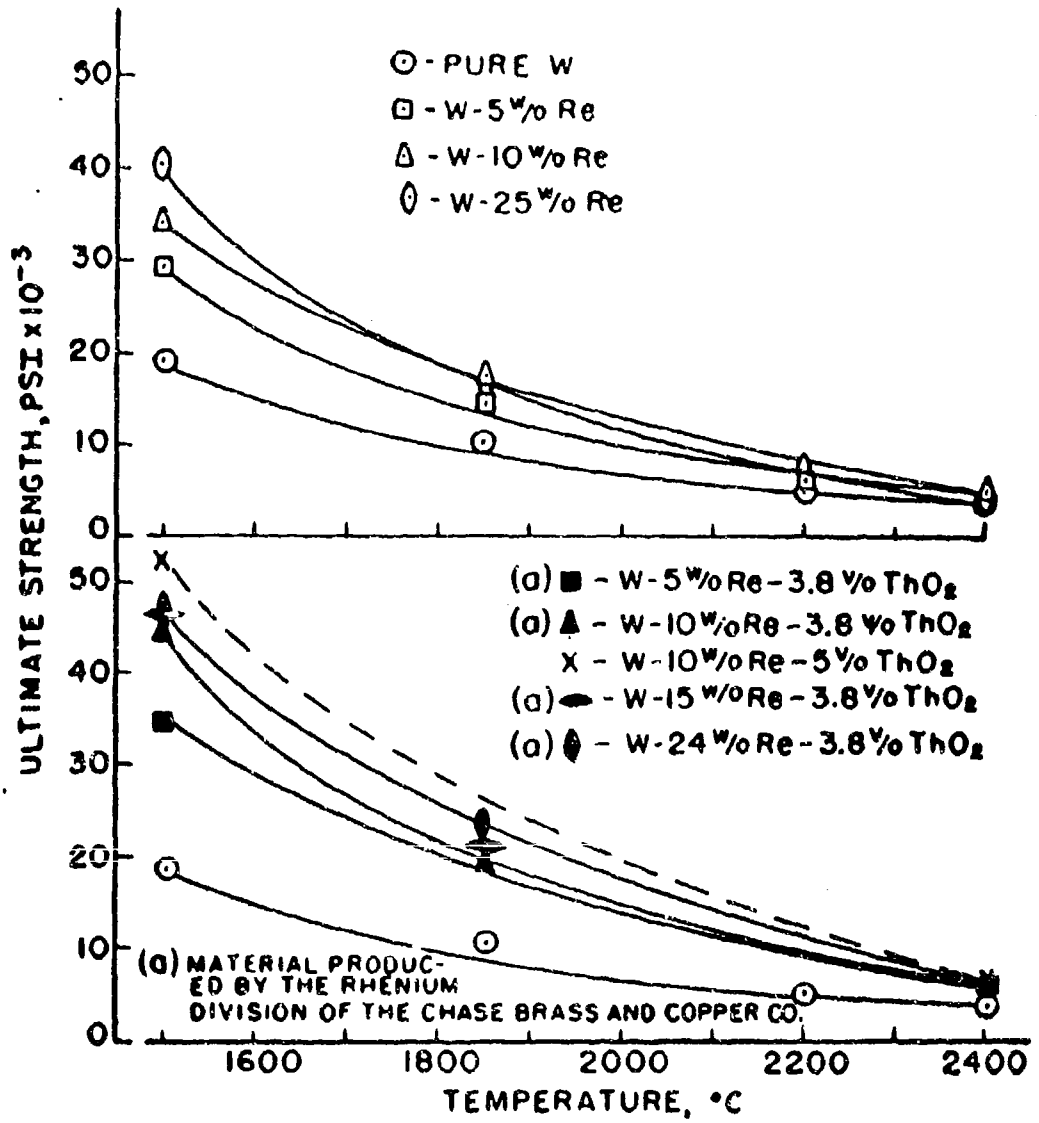

FIG. 43 HIGH TEMPERATURE STRENGTH OF PURE TUNGSTEN IN COMPARISON WITH W-Re AND W-Re-ThO_2 ALLOYS ANNEALED ½ HR. AT 2400 °C ($\dot{\epsilon}$=0.05 MIN^{-1}).

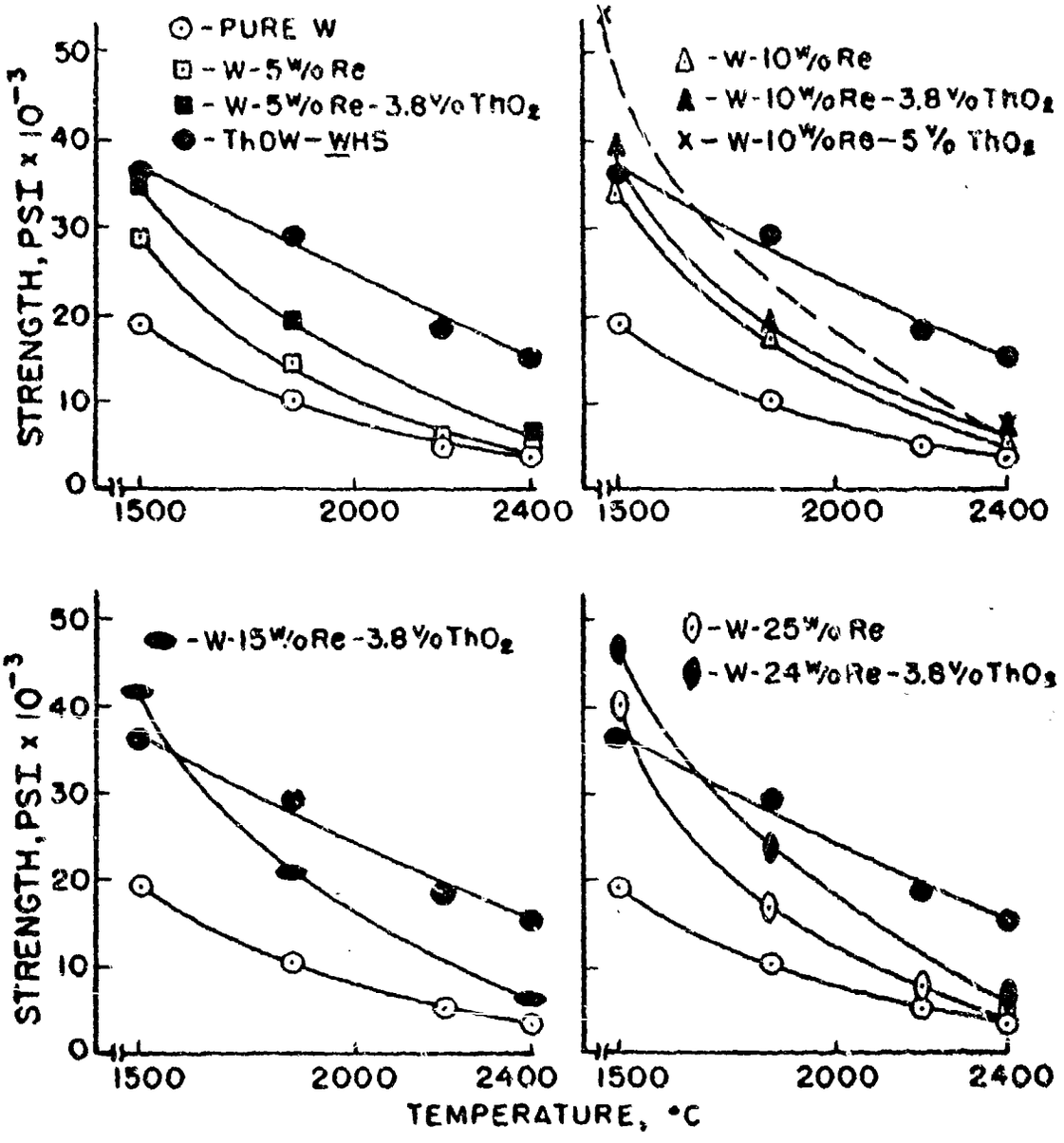

FIG. 44 COMPARISON OF THE HIGH TEMPERATURE TENSILE STRENGTH OF ANNEALED (1/2 HR. 2400°C) W-Re AND W-Re-ThO_2 ALLOYS WITH PURE W AND ThOW-WHS ($\dot{\epsilon} = 0.05\ MIN^{-1}$).

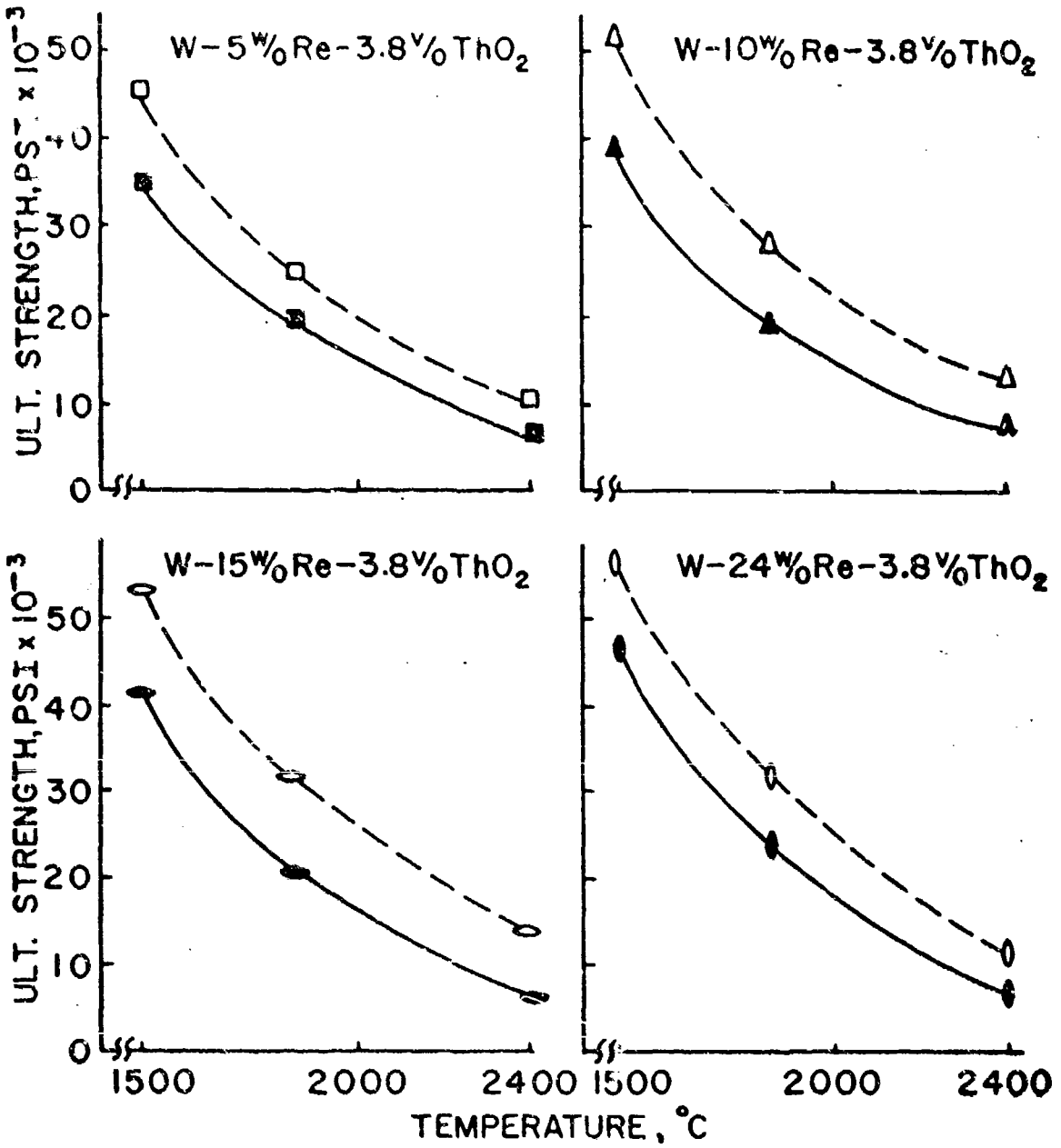

FIG. 45 THE EFFECT OF STRAIN RATE ON THE HIGH TEMPERATURE TENSILE STRENGTH OF W–Re–ThO_2 ALLOYS (—— $\dot{\epsilon}$ = 0.05 MIN^{-1}; – – – $\dot{\epsilon}$ = 2.0 MIN^{-1}).

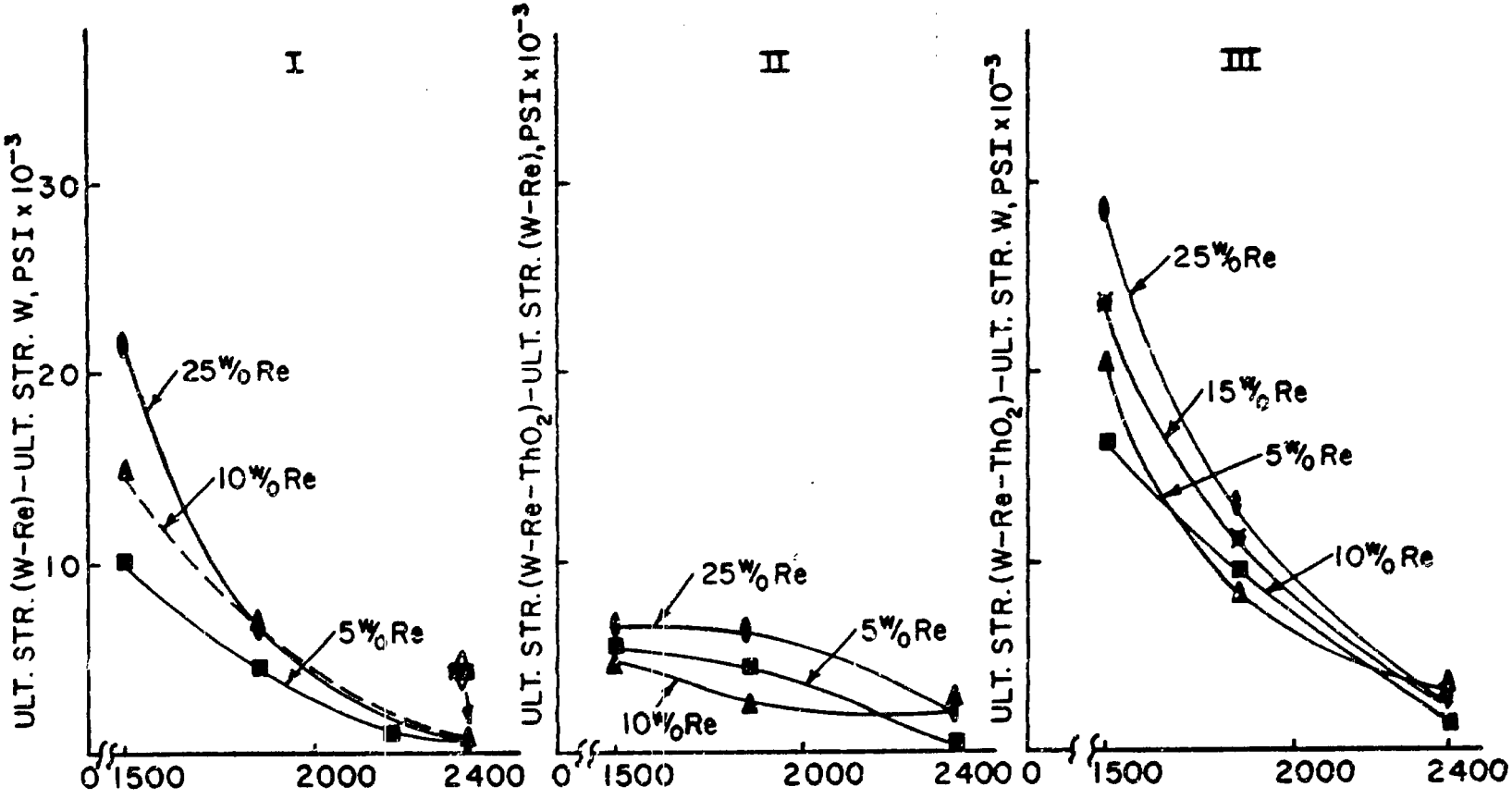

FIG. 46 INCREMENTAL CONTRIBUTIONS OF: (I.) RHENIUM TO THE STRENGTH OF PURE W, (II) 3.8 V/o THORIA TO THE STRENGTH OF W-Re ALLOYS, AND (III) RHENIUM + THORIA TO THE STRENGTH OF PURE TUNGSTEN ($\dot{\epsilon} = 0.05$ MIN^{-1})

is thus much greater for the alloy with the highest rhenium concentration (Control No. 3, 25 w/o Re).

The 3.8 v/o thoria dispersion improves the strength of all W-Re alloys. For the low rhenium concentrations (5 w/o and 10 w/o Re), the thoria contribution at 1500°C is large (~50%); for the high rhenium concentration (25 w/o Re), its contribution to the strength at the same temperature is < 20%. In general, the strength increment due to the dispersed second phase of thoria is much less temperature dependent than that due to the rhenium solid solution. The additive effect of both the rhenium and the thoria is such that an improvement in strength (> 5000 PSI) is achieved up to 2000°C for all low rhenium concentrations.

The strength increment due to rhenium plus thoria at 1500°C is equal to or exceeds that resulting from thoria alone (Fig. 44). But in no case are these rhenium containing alloys stronger than W-3.8 v/o ThO_2 (ThDW-WHS) at temperatures > 1700°C.

As it is normally observed, the tensile strength of the W-Re-ThO_2 alloy increases with increasing strain rate (Fig. 45). The strength increment resulting from a change in strain rate from 0.05 min^{-1} to 2.0 min^{-1} appears to be little affected by either rhenium concentration or by temperature.

C. Discussion of Results

The most important result is that rhenium is deleterious to the strength imparted to pure tungsten by a fine thoria dispersion at temperatures exceeding 1700°C. Two factors can account for this effect: (1) particle size distribution, and (2) the effects of rhenium on recrystallization and dynamic recovery.

1. As shown in Fig. 47a for the alloy CBC-2, which is representative of all the CBC alloys, the particle distribution is rather coarse. In contrast, the alloy ThDW/Re-2 was prepared from ThDW-2 (known to contain a fine dispersion) and exhibits a much finer dispersion (Fig. 47b) than the CBC alloys. The finer dispersion of the latter alloy is also indicated from its much higher strength at 1500°C (Fig. 44). In fact, with the exception of ThDW-1, this alloy had the highest tensile strength (53,100 PSI) of all alloys tested at 1500°C. It can thus be said that ThDW/Re-2 has a fine dispersion which, however, is rendered ineffective by rhenium at high temperatures (5600 PSI vs. 16000 PSI of the best W-ThO_2 alloy).

2. The W-Re and W-Re-ThO_2 alloys, as distinct from the W-ThO_2 alloys, completely recrystallize when annealed at 2400°C for 1/2 hour, whereas only recovery occurs in the W-ThO_2 alloys. This essentially equiaxed structure is shown in Figs. 48a and 48b for CBC-2 and ThDW/Re-2. Micrographs of gage sections of

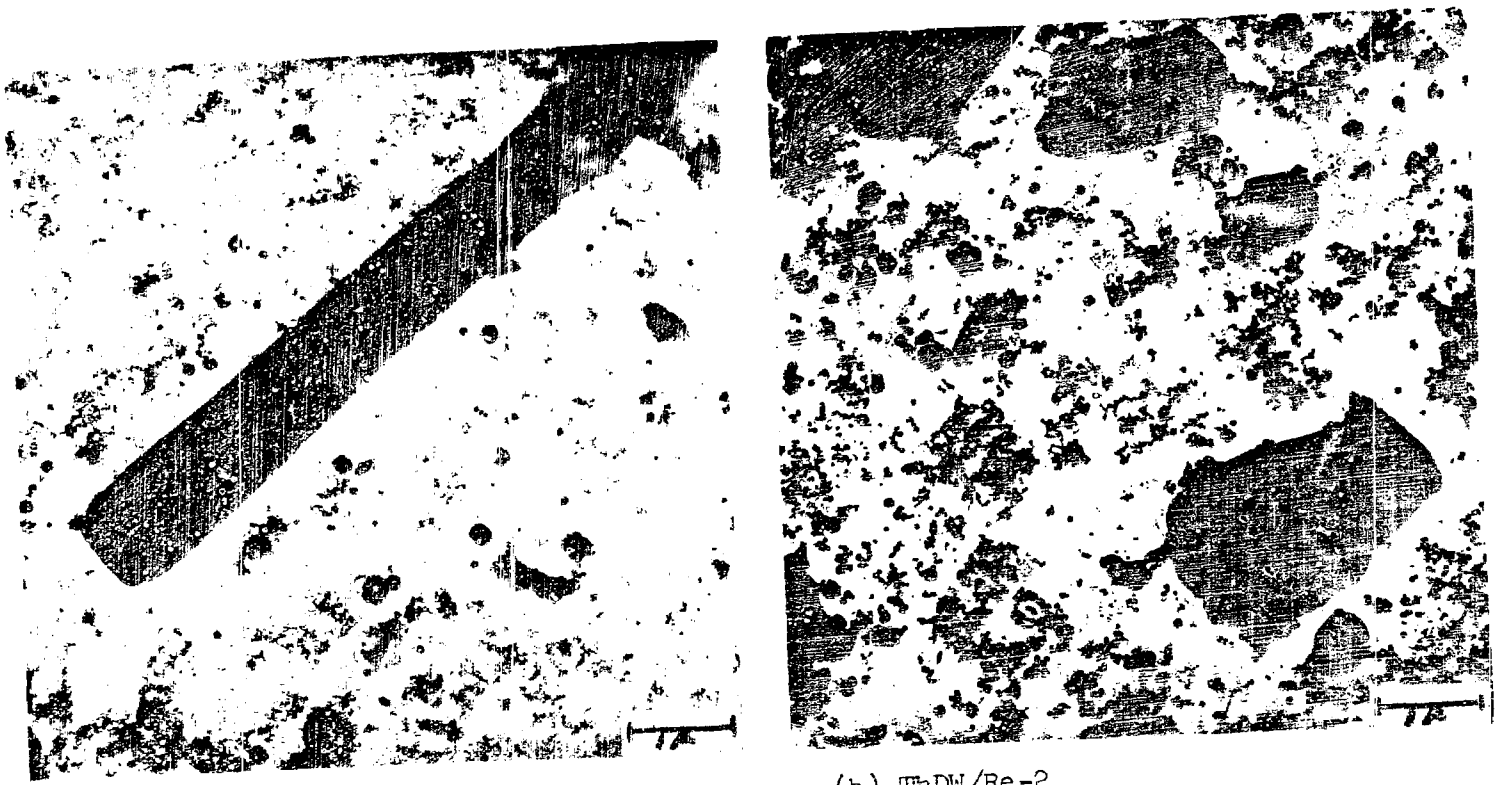

(a) CBC-2

(b) ThDW/Re-2

Fig. 47 Extraction Replicas of W-Re-ThO_2 Alloys - 15000X

(a) CBC-2 (W-10 w/o Re-3.8 v/o ThO_2)-300X

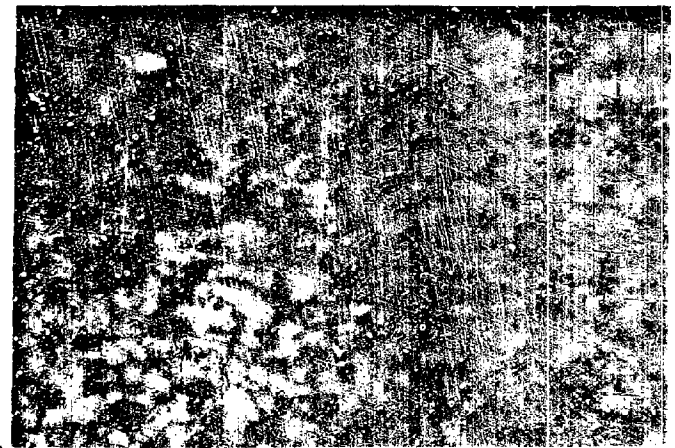

(b) ThDW/Re-2 (W-10 w/o Re-5 v/o ThO_2)-1500X

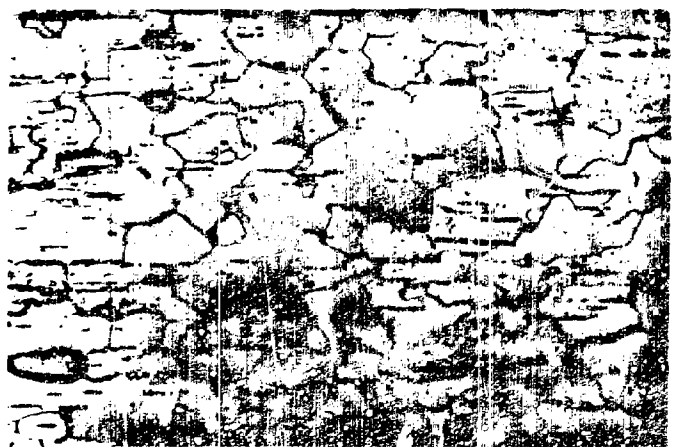

(c) CBC-2 (W-10 w/o Re-3.8 v/o ThO_2)-300X

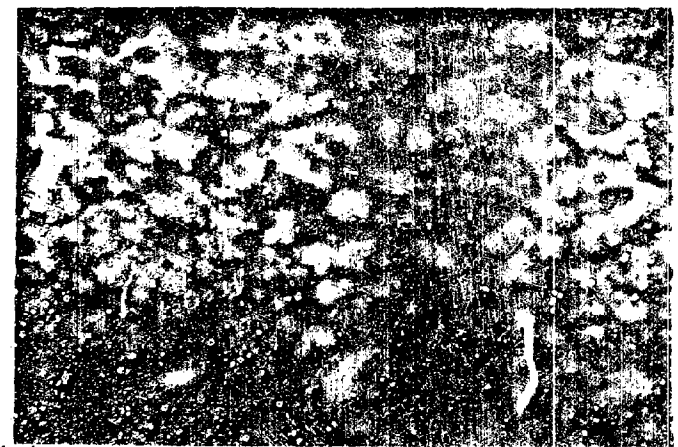

(d) ThDW/Re-2 (W-10 w/o Re-5 v/o ThO_2)-1500X

Fig. 48 Photomicrographs of W-Re-ThO_2 Alloys - Top: After Annealing at 2400°C for 1/2 Hr. Bottom: After Testing to Fracture at 1500°C Following Annealing at 2400°C for 1/2 Hr.

the same alloys tested to fracture at 1500°C are reproduced in Figs. 48c and 48d. This comparison clearly shows that the structure morphology has not changed and the grain size is the same as or larger than that of the recrystallized materials. The main factor, therefore, by which rhenium suppresses the high temperature strength is via its effect on promoting recrystallization and dynamic recovery by increasing the mobility of grain boundaries in these alloys.

This is corroborated by the stress-strain behavior of the higher strength W-Re and W-Re-ThO_2 alloys (Fig. 49), which shows that a dynamic recovery type mechanism is active. In this case, as previously noted (37), the negative slope of the stress-strain curves after small strains is not the result of plastic instability.

IV. SUMMARY

This report marks the end of an extended and successful effort aimed at developing a dispersed second phase alloy of tungsten with superior strength properties in the temperature range 3500 to 5500°F. In the course of this effort, many disparate approaches have been attempted and many hypotheses have been confirmed or disproven. It is thus only appropriate that the work be reviewed, the achievements be put into proper perspective, and guidance be given to further endeavors in this field.

The highest strength dispersed second phase alloy developed in all this work is the alloy W-3.8 v/o ThO_2 (ThDW-WHS). Its development has been closely paralleled by the concurrent development of high temperature testing facilities, hot compaction methods, extrusion techniques, and electron metallography. In very early work (2, 3) an alloy of this same composition was investigated together with other dispersed second phase alloys of tungsten (W-ZrO_2, W-HfO_2, W-SiO_2, W-TaC, W-NbC, W-WB, W-W_2B and W-B_4C). Testing was then conducted up to 3000°F and evaluation was primarily performed by optical microscopy. The tensile test results favored this W-ThO_2 alloy and a W-TaC alloy over all the other alloys. The W-0.38 w/o TaC alloy was later found to lose its strength advantage at temperatures above 3500°F because of instability of the TaC second phase.

Considering the W-ThO_2 alloy system, the opinion prevailed that high strength at high temperatures could be achieved if only a fine enough thoria dispersion could be retained through processing into the worked alloy. At that stage, the W-ThO_2 alloy showed its best properties when it was prepared by slurrying WO_3 with a $Th(NO_3)_4$ solution, followed by firing in air at

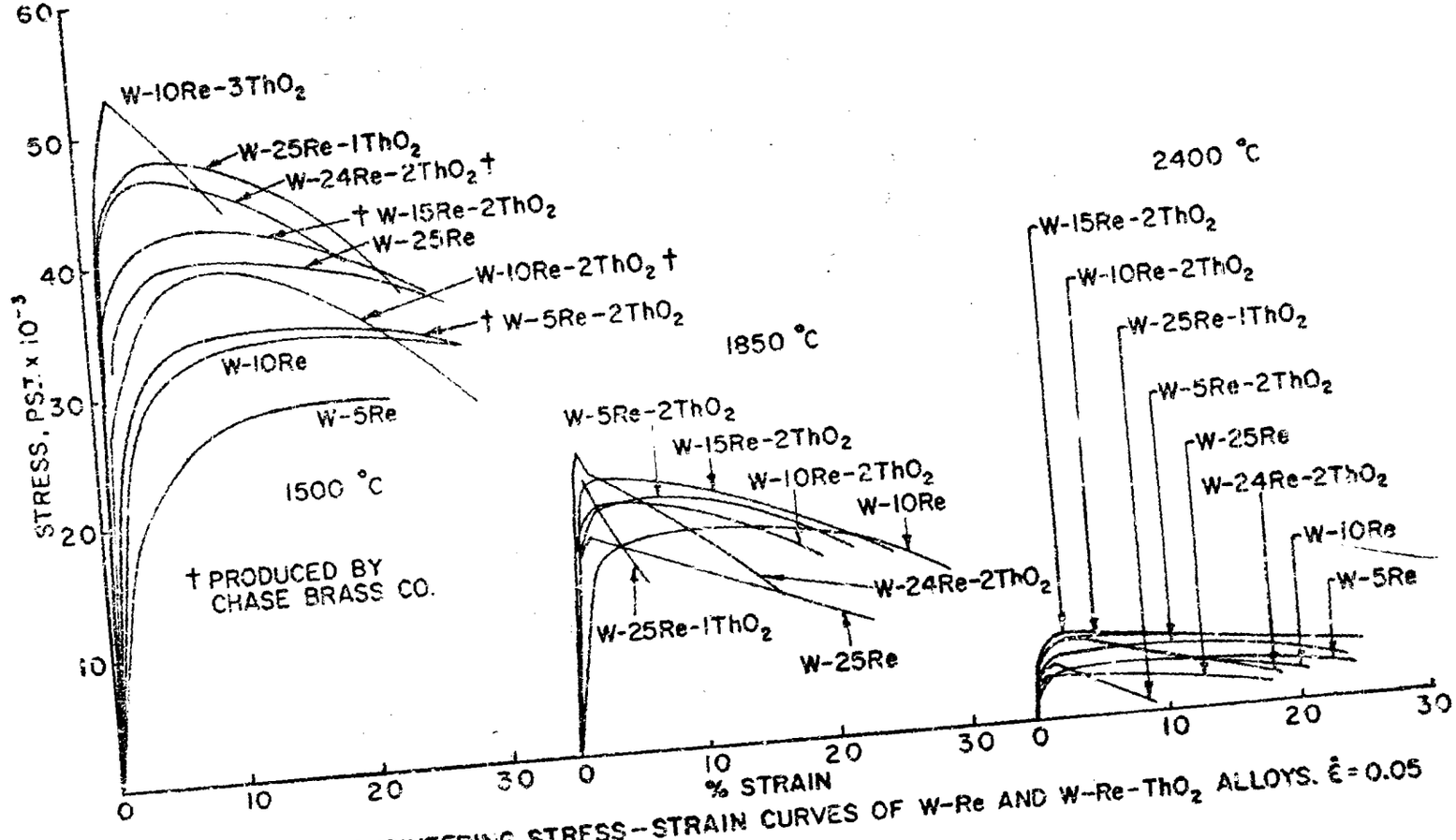

FIG. 49 SUMMARY OF ENGINEERING STRESS–STRAIN CURVES OF W-Re AND W-Re-ThO_2 ALLOYS. $\dot{\epsilon} = 0.05$ MIN^{-1} ANNEALED ½ HR. AT 2400 °C

800°C, and, subsequently, by reduction to metal powder in H_2. Tensile properties at 3000°F are summarized in Table 21 for this alloy as well as for other W-ThO_2 alloys made by other methods under these programs. A similar alloy, the second alloy listed in Table 21, made by a co-precipitation technique outlined in Table 21 had lower tensile strength. In a subsequent approach, a W-1.9 v/o ThO_2 alloy was prepared by dry blending of WO_3 powder with submicron size thoria powder purchased from the Vitro Company, but this alloy had strength properties which were barely better than those of pure tungsten.

The hypothesis was then advanced that the failure to realize strength levels in the W-ThO_2 system, theoretically predicted by the simple Orowan equation, was the result of agglomeration of the second phase during consolidation because of the high temperatures used in self-resistance sintering. With this in mind, another alloy, W-3.8 v/o ThO_2 (#4, Table 21), was consolidated by hot pressing instead of self-resistance sintering and was worked first by extruding instead of swaging. Its properties in the extruded condition were still not satisfactory; however, considering the relatively unworked state of the alloy, they were encouraging. Still working on this hypothesis, a new program was initiated which encompassed the screening of 11 alloy systems, including W-ThO_2. All alloys were made by milling (which had shown promise for ultrafine comminution) and hot compaction with Dynapak extrusion as the breakdown method. Again, the W-ThO_2 alloy (No. 5) exhibited the best properties of all the alloys screened from the combined standpoints of high temperature strength and fabricability. However, electron microscopy, employed extensively by this time, revealed that hot compaction did not prevent agglomeration from occurring, and the present work has, in fact, shown that the method of consolidation is of secondary importance.

The results from the screening program encouraged another attempt to produce a superior W-ThO_2 alloy, but this time with primary emphasis on chemical techniques of powder preparation. The program evolved along this line has culminated in the development of a very high strength W-3.8 v/o ThO_2 alloy (#7 in Table 21), now available in rod form. The tensile properties of this alloy combined with information on particle size and interparticle spacing obtained by electron microscopy have demonstrated that dispersion strengthening of tungsten at extremely high temperatures (4000-5000°F) is now a reality.

When better fabricability is desired, this can be achieved by reducing the ThO_2 concentration of the alloy (Alloy #6, Table 21), yet the strength properties are still significantly improved over those of pure tungsten.

Table 21

Evolution of a High Strength W-ThO_2 Alloy*

Preparation Technique	Strength at 3000°F 0.2% Y.S. (PSI)	Strength at 3000°F Ult. S. (PSI)
1. Submicron precipitated tungsten oxide + $Th(NO_3)_4$ → fire in air (600°C) → reduce in H_2 → press and sinter → swage.	21,000(a) 10,300(b)	27,000(a) 15,200(b)
2. K_2WO_4 + Th/HCl sol. → copp't in COOHCOOH/HCl → wash and dry pp't. → fire in air (800°C) → reduce in H_2 → press and sinter → swage.	20,000(a)	21,500(a)
3. WO_3 + powder of submicron size 1.9 v/o ThO_2 → dry blend → reduce in H_2 → press and sinter → swage.	10,500(d)	14,500(d)
4. The same as #1, except hot pressed and extruded.	19,000	25,000
5. Tungsten oxide from APT + $Th(NO_3)_4$, reduce in H_2 → hot press → Dynapak extrude → swage	23,000(b)	24,000(b)
6. Same as #5, except 1.9 v/o ThO_2 and self-resistance sintered.	18,000(c)	20,000(c)
7. Same as #5, except self-resistance sintered.	30,000(d)	33,000(d)

* Except otherwise noted, annealed at 2400°C for 1/2 Hour.

(a) Annealed 1/2 Hour at 1600°C
(b) Annealed 1/2 Hour at 2200°C
(c) Extrapolated from higher temperature data
(d) Interpolated from tensile data

The key to the ultimate strengthening obtained in this alloy is deduced to be the requirement that the tungsten oxide particles must have a high degree of porosity for the $Th(NO_3)_4$ solution to be absorbed in an effective fashion. In the subsequent H_2 reduction, the thoria which forms is either tightly embedded on the surface or occluded in the tungsten particles.

This deduction is supported by two facts: (1) concentrations >4 v/o of thoria do not significantly improve the strength of this alloy and (2) clusters of discrete particles in the size range 50-500Å which are revealed by electron microscopy cannot be conceived to arise in any other fashion in view of the particle size of the oxide powder ($\sim 20\mu$). A similar concentration effect has been observed in the Ni-ThO_2 system (33) where thoria concentrations >4 v/o do not add measurably to strengthening. Thoria which has not been absorbed by the oxide particles is likely to agglomerate because of its higher mobility during the drying process and possibly in subsequent processing steps, particularly consolidation. Impurities may accelerate this process.

The exceptional properties of ThDW-WHS as a function of working variables have only been explored to a limited extent in the present work. Certainly, thermo-mechanical history as a variable still needs to be investigated and fabrication into sheet, rather than rod, is essential to exploit the alloy for practical application. Two approaches suggest themselves for a sheet rolling program:

(1) Roll from self-resistance sintered (1/2 x 1-1/2" cross section) and forged bars.

(2) Roll sheet bars extruded from either hydrostatically compacted and sintered billets or hot pressed billets.

In both of these approaches, considerable effort will be demanded to optimize properties as a function of working schedule.

Any advantage which appeared to be possible by the addition of rhenium has been negated by this work. Although rhenium can be expected to improve the low temperature ductility of the W-ThO_2 system, the loss in high temperature strength defeats the objective of this effort. Furthermore, it is yet to be resolved whether or not the best ductility has been achieved in the W-3.8 v/o ThO_2 alloy. The fundamental ramifications of these findings have broader significance and should be studied.

V. REFERENCES

1. Sell, H. G., Morcom, W. R., King, G. W., and Cerulli, N. F., "Development of Dispersion Strengthened Tungsten Base Alloys", AFML-TR-65-407, Part I, November, 1965.

2. Atkinson, R. H. and Staff, "Physical Metallurgy of Tungsten and Tungsten Base Alloys", WADD-TR-60-37 (May, 1960).

3. Sell, H. G., Keith, G. H., Koo, R. C., Schnitzel, R. H., and Corth, R., "Physical Metallurgy of Tungsten and Tungsten Base Alloys", WADD-TR-60-37, Part II (May, 1961).

4. Maykuth, D. J., Grube, K. R., Ogden, H. R., Gilbert, A., Jaffee, R. I., and Blocher, Jr., J. M., "Further Development of a Ductile Tungsten Sheet Alloy", Bureau of Naval Weapons Contract N600(19)61982 Final Report, Period May 19, 1964 - October 31, 1965.

5. Kelly, A. and Nicholson, R. B., "Precipitation Hardening", Progress in Material Science, Vol. 10, No. 3, 336, Pergamon Press (1963).

6. Fisher, J. C., Hart, E. W., and Pry, R. H., Acta Met. 1, 336 (1953).

7. Jeffries, Z., Trans. AIME, 70, 303 (1924).

8. Anders, R. J., Alexander, G. B., and Wartel, W. F., Metals Progress 82, 88 (1962).

9. De Pierre, V. and Saul, G., "Effect of Thermo-mechanical Processing Variables on the Short Time 3000°F Tensile Properties of W-0.6 w/o Cb", WADD-TDR-63, 782, 1963.

10. White, J. E. and Jurkowitz, M. M., "Hot Pressing of Tungsten Powder", Contract No. AF04(695)-269, Report No. TDR-269(4240-10)-1, August, 1963.

11. Schneider, P., Chem. and Physics, 28, No. 4, 675 (1958).

12. Dushman, S. and Langmuir, I., Phys. Rev., Vol. 20, p. 113 (1922).

13. Koo, R. C., "Electron Microscopy", Sixth International Congress for Electron Microscopy, Kyoto, Japan, p. 573 (August, 1966).

14. Ashby, M. F. and Eheling, R. - To be published.

V. REFERENCES (cont'd.)

15. Kochs, V. F., Acta Met., 14, 11, p. 1628 (1966).

16. Cahn, R. W., "Recrystallization Grain Growth, and Textures", A.S.M., Metals Park, Ohio, October, p. 99, 1965.

17. Bailey, J. E., and Hirsch, P. B., Proc. Royal Soc., 267A, 11 (1962).

18. Orowan, E., "Dislocations in Metals", AIME, New York, p. 181 (1954).

19. Cahn, R. W., Proc. Royal Soc. (London), 63A, 323 (1950).

20. Petch, N. F., Phil. Mag., 1, 186 (1956).

21. Koo, R. C., Trans. AIME, 227, 280 (1963).

22. Stokes, R. J. and Cottrell, R. J., Proc. Royal Soc. A233, 17 (1955).

23. Armstrong, P. E. and Brown, H. L., Trans. AIME, 230, 5, p. 962 (1964).

24. Hirsch, P. B., J. Inst. of Met., 86, 13 (1957-58).

25. Ashby, M. F., Ph.D. Thesis, Cambridge University, 1961.

26. Seeger, A., Phil. Mag., 46, 1194 (1955).

27. Schoeck, G. and Seeger, A., Acta Met., 9, 382 (1961).

28. Schoeck, G., "Mechanical Behavior of Metals at Elevated Temperatures", McGraw-Hill Book Company, Inc., New York, p. 100, 1961.

29. Andelin, R. L., Knight, J. D., and Kahn, M., Trans. AIME 233, p. 19 (1965).

30. Hart, E. W., "Relation of Properties to Microstructures", A.S.M. p. 95 (1953).

31. Gilbert, E. R., Flinn, J. E., and Yaggee, F. L., "Fourth Symposium on Refractory Metals", AIME, October, 1965 - To be published.

V. REFERENCES (cont'd.)

32. King, G. W., Sell, H. G., Trans. AIME, 233, 1104 (1965).

33. Fraser, R. W., Meddings, B., Evans, D. J. I., and Mackiw, V. N., "Modern Developments in Powder Metallurgy, II", Plenum Press, 1966.

34. White, J. E., Ca[illegible]an, R. D., Trans. AIME, 230, 1298 (1964).

35. Booth, J. G., Jaffee, R. I., and Salkovitz, E. I., "Metals of the Space Age", Plansee Proceedings, 1964, Fifth Plansee Seminar, p. 457, Springer, 1965.

36. Geach, G. A. and Hughes, J. E., "The Alloys of Rhenium with Molybdenum or with Tungsten Having Good High Temperature Properties", Proceedings, Second Plansee Seminar, Metallwerk Plansee A. G. Reutte, Austria, p. 246, 1955.

37. King, G. W., Morcom, W. R., Sell, H. G., "The High Temperature Tensile Properties of Tungsten and Tungsten-Rhenium Alloys Containing a Dispersed Second Phase", Fourth Symposium on Refractory Metals, French Lick, Indiana, October 3, 1965.

UNCLASSIFIED
Security Classification

DOCUMENT CONTROL DATA - R&D

(Security classification of title, body of abstract and indexing annotation must be entered when the overall report is classified)

1. ORIGINATING ACTIVITY (Corporate author)	2a. REPORT SECURITY CLASSIFICATION
Westinghouse Electric Corporation Lamp Division Bloomfield, New Jersey	UNCLASSIFIED 2b GROUP

3 REPORT TITLE

Development of Dispersion Strengthened Tungsten Base Alloys

4 DESCRIPTIVE NOTES (Type of report and inclusive dates)

Summary Report 1 May 65 thru 30 Apr 66

5 AUTHOR(S) (Last name, first name, initial)

Sell, Heinz G., Morcom, William R., and King, George W.

6. REPORT DATE	7a. TOTAL NO. OF PAGES	7b. NO. OF REFS
November, 1966	112	37

8a. CONTRACT OR GRANT NO.	9a. ORIGINATOR'S REPORT NUMBER(S)
AF33(615)-1698 b. PROJECT NO. 7351 c. d. 735101	9b. OTHER REPORT NO(S) (Any other numbers that may be assigned this report) AFML-TR-65-407, Part II

10. AVAILABILITY/LIMITATION NOTICES

Qualified users may obtain copies of this report from the Defense Documentation Center.

11. SUPPLEMENTARY NOTES	12. SPONSORING MILITARY ACTIVITY
	Research and Technology Division Wright-Patterson Air Force Base, Ohio

13. ABSTRACT

The mechanical properties of a W-3.8 v/o ThO_2 alloy with superior high temperature tensile and creep strength have been determined from room temperature to 3000°C. This alloy has been produced by two separate techniques in rod form. The alloy has been found to exhibit a tensile strength as high as 15,500 PSI at 2400°C and at a strain rate of 0.05 min^{-1} and a 1 hour creep rupture strength as high as 12,500 PSI at 2200°C. The DBTT of this alloy annealed at 2400°C for 1/2 hr. is 190°C.

Four experimental W-5.7 v/o ThO_2 alloys have been produced to investigate the effects of chemical processing parameters on dispersoid distribution and strength properties. The high temperature strength properties have been essentially reproduced in alloys in which the thoria dispersion was added to tungsten oxide. In those alloys in which the thoria dispersion was added to the metal powder, the strength improvements were much smaller.

A high temperature strength evaluation was also made on W-Re-3.8 v/o ThO_2 alloys having 5, 10, 15 and 25 w/o Re concentration. These alloys have significantly lower strength above 2000°C than the ThDW-WHS (W-3.8 v/o ThO_2) alloy.

DD FORM 1 JAN 64 1473

UNCLASSIFIED
Security Classification

UNCLASSIFIED

Security Classification

14. KEY WORDS	LINK A		LINK B		LINK C	
	ROLE	WT	ROLE	WT	ROLE	WT
Tungsten-base alloys Dispersion strengthened tungsten Thoria dispersoids Powder metallurgy - Chemistry Tungsten-thoria alloys Tungsten-rhenium-thoria alloys Extrusion Chemical stability High temperature strength Tensile strength Creep strength Electron microscopy						

INSTRUCTIONS

1. ORIGINATING ACTIVITY: Enter the name and address of the contractor, subcontractor, grantee, Department of Defense activity or other organization *(corporate author)* issuing the report.

2a. REPORT SECURITY CLASSIFICATION: Enter the overall security classification of the report. Indicate whether "Restricted Data" is included. Marking is to be in accordance with appropriate security regulations.

2b. GROUP: Automatic downgrading is specified in DoD Directive 5200.10 and Armed Forces Industrial Manual. Enter the group number. Also, when applicable, show that optional markings have been used for Group 3 and Group 4 as authorized.

3. REPORT TITLE: Enter the complete report title in all capital letters. Titles in all cases should be unclassified. If a meaningful title cannot be selected without classification, show title classification in all capitals in parenthesis immediately following the title.

4. DESCRIPTIVE NOTES: If appropriate, enter the type of report, e.g., interim, progress, summary, annual, or final. Give the inclusive dates when a specific reporting period is covered.

5. AUTHOR(S): Enter the name(s) of author(s) as shown on or in the report. Enter last name, first name, middle initial. If military, show rank and branch of service. The name of the principal author is an absolute minimum requirement.

6. REPORT DATE: Enter the date of the report as day, month, year; or month, year. If more than one date appears on the report, use date of publication.

7a. TOTAL NUMBER OF PAGES: The total page count should follow normal pagination procedures, i.e., enter the number of pages containing information.

7b. NUMBER OF REFERENCES: Enter the total number of references cited in the report.

8a. CONTRACT OR GRANT NUMBER: If appropriate, enter the applicable number of the contract or grant under which the report was written.

8b, 8c, & 8d. PROJECT NUMBER: Enter the appropriate military department identification, such as project number, subproject number, system numbers, task number, etc.

9a. ORIGINATOR'S REPORT NUMBER(S): Enter the official report number by which the document will be identified and controlled by the originating activity. This number must be unique to this report.

9b. OTHER REPORT NUMBER(S): If the report has been assigned any other report numbers *(either by the originator or by the sponsor)*, also enter this number(s).

10. AVAILABILITY/LIMITATION NOTICES: Enter any limitations on further dissemination of the report, other than those imposed by security classification, using standard statements such as:

(1) "Qualified requesters may obtain copies of this report from DDC."

(2) "Foreign announcement and dissemination of this report by DDC is not authorized."

(3) "U. S. Government agencies may obtain copies of this report directly from DDC. Other qualified DDC users shall request through

_____."

(4) "U. S. military agencies may obtain copies of this report directly from DDC. Other qualified users shall request through

_____."

(5) "All distribution of this report is controlled. Qualified DDC users shall request through

_____."

If the report has been furnished to the Office of Technical Services, Department of Commerce, for sale to the public, indicate this fact and enter the price, if known.

11. SUPPLEMENTARY NOTES: Use for additional explanatory notes.

12. SPONSORING MILITARY ACTIVITY: Enter the name of the departmental project office or laboratory sponsoring *(paying for)* the research and development. Include address.

13. ABSTRACT: Enter an abstract giving a brief and factual summary of the document indicative of the report, even though it may also appear elsewhere in the body of the technical report. If additional space is required, a continuation sheet shall be attached.

It is highly desirable that the abstract of classified reports be unclassified. Each paragraph of the abstract shall end with an indication of the military security classification of the information in the paragraph, represented as *(TS)*, *(S)*, *(C)*, or *(U)*.

There is no limitation on the length of the abstract. However, the suggested length is from 150 to 225 words.

14. KEY WORDS: Key words are technically meaningful terms or short phrases that characterize a report and may be used as index entries for cataloging the report. Key words must be selected so that no security classification is required. Identifiers, such as equipment model designation, trade name, military project code name, geographic location, may be used as key words but will be followed by an indication of technical context. The assignment of links, rules, and weights is optional.

END

UNCLASSIFIED

Security Classification